3D Silicone Whipping Additive Manufacturing (SWAM): Technology, Applications, and Research Needs.

by

Gurkamal Saggu

A thesis
presented to the University of Waterloo
in fulfillment of the
thesis requirement for the degree of
Master of Applied Science
in
Chemical Engineering

Waterloo, Ontario, Canada, 2022

Author's Declaration

I hereby declare that I am the sole author of this thesis. This is a true copy of the thesis, including any required final revisions, as accepted by my examiners.

I understand that my thesis may be made electronically available to the public.

Abstract

Additive manufacturing has become increasingly popular and is developing in many technologies. This thesis focusses on the additive manufacturing with paste technology, more specifically the goal is to further develop a technology for SWAM (Silicone Whipping Additive Manufacturing). SWAM uses a device similar to a traditional filament 3D printer, but it deploys a paste supplied by a pump instead of feeding a thermoplastic filament through a heated nozzle. There are many parameters that are common to both technologies, but the role of several variables is still not described or discussed in the literature. This is relevant because there are limited technologies capable of exploring the advantage of additive manufacturing with soft or elastomeric materials. A successful SWAM technology be used for developing prototypes that require soft materials, like seat cushion for automotive applications and used in tissue for soft robotics.

One of the key parameters controlling the properties of a part manufacture by SWAM is the whipping mechanism of the paste. In this thesis, experiments are presented based on the relationship of SWAM parameters and "Line Printing" characteristics. Line Printing is an experimental method developed here to obtain further insight on the mechanism of SWAM and to enable correlation between SWAM parameters and properties of printed parts. The whipping extrusion techniques has successfully elucidated the liquid rope coiling effect. The SWAM parameters were selected as: Print speed of the nozzle, Diameter of the nozzle, Flow rate of the silicone feed, and Deposition height of the falling silicone paste. Whereas the Line Printing characteristics such as Filament deposition height, Filament line width and Filament loops have been determined. Filament loops are further subdivided into Single loops and Multiple loops.

As a result, Line Printing may be defined as the novel free forming techniques for reproducing a single segment of the desired feed onto the printed bed using various forms of fabricating methods. It may also be called filament printing, filament fabrication, or line prototyping. It would be an aim to study the behavior of the material deposition as well as its transformed deposition ranging from straight-line printing to multiple or mixed-looped line printing. Hence, novel empirical relationships can be generated based on two boundaries elementary parametric conditions that are print speed and the other is flow rate. A novel parameter named G_L ratio was introduced here to describe the transformation of the filament through filament characteristics. It would thoroughly define the feed flow dropping criterion. It is the ratio of the change in the feed flow rate to the change in the print speed of the nozzle

while the other parameters are held constant. Five transformations of the line filament have occurred which are named as straight line, zig- zag/wavy loop filament, single loops filament, mix loops filament and multiple loops filament. Out of the 5, there are two unstable states, and the rest are stable states. Instability of filament is relatively high at the transition state because of the changing patterns of the silicone rope coiling effect, where G_L is equal to unity. Line printing can be formed into multiple layers thus producing the bulk form which would be a porous structure, thus giving rise to a 3D shape due to controlled deposition of the filament due to the X-Y-Z location of the nozzle.

In automotive applications, this technique can be used to create prototypes for an in-seat car cushion as a substitute for polyurethane (PUR) seat cushions. Herein, silicone has been used because of its versatile applications. The in-seat silicone cushions have been produced to perform force-deflection test to identify the mechanical feature. Viscoelastic properties of silicone concluded that novel SWAM can print lower density in-seat cushion along with variable firmness. The printed cushion showed that they can withstand the applied force for a longer time-period without decreasing with time. This feature would reveal that silicone can be a good material for seat cushioning.

Hard-skinned robots can be modified to humanoid robots which would be ideal in the education system, especially for the autistic children. Soft tissue mimicking materials have been obtained through the line printing technique of the novel SWAM. Parts can be printed to resemble the firmness of fat and muscle tissues due to the displayed similar properties to that of real tissues through mechanical experiments. This could be applied in robots assisting autistic children for example, so they would learn response to external stimuli through humanoid robots in a more natural interactive environment.

Acknowledgements

I would like to express the deepest appreciation to **Professor Leonardo Simon**, my supervisor, for his mentoring and assistance during my master's research and studies, along with his persistent encouragement and forbearance with my mishaps during the COVID-19 pandemic. It has been a privilege to work with him, and I can't emphasize him enough for entrusting me with this tremendous training opportunity.

Professor Rosane Rech, my co-supervisor**,** has graciously allowed me to utilize the R-Code Software to analyze Line Printing Characteristics through her teachings. She assisted me the best in organizing my theses as well. I would like to express my appreciation to her for the insightful remarks on my theses and further she assisted me greatly in the hard times of pandemic.

I would also want to convey my gratefulness to my professor's research colleagues, **Andrew Finkle**, **Douglas A Casetta**, **Maryam Bagheri**, **Chong Meng**, and **Mirela Vanin** for their unwavering support. I would never forget the immense assistance of my Co-op Students, **Luke Young**, **Adnan Fakhouri**, and **Melina Brajuka**.

This research could not have been done without funding from **Ford Motors Company, Detroit, U.S.A** and the **Ontario Centers of Excellence**. I want to express my gratitude working with **Dr. Ellen Lee** *&* **Dr. Janice Tardiff,** Ford Researcher in Advanced Engineering.

A special thanks to my younger brother, **Anmol Saggu**, with whom my childhood memory is incomplete, for supporting me in every aspect of my life and being there in the arduous times of pandemic in which I was feeling low for several times. And he fueled me up with confidence every times.

I would also want to express my sincere gratitude to my elder cousin, **Surinderpal Singh**, and my younger sister **Rajwinder Bassi**, for always pushing me and being the greatest source of happiness in my career.

I would want to voice my gratitude to God, **Waheguru**, for his mercies.

This thesis is wholly dedicated to beloved parents. Lastly, I would like to show my devotion to my parents, **Sardar Manjinder Singh,** and **Davinder Kaur**, and to my late grandparents, **Sardar Nirmal Singh Saggu**, and **Mohinder Kaur**, for always trusting in me and pouring me with affection, care, and encouragement. Without their prayers, none of this would have been possible.

Table of Contents

List of Figures

List of Tables

Chapter 1

Introduction

1.1 Motivation

The developments of 3D printing open up various possibilities in manufacturing --- from low-cost manufacturing to a lean approach to design and development [1]. 3D Printing with silicone is one of the greatest breakthroughs in the field of additive manufacturing in recent years [2]. Silicone 3D printing has a potential to democratize its uses in the production of goods --- varying from food to medical supplies, to automotive and electronic applications [3]. The 3D printing market in the North America was valued at 11.58 billion USD in 2019 and is expected to expand by 14% from 2020 to 2027 [4], as shown in the Figure (1.1) below:

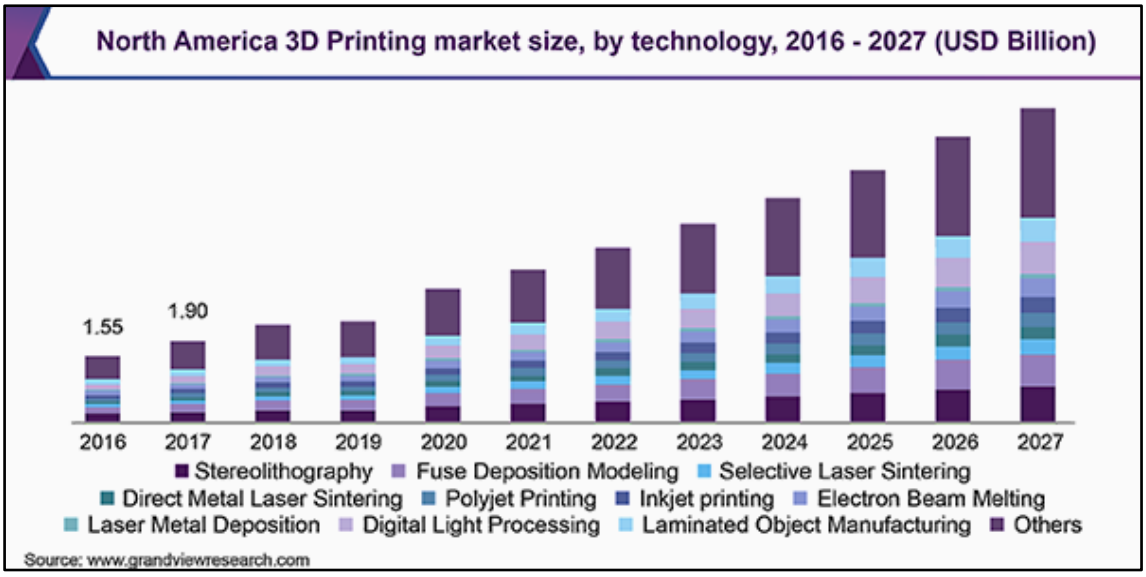

Figure 1.1: The market size of the 3D printing in the North America from 2016 to 2027 [4] (source: www.grandviewresearch.com)

Large industries, such as automotive, electronics, aerospace/defense, and healthcare, are contributing to higher shares for the extensive adoption of 3D printing [5]. Prototyping, customizability designing, and scaling are important factors that will fuel the growth of the industrial segment soon.

The historical review shows that numerous materials (resins, plastic powder, filament, and hot-melt plastic ink) were used in the 1980s for patents in the rapid prototyping field. 3D printed soft actuators seemed to occupy its place in additive manufacturing. Soft actuators are materials which are relatively soft and can change shape and size in response to any external stimuli. Most of the existing soft

materials are fabricated by conventional methods, such as molding, casting, soldering, and piston-type extrusion, which need manual fabrication of materials, post-assemble processing, and protracted iterations until the final product is achieved. Researchers are still exploring an appropriate manufacturing approach for the effective fabrication of soft structure, as shown in the Figure (2). However, the production is still limited to the raw materials and equipment.

Ironically, the reason why silicone has not been used as the raw material in 3D paste printing although it seemed to be an attractive printing material is because it is not possible to melt silicone by heat exposure. Furthermore then print silicone structure layer by layer like additive manufacturing with metals and thermosetting polymers [2]. For these reasons, several researchers and companies have tried to develop materials that would replicate them, although this has never happened again. Herein, the soft structure has been prototyped and fabricated by the novel 3D printing technique, which has been named as Silicone Whipping Additive Manufacturing (SWAM). Soft Structure has been photographed by Gurkamal Saggu in the Figure (1.2) below.

Figure 1.2: Soft part fabricated by Silicone Whipping Additive Manufacturing (SWAM), illustrating the flexibility of silicone-made soft structure. The deformation of the part being squeezed is reversible. (Source: By Gurkamal Saggu)

In automotive sectors, car seats have widely evolved with the knowledge of ergonomics over time in terms of comfort and safety. As a simple explanation, polyurethane has been a trendy and flexible open structure as a substitute for elastomers because it is inexpensive [6]. It is used as an upper comfort layer

in the innerspring car seat, as shown in the Figure (1.3). At this point, one may be wondering if PUR inner seat cushions are like silicone inner seat cushions. Although, both are a type of elastomers, they are quite different in terms of chemical and mechanical applications.

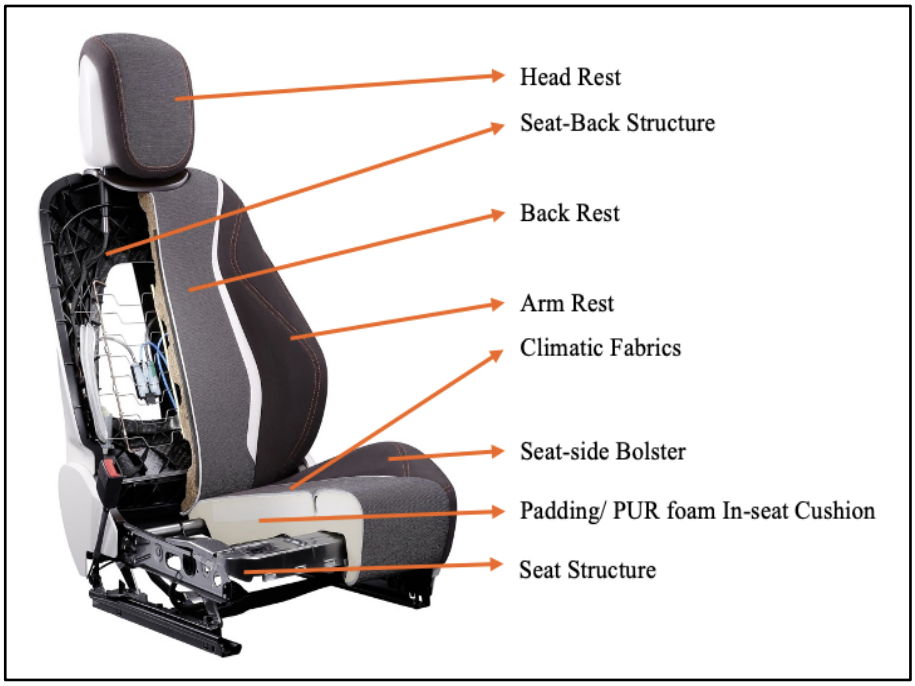

Figure 1.3: Demonstration of Automotive seat design structure [7], labelling the features: Head Rest, Seat-Back Structure, Back-Rest, Armrest, Seat-side Bolster, Padding (PUR foam In-seat Cushion), Climatic Fabrics, and Seat structure. (Source: By Johnson Controls and labelled by Gurkamal Saggu).

Polyurethane seat cushions are better when used occasionally by the user (short periods). However, silicone seat cushion fills the void of the automotive cushion for regular use (extended periods in seat). Unlike PUR, silicone cushion would offer outstanding comfort that could alleviate pain that occurs during longer periods of driving. The mobility of one side of silicone cushion will not be easily felt on the other side. In fact, most consumers have been looking for an orthopedic seat cushion. Unfortunately, the resiliency of high graded PUR cushion does not match that of silicone-printed cushion.

In addition, flexible PUR structures are highly flammable materials. Flexible PUR structure fire safety is only appropriate when the material is properly protected from the fire source [8]. Numerous investigations have been established regarding the flame retardant systems for PUR cushions. Liang co-workers reported that the PUR fire retardancy can be increased by structural influence of organophosphorus [9]. Furthermore, they added DOPO - phosphonamine to PUR foam to increase flame retardancy [10]. Price and co-workers investigated the flame retardancy and smoke suppression

could be done with the addition melamine in compressible PUR compliance [11]. By 2008, Andersson and co-workers introduced a novel fire-retardant system for PUR polymeric foams [12]. Many literatures have only been focused on the new advances in the flame retardant and flexible PUR seat cushions because it represents a hazardous to vehicle occupants. In addition to their flammability, a burning PUR cushion in the car accidents form carbon monoxide (CO), hydrogen cyanide (HCN) and other toxic gaseous particles on decomposition and combustion. [13]. The toxic hazards associated with fire and instability of victims to escape the fire environment can attributed to these main risks: heat, smoke, and harmful fuel products [14]. Escaping time is the interval between the ignition time and the time after which the conditions become ineffective, since the victim can no longer take effective action to save himself. This may be the result of bright and congenital heat exposure; blurred vision due to smoke; unbreathable toxic gases and high-respiratory irritation [15]. Heat, smoke, and flammable gases can disrupt survival, thereby increase fatality risk by damaged lung and sometimes cause death. Ironically, North America has the largest PUR market situated at 95% [16].

There is some controversy in the literature about overall toxicity of PUR foams and fire retardants' effects. This is due the wide range of fire retardants found in PUR foams suggesting that toxicity will follow the general trends in literature for flammable materials [13]. However, silicone foam has fire-retardant property since it can bear a high range of temperature.

In soft robotics sectors, there has been a growing interest in the humanoid robots in education for learners on the autism spectrum [17]. Autism is the spectrum of lifelong neonatal developmental conditions related conditions that offers a person's inability to interact with others and experience the world around them [18]. Autistic children seemed to be particularly interested and motivated by robots, presumably due to the fact that they are interactive though programmed and ultimately rule-based devices [19]. Because of this intellectual disability, autistic children have impaired social communication and interactions, eccentric behavior, and social or emotional reciprocation which differs from the average person. For instance, autistic children may be in the middle of a conversation with someone who is very upset; however, they may not be able to recognize emotions and would not make the emotional connection that the other person is upset. Since, they lack these social skills, they may act or speak inappropriately. This is where humanoid robots could help [17], [20].

A robots' exterior is simply hard plastic, as shown in the Figure (1.4); nevertheless, robots will soon be able to appear more human-like with the help of 3D printing. The replication of tissue like muscles, fat, and skin using silicone will fill this gap in soft robotics. Thereby, counterfeit silicone tissue can be

added to the teaching effect of the robot in the sense of providing comfort and authenticating experience. Since autistic children will learn to associate robots like a real human or person.

Figure 1.4: Demonstration of the Hard-surfaced robotic hand touching the human hand [21] (Source: By Carrie Duarte)

Herein, SWAM technology has been used to print useful lightweight and elastomeric silicone structures with the motivation to be relevant for new seat development and tissue for soft robotics. SWAM is the novel type of paste additive manufacturing which uses the concept of line printing based on falling liquid (silicone) rope effect. These highly durable and temperature resistant structures could mimic inner-seat automotive cushions, that could replicate PUR cushion. Besides being good viscoelastic and biocompatible materials, printed silicone soft structures could be the suitable tissues for the robots.

Furthermore, SWAM would complement traditional methods of casting and injection molding that were facing many problems as categorized below:

a) Limited product development.

b) Increased tooling and capital investment.

c) Inflexible production

d) Difficult high scale of product

e) Long time process.

1.2 Project Objectives

The goal of this project is to identify conditions conducive to 3D printing of silicone paste at room temperature. The specific project objective is:

1. Determine the relationship between SWAM apparatus parameters and printed characteristics of silicone line printing.
2. Identify and evaluate parameters in the mechanism of liquid rope coiling that are relevant in silicone paste 3D printing.
3. Develop a potential criterion for the identification of materials suitable for SWAM apparatus.
4. Prototyping parts with characteristics suitable for automotive seat cushion, inner-seat cushion with variable density and firmness.
5. Prototyping the tissue replica of the humanoid robots with variable density and stiffness.

1.3 Organization of Document

The thesis is divided into the following chapters:

1. Chapter 1: Identify the motivation for this research based on the challenges of polyurethane in automotive seat and the opportunity for tissue in soft robotics.
2. Chapter 2: This chapter illustrates the background of the 3D printers and the external systems and reviews the features with their applications. The chemistry of silicone, liquid rope coiling effects and its four regimes, automobile in-seat cushions, and humanoid soft robots have all been addressed in this section.
3. Chapter 3: The materials and procedures of the SWAM are demonstrated in this chapter. It commences with the SWAM installation and configuration method, then progresses on to line printing, in which the documentation process is statistically validated by imaging and measurements of six filament characteristics. Moreover, it terminates with bulk printing and mechanical compression testing of all specimens.
4. Chapter 4: This chapter outlines the printed filament characteristics, including results and discussion; statistical analysis of filament characteristics as a function of G_L ratio; and the transformation of filament characteristics with reference to the four printing parameters. Use of SWAM for seat cushioning and tissues for soft robotics has been thoroughly investigated.
5. Chapter 5: This chapter marks the conclusion of the thesis.

Chapter 2
Literature Review

2.1 Motivation

3D Printing is a method for creating 3D objects with the aid of Computer-Aided Design (CAD) software. The fabrication is based on the layering ability of the raw material used, thus it is also known as Layered or Additive Manufacturing (AM) [22], [23].

As of 2019, Additive Manufacturing is considered as a compatible industrial-production technology. Adopting this technology is to provide the repeatability, accuracy, interchangeability in the manufacturing of the ergonomic products ranging from automotive to biomedical industries [24], [25].

Commercially, a wide range of materials has dominated in the field of manufacturing, such as stainless steel, plastics, polymers, resins, and ceramics. Tailoring molecular structure, using AM techniques remains challenging as detailed additive techniques are limited to better determining and testing the printability of new material systems. However, researchers are continually developing novel empirical and analytical approaches to address this challenge and to optimize printing parameters [26], [27].

To date, researchers have been investigating the printability of elastomers using different AM techniques, which is highly attractive for the manufacturing of soft and stretchable structures. Due to their inherent material properties, many challenges of printing elastomers remain specific either to the printer or combination of the polymer and the printer. Elastomers are desirable in the automotive applications (e.g., for tires, gaskets, seat cushioning), soft robotics (e.g., actuators, vascularized tissues, shape morphing materials), in consumer products (e.g., shoe soles, bicycle grips), and aircraft industry.

The literature on the extrusion-based AM of soft elastomeric components is rather limited. This is perhaps due to the lack of materials known as thermoplastic elastomers having properties suitable for additive manufacturing. The relationships between printing parameters, material characteristics and properties of final printed product are still in its infancy.

2.2 3D Printing

There is no way to chronicle the advancement of Additive Manufacturing (AM) without acknowledging its commercialization in the past few decades. The progress in stereolithography (SL) was the sign of emergence of the AM in 1987. The early 1990s, Stratasys, Cubital, Helisys, DTM, and Teijin Seiki commercialized new technologies of additive manufacturing such as Fused Deposition Modelling (FDM), Solid Ground Curing (SGC), Laminated Object Manufacturing (LOM), Selective Laser Sintering (SLS), and Solid form Stereolithography respectively [28]. With the myriad inventions in the AM technology, several systems were made to classify the AM processes, e.g., Ming C. LEU summarized the division into four categories according to the state of starting material used as in Table 2.1 [29].

The different 3D printers do not use the same printing technology to print layers to form finished products. Some techniques liquefy or melt the raw material, whereas some use high powered laser to cure photoreactive resin to print the object. Unlike subtractive manufacturing, these processes do not waste material [30].

Molding and casting are the technique generally used for the manufacturing of soft elastomeric components, as shown in the Figure (2.1). However, these methods are not suitable for producing parts having low production volume, low cost, and complex internal geometries. AM techniques have the potential to facilitate complex customization from soft to hard elastomeric components [31], [32].

Figure 2.1: Illustration of Silicone Casting of Shoes' sole [33]. (Source: https://www.structur3d.io/photos).

3D printing extrusion- based methods are based on the technique where the materials are extruded through nozzle and fabrication of the object is controlled by a three-axis (X-Y-Z) motion control system. Extrusion-based methods, such as Fused Deposition Modeling (FDM) and Direct Ink Writing (DIW), are most used due to their low material cost and ease of use.

Fused Deposition Modeling (FDM) uses continuous thermoplastic filament material, such as Acrylonitrile Butadiene Styrene (ABS), Polylactic (PLA), Thermoplastic elastomers (TPE), Polyethylene terephthalate glycol (PETG), etc. It is also the most used technology for prototyping as well as for modelling. It fabricates the part layer-by-layer by extruding the melted thermoplastic material out of the nozzle [30]. After the deposition of a given layer, the vertical axis of the nozzle moves up by the previous layer thickness, and the new layer is deposited [34]. The resolution of the constructs is particularly dependent on the nozzle diameter. Though FDM is known as Extrusion Technique, it is not suitable for printing paste-like material such as hydrogel or RTV silicones, a type of silicone that cures at room temperature and RTV is a general term for Room-Temperature-Vulcanizing. FDM process is a less expensive process than SLA, to a point that makes it suitable for home use or recreative applications. The level of accuracy and surface finishing provides are worth the manufacturing cost [26], [30], [31].

Table 2. 1: Working Principle of AM processes [29].

State of starting material	Process	Material preparation	Layer creation technique	Phase change	Typical materials	Applications
Liquid	SLA	Liquid resin in a vat	Laser scanning/ light projection	Photopoly-merization	UV curable resin, ceramic suspension	Prototypes, casting patterns, soft tooling
	MJM	Liquid polymer in jet	Ink-jet printing	Cooling & photopoly-merization	UV curable acrylic plastic, wax	Prototypes, casting patterns
	RFP	Liquid droplet in nozzle	On-demand droplet deposition	Solidification by freezing	Water	Prototypes, casting patterns
Filament/ Paste	FDM	Filament melted in nozzle	Continuous extrusion and deposition	Solidification by cooling	Thermoplastics, waxes	Prototypes, casting patterns
	Robocasting	Paste in nozzle	Continuous extrusion	–	Ceramic paste	Functional parts
	FEF	Paste in nozzle	Continuous extrusion	Solidification by freezing	Ceramic paste	Functional parts
Powder	SLS	Powder in bed	Laser scanning	Partial melting	Thermoplastics, waxes, metal powder, ceramic powder	Prototypes, casting patterns, metal and ceramic preforms (to be sintered and infiltrated)
	SLM	Powder in bed	Laser scanning	Full melting	Metal	Tooling, functional parts
	EBM	Powder in bed	Electron beam scanning	Full melting	Metal	Tooling, functional parts
	LMD	Powder injection through nozzle	On-demand powder injection and melted by laser	Full melting	Metal	Tooling, metal part repair, functional parts
	3DP	Powder in bed	Drop-on-demand binder printing	–	Polymer, Metal, ceramic, other powders	Prototypes, casting shells, tooling
Solid sheet	LOM	Laser cutting	Feeding and binding of sheets with adhesives	–	Paper, plastic, metal	Prototypes, casting models

DIW is another Extrusion-based AM technique which is used for the printing paste or ink/gels with higher viscosities, to recover its rigidity after extrusion. In this technique, a suitable material should possess specific rheology to be processed. The material should be thixotropic; thus, its viscosity decreases under shear strain. Fillers, such as silica particles, nano-clay, are commonly blended with the polymer resin to achieve the described rheological properties. [26] The Herschel- Bulkley model is often used to describe such paste.

Like Robocasting, Freeze-Form Extrusion Fabrication (FEF) was developed at Missouri University of Science and Technology. The solidification of the material after printing is achieved by freezing the deposited aqueous paste. Proper paste viscosity and consistency, straight walls and flat tops can be modelled using a support bath. It has an exclusive ability to make functionally graded components from multiple materials including reduced organic binder [26], [31], [34], [35]. DIW is also considered cheaper as well as environmentally additive technology. The resolution of the final products is usually defined by the nozzle dimension.

Recent 3D printing has many things in common to was previous observed as Paste Printing. However, the materials used in this technique have been restricted to a very limited range due to lack of available apparatus designs. With the continuous advancements in 3D-Printing, the authors have identified two main constructive designs for paste and clay extrusion devices. In 1975, Robert A. Bemm [36] introduced the first piston-type extruder, like a syringe which is electrically or pneumatically actuated. With the help of an electric motor, the linear translation has been achieved using a pinion rack mechanism as shown in the Figure (2.2). The apparatus was designed for the edible pastes, confections, and bakery products.

A similar extruder design was used by RichRap (2012), named Universal Paste Extruder, shown in the Figure (2.3). This design was reported to be capable of ceramic and food 3D printing. This device uses a drive belt mechanism to drive a piston that extrudes the material through the nozzle. Nevertheless, this design has some limitations to several aspects. The efficiency of this extruder design is restricted to only fabricating small-volume objects because of low amount of raw material in the extruder tube. The dynamic capabilities of the 3D Printer have also been affected by raised center of gravity due to the additional weight of the piston, installed over the printer head. The feedstock retraction function cannot be used during the fabrication, though the design uses pneumatically actuated pistons [37].

The second constructive design was commercially launched by WASP in 2016 [38] that are adaptable to other 3D printers for ceramic materials. This design uses an electrically actuated auger screw to extrude the feedstock through a nozzle. It also includes a separate container in which the pressurized feedstock is stored along with the extruder. The extruder allows the feeding of the material during the printing process to model large objects. The fabrication of large objects demands additional drive elements, such as electrical motors, compressors, and pneumatic valves. As a result, it increases the complexity of the 3D-Printer design and makes it difficult to be a suitable system that can be a drop-in replacement for any thermoplastic extruder.

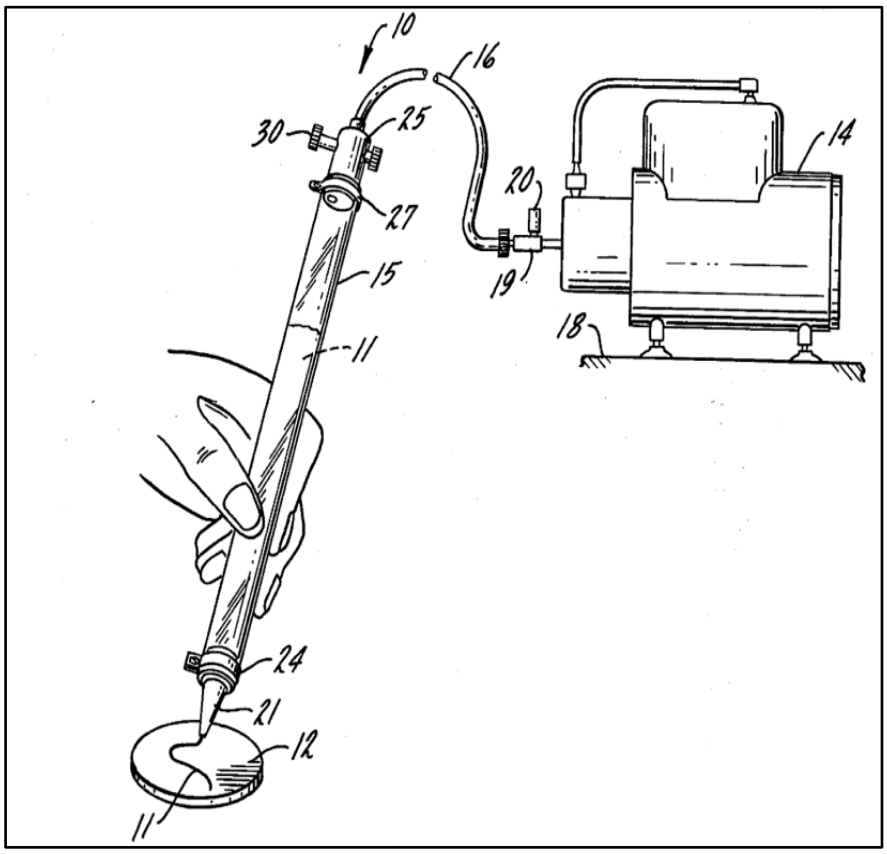

Figure 2.2: Piston-type Extruder by Robert A. Bemm [36]

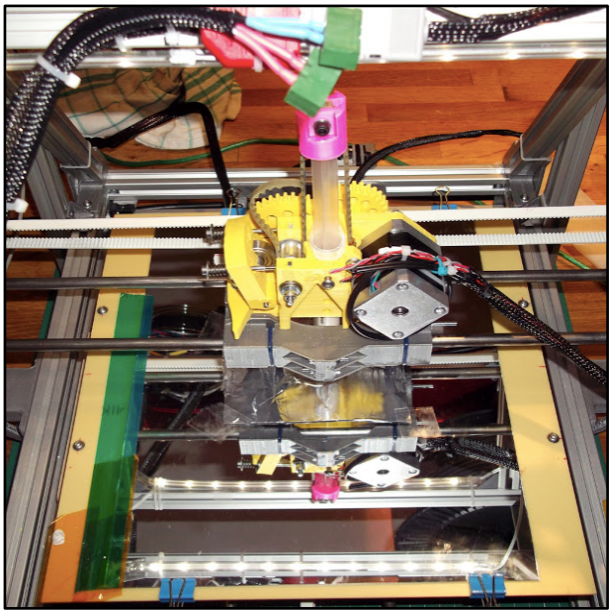

Figure 2.3: Universal Paste Extruder by RichRap [37]

Catalin G. Amza in 2017 [39] with other researchers has eliminated some of the limitations of the aforementioned paste extruder equipment by introducing the Hardware Add-On for Desktop 3D printers. The Hardware is a paste extruder, successfully incorporated with stepper motor, ceramic heating cartridge, thermistor, and DC fan. Though it is a simple extruder with lesser drive elements, it is mounted on the desktop 3D printer replacing standard thermoplastic filament extruders. Furthermore, one can also control the flow rate and print speed to accommodate the certain needs for the extruded feedstock.

2.3 3D printing Materials

New industrial printing materials and machines are sold every year to meet the growing demand for the production technology. Encouraged by these new product possibilities, there is a growing challenge that prevents companies, engineers, and researchers from understanding the technology advances and potential economic benefits of AM.

2.3.1 TPE (Thermoplastic Elastomer)

TPE is a thermoplastic material with rubber-like properties. The components that are 3D printed in TPE are highly durable with good chemical, heat, and tear resistance. This highly durable polymer combines both elastomeric and thermoplastic properties. What makes this material so appealing to manufacturers is that it can return to its original form without any damage after a short tug. This is only possible due to its rubber like features, which make 3D printing an ideal choice for applications that need to be impact and vibration resistant.

In addition, TPEs have better chemical stability and better resistance to abrasion and wear and tear. Another advantage is that TPEs are generally heat resistance which allows it to be sterile. Furthermore, 3D printed scaffolds with these types of materials are suitable for many industrial and medical applications as well as functional prototypes.

2.3.2 TPU (Thermoplastic Polyurethane)

TPU is a flexible polymer with good physical properties, high thermal stability, and good chemical resistance. This 3d printing material has been engineered to mimic rubber-like properties by combining strength with greater flexibility and durability. It has excellent deformation properties and is highly

resistant to dynamic loading. For this reason, parts that are 3D printed in TPU can be easily compressed and applied to a degree that other common plastics (ABS and PLA) cannot. TPUs are softer than TPEs though TPU is a type of TPE with variable level of hardness.

TPU's awesome formwork makes detail and compact parts with excellent surface quality. Another advantage of 3D printing material is that it is a real all-rounder capable of creating flexible, semi-rigid or rigid parts that can withstand temperatures up to 80 ^{o}C. Such features are increasing the popularity of 3D printing in TPUs for high performance parts in machinery, aerospace, and automotive applications. Depending on the application, the recycling rate of TPU can go up to 100%. However, TPU has some weaknesses such as longer leading times, non-bio friendly material and its shrinking property during wet conditions [6].

2.3.3 Silicone

Silicone is a biofriendly elastomeric polymer that has unique mechanical, chemical as well as thermal properties. Silicone is a well-known category of elastomers. It is a promising material for AM due to its degree of flexibility and accuracy at which is flow can be controlled. Until recent years, the alternative was to use either casting or molding other materials that sought to mimic properties such as silicone rubber. Compared to conventional methods, 3D printing offers high degree of flexibility and enables the production of parts that are higher in complexity. For those reasons, silicone paste printing has seemed to gain its popularity in automotive and medical industries.

Being a versatile material with unique properties, it can be used for very high-performance applications due to its high environmental resistance. For instance, silicone AM can produce end parts with higher precision that can be sterile. Silicone can withstand extreme temperatures, it also offers good electrical resistance and the possibility of printing counterfeits with various levels of density, stiffness, or firmness. Many industries have waited for this product to be available for 3D printing.

2.3.3.1 Silicone material and its chemistry

Silicone is a thermoset polymer. The word silicone was given by F.S. Kipping in 1901 to describe the general formula of the polymeric substance i.e., $(R_2SiO)_n$ by analogy with ketones. 'Silicon' and 'Silicone' are just two of the words that can be often confusing, but they carry entirely different meanings and usages. Silicon is a chemical element that can be used in making electronic chips and solar cells, due to its crystalline form and semiconducting metalloid properties. Silicones are

compounds made up of silicon (Si), oxygen (O), carbon (C), hydrogen (H), and perhaps other kinds of atoms as well. Different physical and chemical properties can be observed due to the variable composition of the atoms' arrangement in the compound [40]. Silicones are commonly used as silicone oil, silicone resin, silicone rubber, and silicone grease.

Chemically, silicones are often called polysiloxanes or polymerized siloxanes due to the presence of the siloxane repeating unit ($–R_2Si – O – SiR_2 –$). The presence of 'organic' groups (R) attached to an 'inorganic' groups (Si-O) in the backbone gives silicones a wide variety of properties and compositions. Thus, the structure of the material can be linear, branched, cyclic, and caged. They can vary in consistency from liquid to gel to rubber to hard plastic. For instance, polydimethylsiloxane (PDMS) is the most commonly linear – structured siloxane used as silicone oil. Due to their basic and unique polymeric properties, they can be used in sealants and adhesives compositions in the field of automotive and aerospace (for their low and high temperature behavior), lubricants, medicine (for their excellent biocompatibility), cooking utensils (for their thermal resistance), electronic (for their electrical resistance), and building industries (for their multi-substance sealing capability and their good weathering resistance) [41], [42].

Particular attention is given to the silicone crosslinking and its properties, as to address its usage as sealants and structural adhesives, rather than its basic preparation. The various forms of silicones can be obtained due to its unique chemical structure, such as silicone fluids, silicone gels, silicone resin, and silicone elastomers. The physical properties of the silicones and uses depend not only on the chemical structures, but also on the organic groups (-R) attached to the main inorganic chain of the silicones, having the Si-O framework. Linear or cyclic silicone polymers can be easily transformed into 3D network and an elastomer with the help of crosslinking reaction. In simple manner, un-crosslinked silicone behaves like a fluid because it flows upon shear forces and its viscosity can be measured. As the degree of crosslinking increases, so does the firmness and stiffness of the silicone paste until the material changes its behavior from a liquid to a solid. Formation of chemical bonds between adjacent chains can be obtained according to one of the following reactions: crosslinking by radical, addition or condensation reaction [43].

Radical Crosslinking

Efficient crosslinking with radicals can only be achieved where polymer contains vinyl groups[44]. Unlike addition and condensation crosslinking, radical crosslinking does not require a catalyst. Various organic peroxides may serve as free-radical generators for the initiation of this type of crosslinking. This can be done either by heating or radiating. High temperature vulcanized (HTV) silicone rubber can be obtained by incorporating vinyl group into the polymer (0.5 mol % – 1.0 mol %) at elevated temperature. It may be necessary to remove volatiles residues during the curing process [45]. The peroxide curing of HTV rubber is shown in the Figure (2.4).

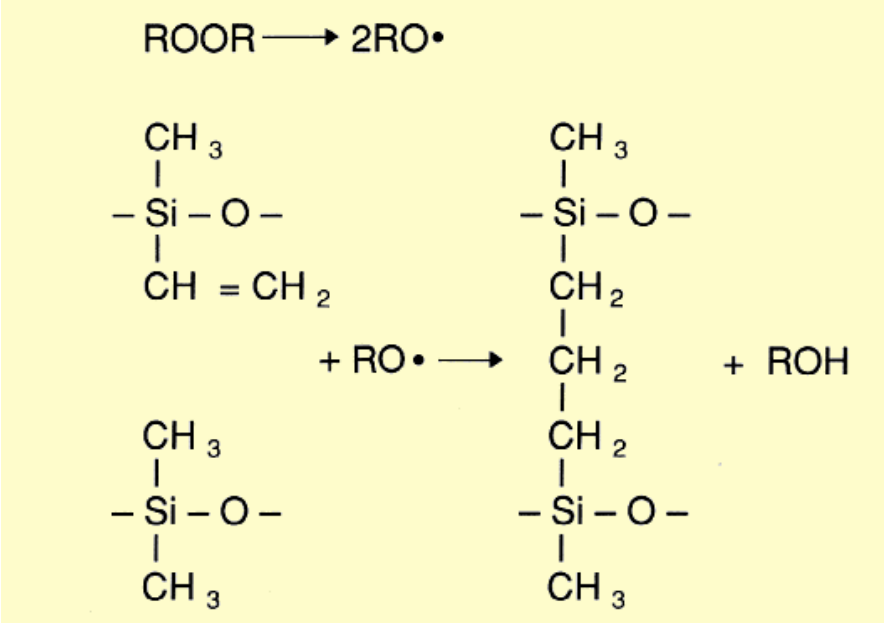

Figure 2.4: Peroxide curing of HTV rubber [45].(Source: https://chemiedidaktik.uni-wuppertal.de/fileadmin/Chemie/chemiedidaktik/disido/en/info/m_fact/crossmod.htm)

Addition Crosslinking

The crosslinking is achieved by reacting the vinyl-end blocked polymers with crosslinking agent containing Si-H groups, in the presence of catalyst such as Pt, Pd or Rh metal complexes. Unlike condensation crosslinking, the curing is impaired by various substances such as sulphur compounds, and many others. For this type of crosslinking, the curing rate is entirely dependent on temperature. Both 1- and 2-parts RTV silicones systems would not encounter chemical shrinkage in this crosslinking, due to absence of by-product during the cure mechanism [43], [45]. The addition curing of RTV-2 rubber is shown in the Figure (2.5).

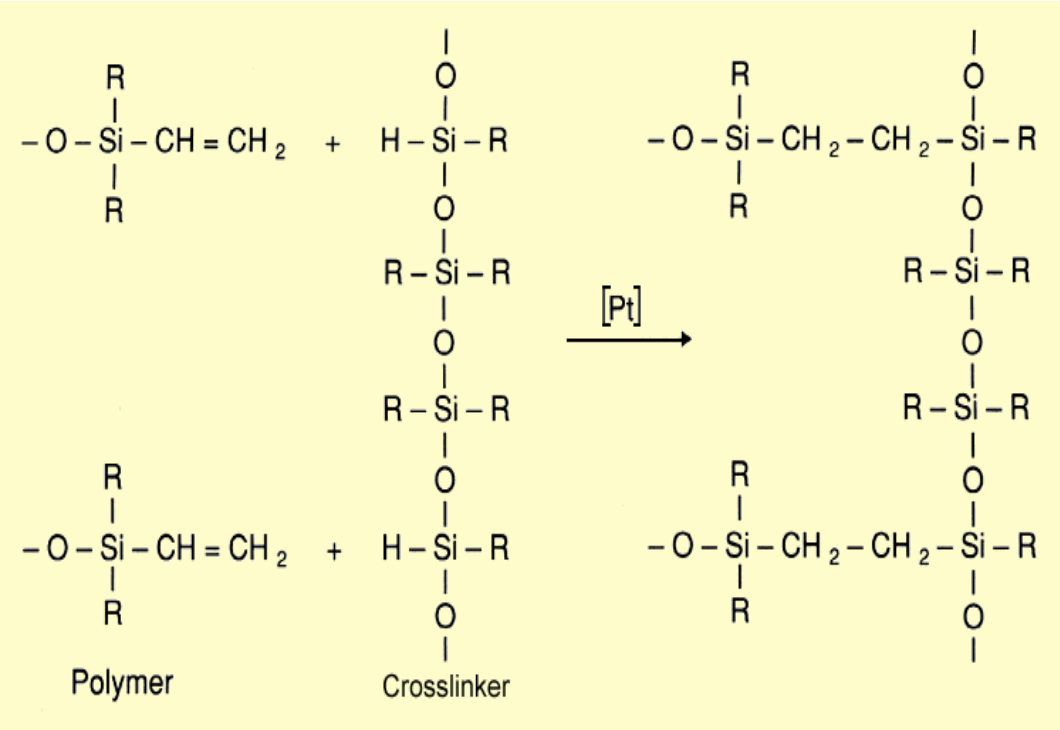

Figure 2.5: Addition curing of RTV-2 rubber [45]. (Source: https://chemiedidaktik.uni-wuppertal.de/fileadmin/Chemie/chemiedidaktik/disido/en/info/m_fact/crossmod.htm)

Condensation Crosslinking

The crosslinking is achieved between hydroxy-end blocked-polydimethylsiloxanes and silicic acid esters on the exposure to the ambient moisture. Dibutyltin dilaurate and dibutyltin dioctoate are the typical catalysts for condensation curing. They catalyze the rate of reaction on the strong accelerating effect of water present in the atmosphere, therefore curing is impaired only by lack of water. Condensation curing is largely independent of temperature [40], [42]. The condensation curing of RTV-2 rubber is depicted in Figure (2.6).

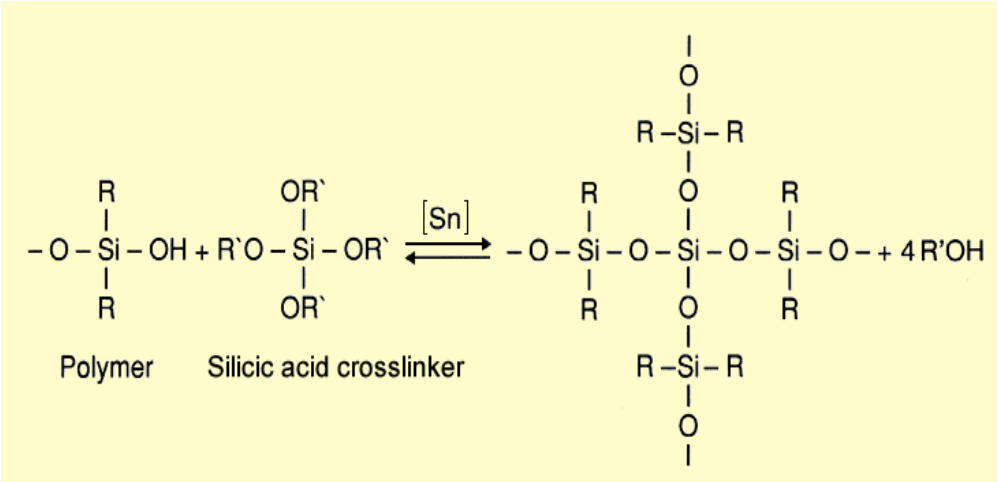

Figure 2.6: Condensation curing of RTV-2 rubber [45]. (Source: https://chemiedidaktik.uni-wuppertal.de/fileadmin/Chemie/chemiedidaktik/disido/en/info/m_fact/crossmod.htm)

2.3.3.2 Silicone Adhesives

Based on organic polymers, silicone has special properties compared to other adhesives because silicone has a distinct chemical backbone. They are very flexible at low temperatures, 75 °C, and have excellent thermal stability up to 200 °C (continuous exposure) and up to 300 °C (exposure for short periods). The properties of silicone remain unchanged to this temperature range. Silicones are tough and resist moisture as well. That is the reason why silicone is chiefly used as adhesives.

Single component silicone adhesives require a moisture content of 5% to 95% for curing. In addition to the presence of moisture, a temperature of 5 to 40 °C is required for curing. The complete curing depends on the thickness of the adhesive film and can take several days. The onset of curing is characterized by skin formation. The few millimeters thickness film can usually heal within 24 hours. Various types of moisture-cured silicones are available depending on the bonding conditions and substrates. Several formulations are used in aircraft and aerospace applications.

Two components silicone adhesives are available with a range of properties and curing rates. However, the initial strength and the strength rate is usually higher than that of moisture-cured silicone. The response to curing can take up to 24 hours. Meter mix equipment is often used to mix the two components of silicone. The two components of silicone are extensively used in the assembly of windows [46].

2.3.3.3 Silicone Sealants

The main difference between adhesives and sealants is that sealants generally have less strength but higher elongation. The main purpose of sealants is to seal assemblies as well as joints by overlooking the environmental conditions. They need to have an adequate flexibility and elongation when they are used between substrates of different thermal coefficients. Sealants usually contain an inert filling material and are formulated by an elastomer to provide required flexibility and elongation. Despite of having great strength, silicone sealants do convey several properties. They provide thermal and acoustic insulation and can act as fire barriers. Sometimes, they also contain electrical properties. They may also be used for filleting and smoothing.

Essentially, sealant perform three main functions with accurate formulations.

1. It bridges the gaps between two or more substrates.
2. It creates a barrier through its own physical properties and by adhesion to the other substrates.
3. It has sealing properties of longer time with good service conditions against severe environments.

Sealants are categorized, into three main classes based on physical form, described below:

One-component sealants are often packaged in the cartridges. No additional equipment is required to apply one-component sealants. These include acrylic solvent-based, butyl solvent-based, latex water-based, silicone and polyurethane.

Two component sealants contain a base component and an activator component. The activator is usually added to the base component and mixed for a desired time-period before application. Bulk guns and mixing equipment are required to prepare and apply the sealants. Two components are often packed in separate buckets. These include epoxy penetrating solvent-based, silicone and urethane.

Sealant tapes are available as sealant on a flexible backing. This includes butyl and silicone tapes and urethane tapes [47].

2.4 Vehicle Fires

Fire protection is crucial to save life and property. Firestops are very effective in saving the lives, and thus reduce damage to building structures, and owned property. Fire extinguishers and fire stop products aid in this objective [48]

Vehicle fire is uncontrollable burning that involves motor vehicles. It is also known as car fire or carbeque, as shown in the Figure (2.7). It is the most common cause of property damage related to fires. Cars may explode if they are burning for too long. A motor vehicle contains a variety of flammable substances, including flammable liquids (gasoline and oil) and solid combustibles (polymers and plastics).

Figure 2.7: SUV car is on fire in Pasadena, California. (Source: https://en.wikipedia.org/wiki/Vehicle_fire#/media/File:Lightmatter_carbq.jpg)

In the Great Britain, accidental car fires are declining but there has been deliberate increase in car fires based on arson activity [49]. However, in case of arson the fire does not start from inside. It is very common that joyriders set fires to stolen vehicle and vandals set fires on to abandoned cars in each and every country [50], [51]. Therefore, it became a law in some EU countries of carrying in-car fire extinguishers [52]. There were approximately 300,000 car fires per year reported in the United States alone from 2003 to 2007, which caused more than 450 causalities [53].

Excessive heat can slowly degrade the rubber material, causing poor performance and premature failure. As such, high temperature applications require high-temperature resistant rubber products that offer reliable performance, if nothing else. Natural rubber cannot be used with temperatures above 85 ^{o}C. However, some synthetic grades of rubber are chemically engineered to withstand temperatures above 300 ^{o}C [54].

PUR is made commercially available after to form various types of foams, sealants, coatings, adhesives, and moldings. The PUR foams can be seen in appliances, automotive parts, carpet padding, in seat cushions, mattresses, composite wood, packaging and so on. PUR can be made as thermoset or as thermoplastic material. On exposure to extreme heat, PUR ignites and burn with harmful gases which include carbon monoxide, hydrogen cyanide and nitrogen oxides. It leaves small amount of char residue. Based on the chemical properties, thermoset PUR can withstand large temperatures unlike thermoplastic and rubber in general. Generally, PUR can be used in the temperature range from -62 to 93 ºC. Special formulated PUR foam can extend its range to as high as 150 ºC [55]. When the thermosets PUR is exposed to extreme temperatures above their limits for long periods of time, they can often cause the following conditions:

1. Weakened physical characteristics.
2. PUR foams usually get sticky by changing its chemical form.
3. PUR may burn which depends on the temperature range and exposure range of flame.

Silicone is a very effective elastomer for temperatures where natural rubber or PUR do not perform well. It offers high temperature resistance and can withstand more than 300 ºC. Although suitable for UV, ozone and weather resistant applications, silicone is recommended for use with specific temperatures and may not always offer the required mechanical properties. But it has good compression set. Some properties such as tear strength, elongation, compression, flexibility, thermal conductivity, and in some cases tensile strength can be far superior to organic rubber at extreme temperature.

Silicone is preferred in rubber industry when the initial shape and perception of mechanical strength are required under extreme thermal stress or sub-zero temperature. Silicone rubber is available in a range of hardness level, expressed as shore A between 10 and 100. It is available in almost in any color and can be a color match. Silicone does not melt but decompose when temperature rises above certain limits. One of the decomposing products is silicone dioxide, also called silica.

Silicones are highly amorphous materials, such that in the solid-state the polymers chains are randomly structured and have no long-range order. Silicones do not have a melting temperature. It does not mean that they are unaffected by heat. They begin to degrade through the process like depolymerization and thermal oxidation. Fortunately, the temperature higher than 300 ºC are normally used during cooking and thus making silicone a great choice for cooking utensils. By comparison, kitchen utensils made of

thermoplastic materials such as polyethene and polypropylene will be dangerous, as they undergo much lower temperature than polymer melting.

Silicone foam is a synthetic rubber which has been used in the North America to stop fires and are usually established within fire-resistance-rated wall and floor assemblies. It is very helpful in preventing the flame spread and smoke from one room to another. When properly installed, silicone foam firestops can be made to comply with building codes. In fact, it includes greater flexibility and dielectric strength. Silicone foam firestops are causing controversy and pressure due to the development of smoke due to pyrolysis of flammable parts inside the foam that emit hydrogen gas, shrinkage, and cracking. Different types of fire sealants are used for their individual properties. Firestop's sealants can be silicone, multilayer or wide. They can be elastomeric, representing 25% to 50 % of their ability to elongate. Useful firestop sealants absorb the energy of the fire to protect what is underneath. Also, it has been reviewed in some of the literature that food graded silicone is a non-toxic polymer made mostly from silica (sand). It can withstand extremes temperature without leaching hazardous chemicals or off-gassing.

2.5 Liquid Rope Coiling

2.5.1 Background

Liquid rope coiling occurs when the viscous fluid is fallen from a fixed height onto a horizontal surface. The instability of falling liquid causes a series of regular coils, as shown in the Figure 2.8. The coiling of the falling viscous liquid has been studied over the last 60 years. The term 'Liquid Rope Coil effect' was first coined by G. Barnes and R. Woodcook in 1958 [56].

Taylor suggested the first theoretical study explaining the similarity of the falling liquid instability with the buckling instability of a solid rope under applied compressive stress [57]. Successive theoretical research based on linear stability analysis determines the critical fall height and coiling frequency. They explained that the instability occurs for low Reynolds numbers and the height greater than threshold height, which depends on the properties of the liquid (viscosity and surface tension) [58]–[60].

Figure 2.8: The rope coiling instability in falling honey. [61]

2.5.2 Structure and Regimes of Falling Liquid

Generally, the falling liquid comprises a long, nearly vertical 'tail' and a helical 'coil' near the horizontal surface, as shown in Figure (2.8). The tail is the part of the flow that precedes bending or twisting to produce the coil, whereas the helical coil of the radius (R) is the settled part of the flow onto the surface [62].

The falling liquid exhibits two elementary velocities, axial velocity (U_1) in the tail section and angular velocity (Ω_1) in the coil section with the radius of the coil at its contact point with the rate (a_1), at varying falling height to form coil onto the flat surface [63]. They are determined based on the flow rate as:

$$Q = \pi a_1 U_1$$

$$Q = \pi {a_1}^2 R \Omega_1$$

The coiling frequency (Ω) could be measured to understand the dynamics of the falling fluid based on the imposed volumetric flow rate (Q) and different falling heights (H), as shown in the Figure (2.9).

The coiling behaviours of the falling liquid are predominantly influenced by three main forces --- viscous force (F_V), gravity force (F_G) and inertial force (F_I). For simplicity, the surface

tension (σ), the property of the surface of a liquid that allows it to resist an external force, due to the cohesive nature of its molecules was neglected due to its minimal effect on the coiling [64]. Surface tension coefficient (γ), the force occurring on the liquid's surface at right angles to a line of unit length on the liquid's surface, is however, important in other related phenomena such as thermal bending of the liquid jets by Marangoni stresses (Brenner and Parachuri 2003) [65].

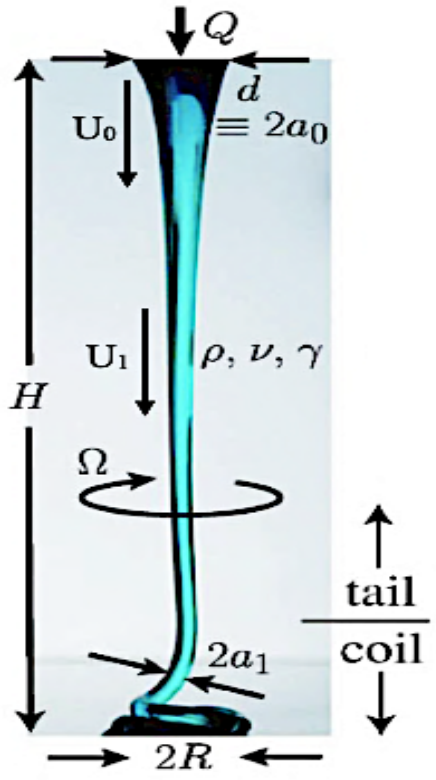

Figure 2.9: Steady-state rope coiling of viscous corn syrup (photographed by Neil Ribe), showing the parameters of a typical laboratory experiment fluid with density (**ρ**), viscosity (**υ**), and surface tension coefficient (**γ**) is injected at a volumetric flow rate (Q) through a hole of diameter (d ≡ $2a_0$) and the falling height (H) of the fluid. The radius of the rope at its contact point with the plate is (a_1), and the radius of depositing fluid is (R). The initial velocity (U_0) of the fluid at the hole tends to attain average axial velocity (U_1) and angular velocity ($\boldsymbol{\Omega_1}$) to form coiling frequency (**Ω**) [62]. The accumulation of material over the flat surface is denoted as mound.

The forces of the falling fluid have been evaluated by Mahadevan (2000) and Ribe (2004) [64], [66] as: -

$$F_V \cong \rho v \mathrm{U}_1 {a_1}^4 R^{-4}$$

$$F_G \cong \rho g {a_1}^2$$

$$F_I \cong \rho \mathrm{U_1}^2 {a_1}^2 R^{-1}$$

The forces acting on the falling viscous fluid can be categorized into three modes --- viscous mode, gravitational mode, and inertial mode. The coiling behaviour is stable in these modes, with different heights, due to the balanced forces.

Probing into deeper details, the modes/regimes were explained based on coiling frequency under the influence of variable heights, as shown in the Table 2.2:

1. Viscous mode: Both gravitational and inertial forces are negligible as compared to the viscous forces. The net viscous force on each fluid element is zero. The coiling occurs in this regime is called viscous coiling (Ω_v). The coiling is entirely caused by the fluid extrusion from the nozzle, like toothpaste squeezed from the tube. Because the flow deforms by twisting and bending with irrelevant stretching, its radius is almost constant, therefore, $a_1 \approx a_0$ and $U_1 \approx U_0$.

2. Gravitational mode: The tail and the coil structure of the falling fluid can be seen distinctly since the gravity becomes a significant factor. The gravity force balances the viscous resistance of fluid to stretching in the tail section and to banding or twisting in the coil section, but the inertial forces are negligible by comparison, therefore, $F_G \approx F_V \gg F_I$. The coiling in this mode is named as gravitational coiling (Ω_G).

3. Inertial mode: Inertial coiling (Ω_I) can be observed because viscous forces that resists bending is balanced almost entirely by inertia, thus, $F_I \approx F_V \gg F_G$. Due to a minor role of gravity, the tail section is perfectly vertical without any sideways.

4. Inertial-gravitational mode: Also, the fourth mode was also observed of having unique and multivalued coiling behaviours when the fall height was increased from the gravitational mode to the inertial mode. The viscous forces are balanced by both gravitational as well as inertial

forces, $F_V \approx F_G \approx F_I$. This transitional state of the coiling behaviour is known as inertial-gravitational (IG) mode.

Besides, they also observed the change in the shape and size of the cone deposited concerning the different falling liquid height (H) and fluid viscosity (υ) [56], [67].

Table 2. 2: Modes or regimes of the falling liquid along with the dominant forces, scaling laws, falling height, coiling radius, and coiling frequency.

Mode/ Regime	Dominant Forces	Scaling Laws	Falling Height	Coiling Radius	Coiling Frequency
Viscous Mode	F_V	-	$H\left(\frac{g}{\nu^2}\right)^{1/3} \leq 0.08$	$R_V \cong H$	$\Omega_V = \left(\frac{Q}{Ha_1^2}\right)$
Gravitational Mode	F_G	$F_G \approx F_V \gg F_I$	$0.08 \leq H\left(\frac{g}{\nu^2}\right)^{1/3} \leq 0.4$	$R_G \cong \left(\frac{\nu Q}{g}\right)^{1/4}$	$\Omega_G = \left(\frac{g\nu Q^3}{a_1^8}\right)^{1/4}$
Inertial-gravitational Mode	F_G F_I	$F_V \approx F_G \approx F_I$	$0.4 \leq H\left(\frac{g}{\nu^2}\right)^{1/3} \leq 1.2$	$R_{IG} \cong$ *not defined*	$\Omega_{IG} = \left(\frac{g}{H}\right)^{1/2}$
Inertial Mode	F_I	$F_I \approx F_V \gg F_G$	$H\left(\frac{g}{\nu^2}\right)^{1/3} \geq 1.2$	$R_I \cong \left(\frac{\nu a_1^4}{Q}\right)^{1/3}$	$\Omega_G = \left(\frac{Q^4}{\nu a_1^{10}}\right)^{1/3}$

1. Viscous Regimes: Mound of the falling fluid is quite high because of several intact coiling periods. This is due to having low falling height and high viscosities.
2. Gravitational Regimes: Falling fluid mound remains low and disappears within one or two coiling periods for greater falling height and/or lower viscosities.
3. Inertial Regimes: Shorter coiling period delays an individual coil to coalesce completely with its predecessor coil.

The falling height and the coiling radius remained the most important factors to describe the liquid rope coiling, however nozzle diameter and flow rate have always been considered as constant parameters. G. Warnes and R. Woodstock explained the rate of coiling (v) as a function of falling liquid height (h) [67]. The coiling frequency had been observed more with an increase in the fall height at the constant flow rate and temperature. It was concluded that

coiling would only occur if the falling liquid would attain sufficient terminal velocity because of its viscosity. Thereby, coiling will not start at zero height.

Later some extensive experimental study of the coiling patterns has been conducted, when a viscous fluid flowed onto a moving surface at different ranges of falling height. Chiu demonstrated the different theory about the coiling behaviours within the three different regimes, based on the new parameter of the speed belt (U_0) at different values of falling height (H). Eleven silicone liquid rope coiling patterns were introduced, namely, steady, meanders, double meanders, sidekicks, coiling, double coiling, figure-of-eight, double-eight, braiding, slanted loops, and w-patterns, as shown in the Figure (2.10) [68].

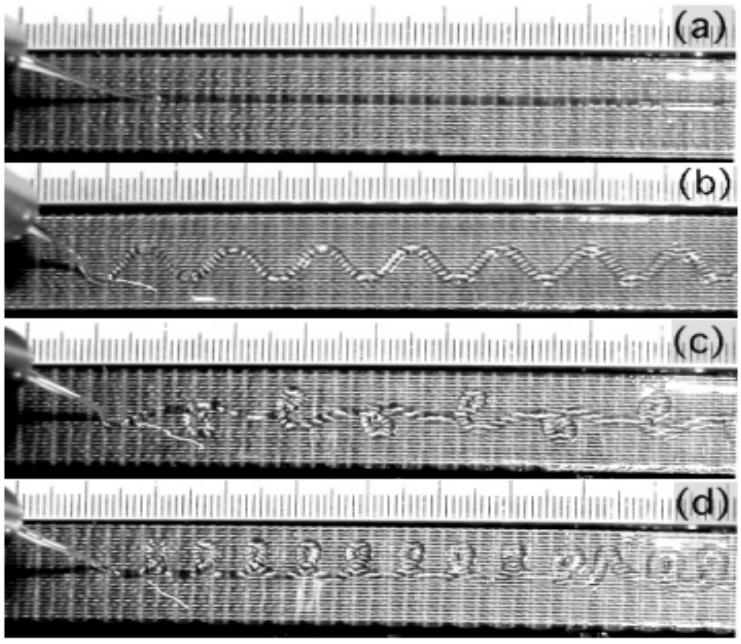

Figure 2.10: The illustration of the states of falling liquid on the belt. The nozzle is on the left and the belt move from left to right. The internal reinforcing mesh of the semi-transparent belt is visible, but the surface of the belt is smooth. The scale is in mm. (a) The steady state. (b) The meandering state. (c) The figure eight scale. (d) The translated coiling state [68].

Tian demonstrated similar Liquid Rope Coiling experiments on high viscosity moisture cured silicone to create silicone foam by additive manufacturing. The dimensions of the coiling patterns were explained on the basic effects of four parameters, Height (H), Flow Rate (Q),

Nozzle Size (D), and Travelling speed (U_0). The coiling patterns were defined as, Steady, Meandering, Figure-of-8, Coiling, and Side Kicks. They were studied on the variation on the two independent variables (Height, H and Travelling Speed, (U_0), while holding the value of the other two independent variables (Nozzle Size, D and Flow Rate, Q) as constant.

However, effects with respective to the other independent variables (Nozzle Size, D and Flow Rate, Q) would still need to be studied in detail. Travelling Speed (U_0) considered the most in parameter in controlling the loops by reducing its value. Thereby, there is no information regarding the multiple loops as one of the possibilities.

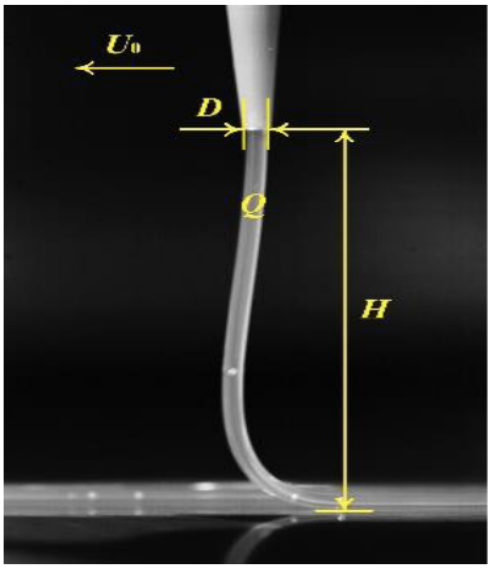

Figure 2.11: The illustration of the falling liquid on the stationary surface. The nozzle is moving right to left with the travelling speed ($\boldsymbol{U_0}$) at the specific height (H). The diameter of the falling liquid is denoted by D with the deposition rate of Q [69].

The literature review demonstrated that the coiling frequency has always been controlled to obtain stable coiling. The transformation of the coiling has been substantially examined over different ranges of the falling height. However, there is a lack of information regarding the coiling transformation related to important parameters including different ranges of the flow rate, print speed and nozzle diameter.

On the contrary, Travelling Speed (U_0) was considered as insignificant parameter in the printing experiments of "Viscous Thread Instability" (VTI) by Lipton, as shown in the Figure (2.11) [69]. Different patterns of coiling effects were induced by modifying deposition parameters as, material flow rate (Q), movement of the print head (P_s), spacing between the path movement (P_w), and layer height (P_h). The study highlighted the production of the complex interconnected structures using VTI technique. These structures have been only constraints to 'Alternate loops' and 'Translated coils' with the controlled printing parameters. Combination of deposition rate (Q), nozzle height (P_h), and spacing between strands (P_w), were considered the favourable parameters for controlling the alternating loops and translating coils, as shown in the Figure (2.12) [69].

Figure 2.12: The demonstration of the Viscous Thread Instability (VTI) by Lipton. The patterns are obtained with the moving nozzle over the print bed with the increased flow rate. This can induce patterns such as meanders (left side), translated coil (middle), and alternating coil (right side) [69].

In summary, the literature in Liquid Rope Coiling indicated that its mechanism has been well established. There are several relevant contributions investigating the relevant aspects of key variables and the possible patterns obtained when printing lines or layers. However, there is a clear lack in the literature regarding other variables relevant to enable the advancement of a technology that could be useful in producing parts with controlled firmness or porosity by exploring SWAN.

2.6 Automotive In-seat Cushion

Paste Additive Manufacturing is still in its infancy to produce an automotive seat cushioning. Profound knowledge is essential, concerning the printing technique and cushioning properties, to model an automotive cushion as accurately as possible. The target of the present section is to give an overview of the mechanical attributes of three customized cushions. Advancements of 3D printing technologies have significantly transformed the potential ways in the domain of manufacturing. For the automotive industry, these advances have opened doors to manufacture newer, safer, lighter, and lower cost-efficient products. The main purpose for adopting this technology is to provide repeatability, accuracy, and interchangeability in the manufacturing of ergonomic products. One of them is an automotive cushion or padding which can be challenging product today.

However, no single cushion material could meet alone the needs of all consumers due to the complexity of function embedded on a seat (comfort, safety, heat/ventilation, air bags, etc.) Many of these factors are interrelated; some factors are attributed to the manufacturing of cushions while others are related the customer needs. Factors that are affecting the comfort would include pressure distribution, efficiency, stability, firmness, moisture, and heat accumulation, and more. Factors that determine the functionality which are mostly related to the material such as density, energy absorption, elasticity, thickness, biocompatibility, flammability, appearance, and so on [70]. Rise in various legislative and industry initiatives regarding, safety, sustainability, and eco-friendly, propels automotive industry to use 3D Printing because of its single-step production.

Springs and rubberized hair were the earliest vehicle seat padding material. The latex foam cushions were, initially, installed in London's buses during 1930s. These foams were considered as the comfort yardstick as compared to former materials. Later that decade, Latex seating was adapted to passenger cars and continually used until the 1960s. Around the same time, polyurethane foam (slab-stock foam) became the mainstream padding material and

replaced latex because of its easier and consistent production process. Another reason was its lower cost.

Over the time, the primary focus was the PU production due its complex polymer chemistry. Polyurethanes are also known as reaction polymers, including epoxies, phenolic, and unsaturated polyesters. Initially, the first flexible PU foam had been manufactured using cast aluminum molding heated in a hot air oven. This hot PU foam production reduced the manufacturing time and material wastage (cutting and gluing) in the production of PU Slab-stock foam. Progressively, the development of cold PU foam offered more advantages over hot PU foam in terms of higher support factor, better flammability resistance and most importantly – its longer resiliency.

The force-deflection for latex high-density foam is 80 kg/m^3 and for PU lower density foam it is 48kg/m^3. One of the superior advantages over latex that PU form is their resilience property even beyond 50% deflection. As a leading member of wide-ranging and highly diverse polymer family, polyurethanes have various structural forms and types. It can either be thermosetting polymer or thermoplastic polymer, thus they are considered in the class of reaction polymers [6].

2.7 Humanoid Soft Robots

Soft robotics deals with the construction of robots with highly compliant materials, which can mimic the behavior of living tissues. Robots with entirely soft bodies have tremendous potential. However, it is very difficult to design manually and control soft robotics with their low mechanical impedance. Currently, hard bodied robots have dominated this field while harnessing the new material for robots is still in its infancy.

Movement may be defined as the act or ability of an entity that move itself from one place to the other. Muscular and flexible soft structure of a living being features the extraordinary versatility and multifunctionality of natural organisms. Such capabilities have inspired robotic engineers to mimic the deformability in bio-inspired soft robots. To achieve this, the design of bio-inspired soft robots must be the perfect blend of sensing, active and passive movements, and control.

Soft robots must have ability of safe human-interaction that exhibits global compliance and robust material interfacing devices. The researchers presented the varied ways to develop human-friendly robots that could be used for physical human-machine interaction. For example, the McKibben hand for grasp assistance, and Rubberwear for robotics arms used on robotic arms which is used for industrial automation [71]

The advances of soft robotics have rapidly gained interest over past few decades. Devising new bio-inspired robotics can bridge the gap between the conventional robots and living beings. This leads to many applications not only in human-interaction but also in health care, locomotion strategies, and disaster relief. However, soft bio-inspired robots remain challenging because of their material, designing, and system integration. Researchers claimed two main objectives should be achieved to produce versatile functional soft robots [72].

1. Replacing hardware modular systems with fully integrated material design that conveys these functionalities.
2. Replacing hard and rigid materials with soft materials which are compatible physically, such as, elastomers, gels, and fluids.

[72] It is hard to address the challenge of conventional approaches without understanding the unique chemical properties of soft materials. Compared to hard surfaced robots, soft robots are composed of flexible material such as gel, elastomers and biological material that exhibit similar rheological and elastic properties to soft matter that found naturally.

2.7.1 **Material Selection**

This is an essential consideration for soft robotic components. The material must exhibit elastic and viscoelastic properties to adapt the mechanical versality and multifunctionality of the soft robots. The myriad issues have been raised in other articles regarding the material of soft robotics. Typical materials which are used in soft robots include urethanes, hydrogel, silicone elastomers, and hydraulic fluids.

Elastomers are highly desirable for this application since they facile broad properties within themselves. These compliant materials are, thereby considered as soft active materials in healthcare in terms of compatibility and safe biological interactions.

Conventionally, robots were constructed with the metals or hard plastics, having an elastic module of $10^9 – 10^{12}$ Pa, whereas most material in living beings, such as, skin, fat tissues, and muscle tissues have

a module of $10^2 – 10^9$ Pa [73]. The nature of the soft robots' tissue must hold a load over a large area for longer time, with low deformation. This conformal nature of soft robotic material could be easily related to the natural tissues that tend to deform elastically when a force is applied without causing damage.

Soft materials found in both biology and soft robotics are viscoelastic. Viscoelasticity is the property of the materials that describes viscous as well as elastic characteristics under impact or stress. Whereas elasticity is usually the result of bond stretching along the planes of ordered structures. Viscosity is the result of molecular or atomic diffusion inside the amorphous structure. Soft robotic tissue can be best described in their storage and loss modules, which represents elastic portion and viscous portion, respectively. In contrast, purely elastic materials do not dissipate energy when a load is applied then removed, such as, steel, bone, and wood. Important features of viscoelastic materials include, stress-strain behavior, high cycle loading, high elastic resilience, high fracture abrasion property, aids in the desired actuation capabilities of robots.

To achieve the full potential of soft robotics numerous key challenges are needed to be addressed. The core challenges revolve around the understanding of the structure property relations of Line printing property and soft robotics' structure.

This thesis will present the comparative performance of four tissue model materials based prepared using SWAN. These materials were prepared based on the experimentation of "Line Printing". As it will be presented, the experiment results have been used to statistically demonstrate that the presented analysis results are of high accuracy.

Chapter 3
Material and Methods

3.1 Material

The raw material used in this thesis was clear, one-part acetoxy cure silicone cure elastomer (DAP® 100% Silicone Rubber Window, Door & Siding Sealant, DAP Product Inc., Baltimore, Maryland) with 0.96 g/cm^3 density. Silicone rubber is the base polymer of the uncured raw material, the composition also includes hydrotreated middle distillate (10-25%), amorphous silica (2.5 – 10%) and silanetriol, methyl-triaceta (2.5-10%).

Silicone gets cured on the exposure to the atmospheric moisture at room temperature with the release of the acetic acid molecules. It can be cured at any working temperature ranges from -35^{0}F to 140^{0}F. The curing was carried out at room temperature in this thesis. It creates a skin over time of 5 to 10 minutes. Its tack free time is 10 to 20 minutes, and the cure handling time is 24 hours. Cured silicone is durable, weatherproof, and flexible to withstand expansion and contraction without cracking. It is also mildew and mold resistant. It is a continuous use product at any service temperature ranges from -40^{0}F to 350^{0}F.

3.2 SWAM Demonstration

SWAM is the abbreviation of the experimental setup called “Silicone Whipping Additive Manufacturing”. SWAM was assembled and based on an open source of Fused Deposition Modeling (FDM) machine (Ultimaker 2+) without using the base heater and filament extrusion. The closed framed extruder (Discov3ry) is used to extrude silicone. The Discovery Complete Extruder is considered as the superlative option for SWAM with FDM printers. It would help in expanding the printing processes in terms of material ranges from silicone to plastic to biomaterial to nano material easily using design slicing software Ultimaker Cura. The extruder is a very easily configurated system, portable, compatible with diverse and customed material. The Ultimaker Cura software was used to derive the G-code files based on the CAD models. Herein, the extruder is pre-integrated and closed framed system. Figure (3.1) demonstrates the apparatus of the Silicone Whipping Additive Manufacturing (SWAN) and its components.

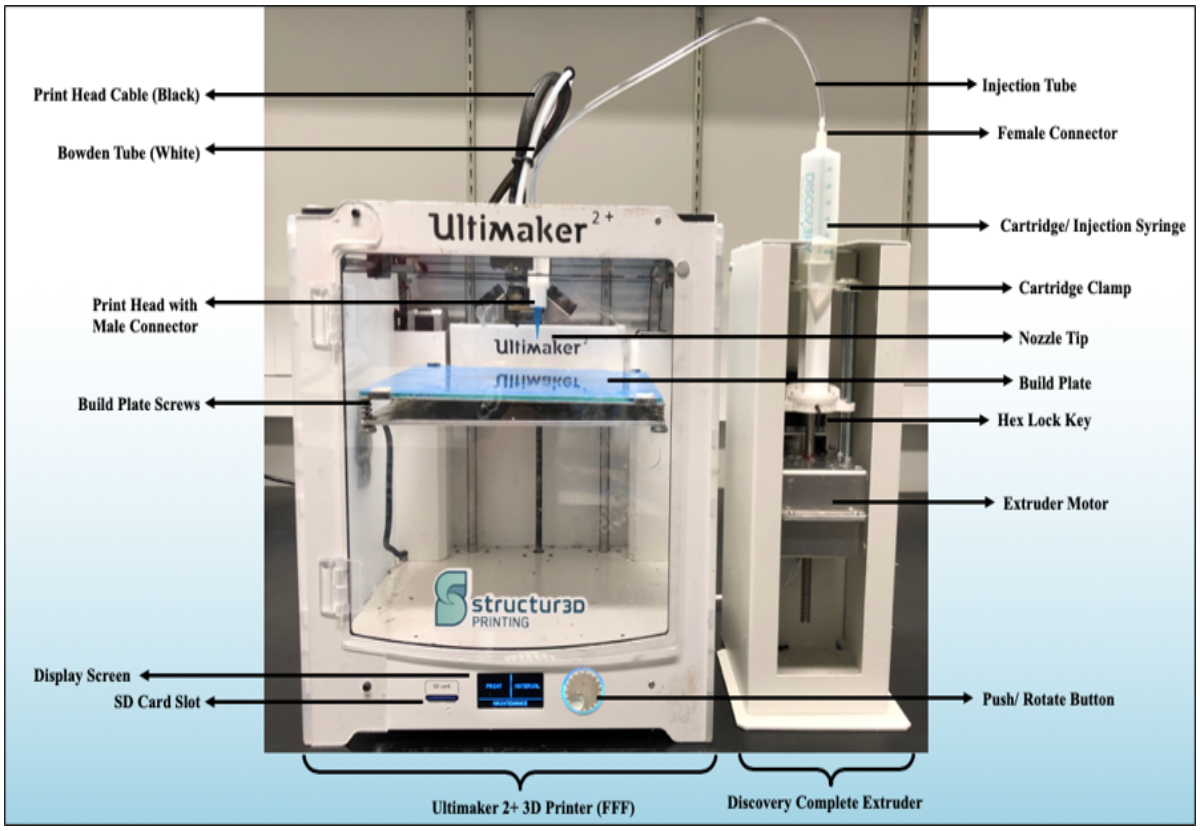

Figure 3.1: Silicone Whipping Additive Manufacturing (SWAM) and its components. (Source: By Gurkamal Saggu)

3.2.1 Installation and Set Up Strategy

When it comes to assuring a high-quality printing, certain strategy was followed to avoid involuntary external effects. It begins with filling of the syringe with silicone by using caulking gun. The filled syringe must not contain any air bubble in it because air bubbles would lead to defects known as breaks while printing. Next, the female connector is fastened to the tip of the syringe and tubing firmly as to prevent minuscule and multiple bubbles. Furthermore, the caulking gun could be used to compress silicone within the syringe to achieve most of the way through the tubing. It would save the extra time on purging later. Finally, slide the end of the tubing through the print head and slide the male connector onto the end of the tubing that can be affixed by pushing it back into the recess of the print head.

The distance should be levelled properly between build plate and nozzle tip. The levelling is done by sliding thin paper or card between nozzle tip and build plate. The level is also maintained by rotating the screws that are located on the four corners of the build plate or the printing bed.

In addition, the fast purging would be done before starting the printing. It would help in building the nominal pressure on the plunger of the syringe for the smooth oozing. It is always controlled with the aid of G-code.

3.3 Line Printing

Line Printing is defined as the novel free-forming technique for reproducing single segment of desired feed onto the printed bed using different form of fabricating methods. In simple words, Line Printing is the printing of the line segment by laying down the desired material onto the printed bed. This technique is also referred to as filament printing, filament fabrication, or line prototyping, as shown in the Figure (3.2). This technique is helpful to study:

1. The behavior of the material deposition during the process of fabrication.
2. The transformation of the material deposition during printing.
3. The characteristics of the deposited segment, to relate the bulk form characteristics.

Figure 3.2: Line Printing over the black surface. (Source: By Gurkamal Saggu)

Reproducing line printing is a relevant step toward understanding the repeatability of patterns during the printing process. Several process variables are involved, and all variables affect the resulting fabrication. In this investigation, only the significant and easy to control parameters were considered depending on the controls available in the Cura software. The process parameters investigated in this

study include Nozzle diameter (D), Gap distance (H), Flow rate (Q), and Print speed (V) and the value were chosen accordingly given in the Table (3.1).

The Line Printing was performed by using various nozzle sizes. The nozzles can be identified by their colors or diameters, as usually done by the nozzle suppliers. The smallest nozzle was the clear nozzle (0.2mm), it made very laborious for the extruder to extrude filament since it required additional pressure and reversive G-code implementations. Due to its smallest area of cross section, it led to very thin filament and distant deposition with slow printing.

The largest size was the olive nozzle (1.60 mm), it required more volume and thicker material deposition to extrude to a point that it failed to participate as a parametric constraint. However, it can be considered as an upper bound in design of experiment (DOE) at one point. Red nozzle (0.25 mm) has manifested more looping effects of very fine filament while testing through line printing. The other nozzles also showed fine and looped deposition. Hence, the highest set value was chosen as grey nozzle (1.19 mm) and the lowest as blue nozzle (0.41 mm) with the median parametric value of green nozzle (0.84 mm).

Furthermore, the Gap Distance has been described as the displacement between the print bed and the nozzle diameter. It is measured in millimeters. Gap distance has been considered to demonstrate the falling effect of the silicone filament onto the printed bed. The effect of the falling silicone rope coiling has been particularly carried out in the gravitational mode. Therefore, Gap Distance was a function of gravity forming different patterns of Line Printing when it varied from 25 mm to 75 mm.

Print Speed is the third important factor which has been taken in mm/s. Print speed has been defined as the movement or the minimum displacement of the print head per unit second on a horizontal direction (X or Y). Its choice was made considering the need to deliver a certain amount of flow. It ranged from 5 mm/s to 10 mm/s.

Flow Rate was the last parametric constraints, it has the unit of ml/min. It may be defined as the volumetric feed through the nozzle diameter per unit time. It was controlled by the device motor to extrude the desired volume of silicone feed through the cartridge, given in appendix A. The flow rate ranged from 0.4ml/min to 0.8 ml/min.

Table 3. 1: Printing Parameters with high and low values.

Printing Parameters	Low	High
Nozzle Diameter (mm)	0.41	1.19
Gap Distance (mm)	25	75
Nozzle Speed (mm/s)	5	10
Flow Rate (ml/min)	0.4	0.8

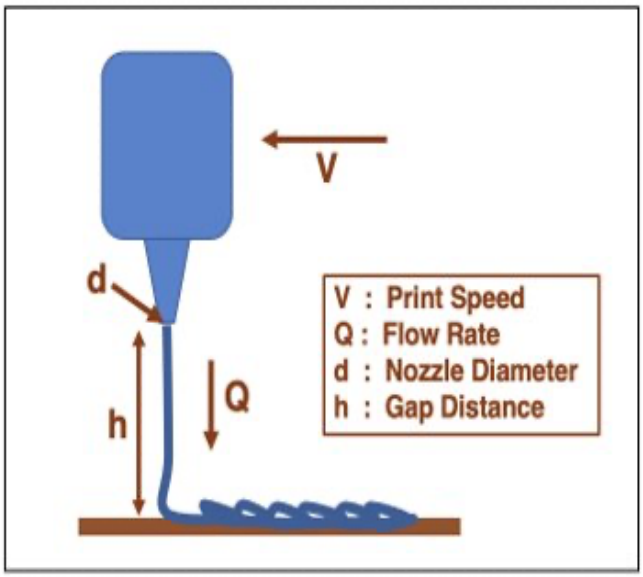

Figure 3.3: Line Printing Process with four mentioned printing parameters. (Source: By Gurkamal Saggu)

The response parameters of Line Printing are measured and analysed to understand the behavior, transformation, and characteristics of material deposition as shown in the Figure (3.3). The response parameters are also called Filament Responses or Filament Characteristics. It is represented as F_x, where F represents Filament, and its subscript x represents a specific characteristic. The Filament characteristics (F_x), such as Filament Diameter (F_D), Filament Deposited Height (F_H), Filament Line Width (F_{LW}), Filament Loop Counts (F_L), Filament Multiple Loops (F_{ML}), and Filament Single Loops (F_{SL}), are described in the later section of this chapter.

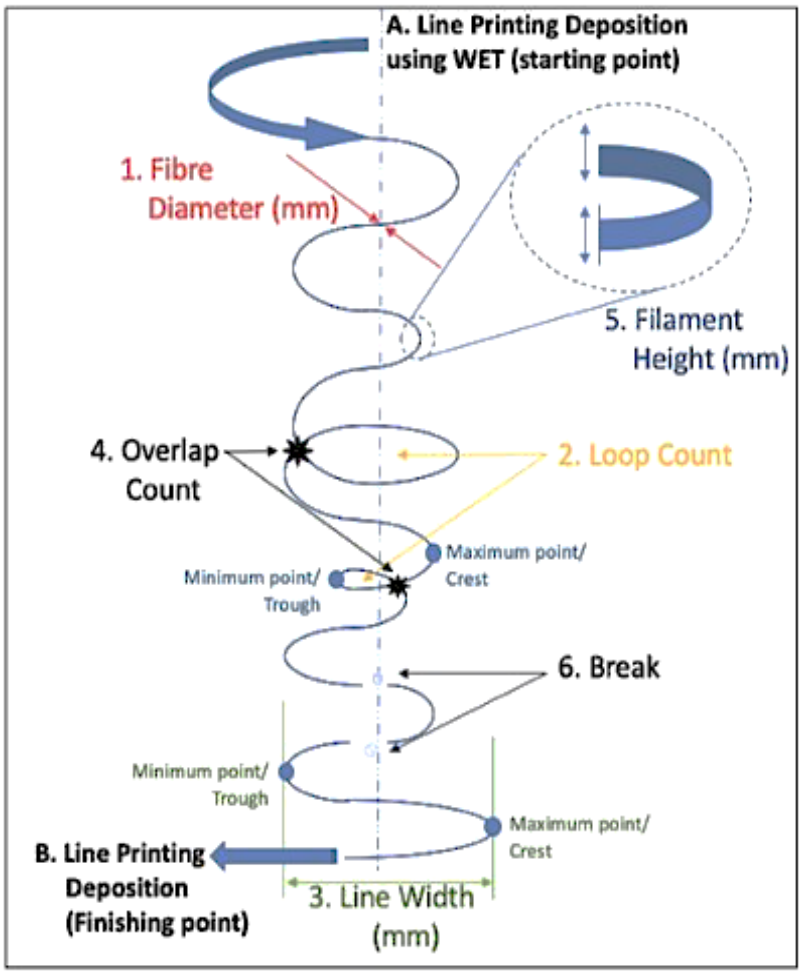

Figure 3.4: Line Printing Deposition starts from the top and finishes at the bottom. (Source: By Gurkamal Saggu)

3.4 Method

3.4.1 Choice of Experiments and Statistical Analysis

For the analysis of Line Printing, the statistical analysis was done by software R Code. The method of statistical analysis is called Design of Experiments (DOE). DOE aided to evaluate the relationship between parametric factors and Line Printing characteristics. Ample data graphics and analysis could be attained since the software is more user friendly.

The Line Printing characteristics can be easily studied in detail. In respective to four parametric factors, the line printing DOE was generated as two level and four factors, 2^4. Each Line Printing was fabricated three times, thus having 3 replicates of each run along with 12 center points. Therefore, the total number

of experiments were constituted as 60 runs. All the 60 runs were fabricated over the black sheet for facile documentation process by analysis image generated with digital photography. The Line Printing was fabricated in three segments as shown in the Figure (3.5).

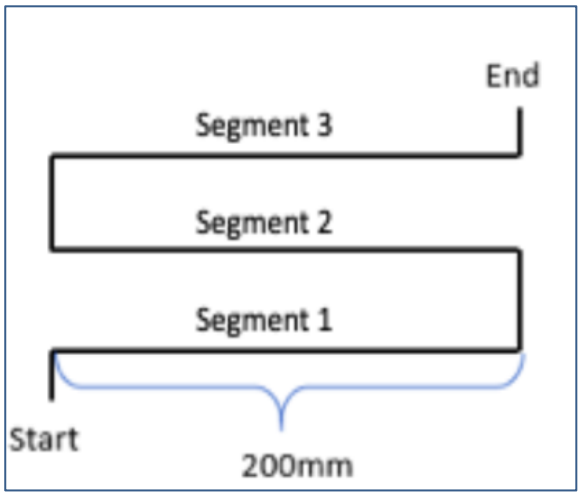

Figure 3.5: Line Printing Pattern. (Source: By Gurkamal Saggu)

Herein, ANOVA justifies the relation of variance to obtain the regression model of each line characteristics with respect to four desired factors. Significant results were achieved by setting alpha value to 10% that can be able to highlight notable effects of the factors. Sometimes, inherent variability is bound to happen which is associated with experiment. This uncontrollable error factor is called noise. If the value of the factor is close to this error bound, then the regression model must be examined thoroughly by omitting it. However, if the value of the factors is already absorbed into the noise, then it is considered as a non- significant factor. It is noted that the assumptions over the combined factor effect are not relatively like the single factor effect.

Only one set of center point is defined to ensure the model's linearity. The confidence level is set to 95% to make good assumption to create a bulk printing model (explained in 3.4.3 section). This confidence level would generate all the data effects under one roof. The curvature factor was not significant before, thus required more testing for the omittance of pointless factors' effects. Whereas it was found to be significant in testing filament line width and loops.

Further, exclusion has been done in respect to the p-value. The p-value supposed to be lower than 0.05 since the confidence level was 95%. Both p-value and F-value measures the desired magnitude as they are inversely related to each other. The higher the F-value, the factor is more relevant while having the

lower p-value and vice versa. Lack of fit has remained due to the proximity of the center points to each other, thus, showing lesser variability.

To conclude, the regression equations of each line printing characteristics and main effects analysis has been established in 4.2 section of the thesis.

3.4.2 Documentation Process

The Surface morphology was analysed by producing the filament fabrication over the black sheet. All the 60 runs were printed for facile documentation process, into qualitative and quantitative data as follows.

3.4.2.1 Qualitative Data: Imaging

A digital photographic Canon EOS 1500D DSLR camera with 18 – 55 mm and 55 – 250 mm Dual Lens was used for imaging of the samples. The camera was mounted on a copy scanner. The criteria that determine the image quality of the printed samples include the number of elements, such as, the type of the printed sheets, printing material used and its appearances, camera lens' mount, how wide the lens' diaphragm opens, and lens' faces, must be adjusted.

The camera was mounted onto the vertical camera frame at the set height distance of 12". The filament printed samples are placed below perpendicularly to the optical axis of the camera's lens, to reproduce equally flat image in the final photograph without distortion. Light source must be right above the camera to avoid the shadow or false reflection of the printed filament. Therefore, the flash of the camera was set to 'OFF' to toe shiny appearance of the filament in the image, due to its reflection.

For sharp and clearer image, manual focussing was adjusted to the zoom of EF 30 cm at $8^{0}15^{"}$ wide angle of the outer lens. It was set using the focus lock buttons located along the circumference of the forward portion of the lens.

3.4.2.2 Quantitative Data: Measurements.

The Line Printing characteristics are also called Filament responses or Filament Characteristics. It is represented as $F_{x,}$ where F is the filament, and its subscript x represents a characteristic. The ImageJ Software was used to analyze the digital images and to catalogue the measurements of all the characteristics except Filament Height deposition (F_H), which is measured by micro screw gauge.

1. Filament Diameter, F_D

The filament diameter is the filament thickness after deposited on the printing bed as shown in the Figure (3.6). It is represented as F_D and measured in mm. A random number generator is used to acquire a set of 10 random numbers from 0-15, as in accordance with the relative length (15 cm) of the measuring ruler. Using the ImageJ software, measurements in the image was set to 1 mm as demarcations on the ruler. The F_D measurement was taken at the right angle to the filament. In some cases.

- If the multiple filaments are sharing the same point on the measuring ruler, then the upper most filament is used to compute the F_D.
- If the upper most filament is vague due to the layered overlapping, the filament immediately below was used for the record.

The final recorded data is the average of the 10 measurements.

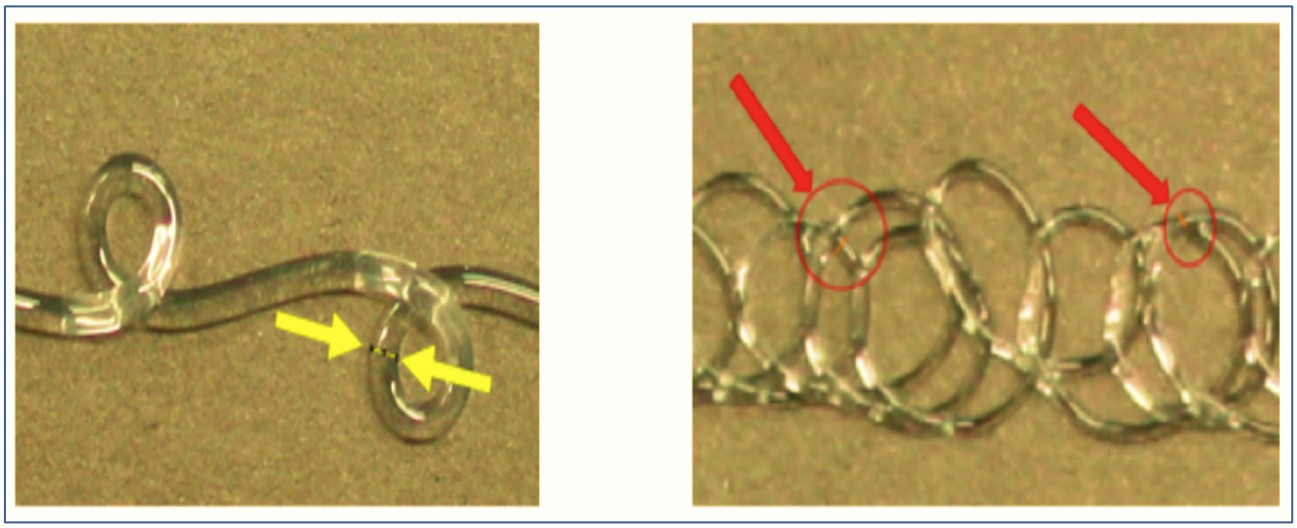

Figure 3.6: Measurements of Filament Diameter, $\boldsymbol{F_D}$. (Source: By Gurkamal Saggu)

2. Filament Deposited Height, F_H.

The Filament Deposited Height $(\boldsymbol{F_H})$ is the second response which is also measured in mm. It is the only response which was measured by using micro screw gauge as shown in the Figure (3.7). The measurement point is taken in two ways.

- At the overlapping point of the filament, $\overline{\boldsymbol{F}}_{\boldsymbol{H,op}}$.

- At the non-overlapping point of the filament, $\bar{F}_{H,nop}$.

The height of the deposition seemed to be same at all the points of the segment. The end points of the segment are considered for measurement, as fact, that the amount of the filament is greater at the starting of the filament than to its ending.

The average height (F_H) is measured by excluding the width of the paper (0.223 mm) from the final measurement of the printed samples. Mathematically,

$$F_H = \left\{\left(\frac{\bar{F}_{H,op} + \bar{F}_{H,nop}}{2}\right) - (\dot{W}_p)\right\}$$

Where, F_H is the average filament deposition height, $\bar{F}_{H,op}$ is the mean average width measured on the overlapping points of the filament, $\bar{F}_{H,nop}$ is the mean average width measured on the non-overlapping points of the filament, and $\dot{W}_p$ is the width of the printed sheet (black).

It should be noted that the thickness width proofs more amount of deposited silicone i.e., more volume has been deposited.

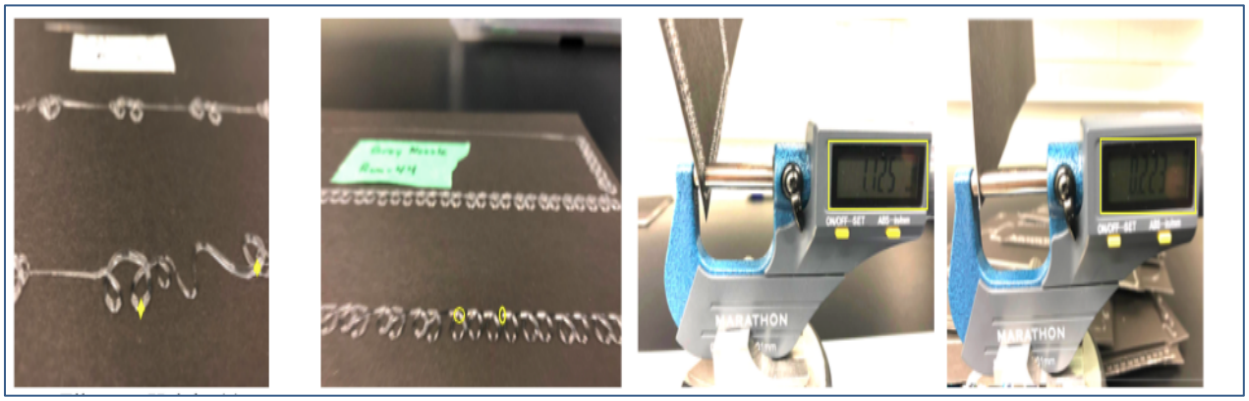

Figure 3.7: Measurements of Filament Deposition Height, F_H. (Source: By Gurkamal Saggu)

3. Filament Line Width, F_{LW}.

The linear spreading of the filament can be noted by measuring filament line width, between the maximum and minimum horizontal distance of the spread filament on the sheet. It is denoted by F_{LW}. and measured in mm.

Setting of the scale is done, in the units of mm converted from pixels, in ImageJ software. Due to the filament transformation from steady state to looped state (discussed in 4.4 section), the F_{LW} measurements is done in the following steps, as shown in the Figure (3.8):

- If the filament is deposited in a wave or having more wavy fabrication other than a smaller number of loops, the point of measurement is considered as the horizontal distance between the crest (maximum point) and the trough (minimum point) of the filament.
- If there is a loop near the point of measurement, the width of the loop is taken instead of the actual point of measurement. The width is evaluated from point of loop's intersection to its circumference.
- When the measurement point falls nearby smaller and larger loop, the larger loop will be considered to evaluate F_{LW}..
- When the measurement point lies on the region of clustered loops, the largest loop of the region is considered for F_{LW}..

The line width is calculated as average of the 10 random numbers which are chosen as 10 measurement points. Large deviation of the line width defines the large spreading or large divergence from the mean point.

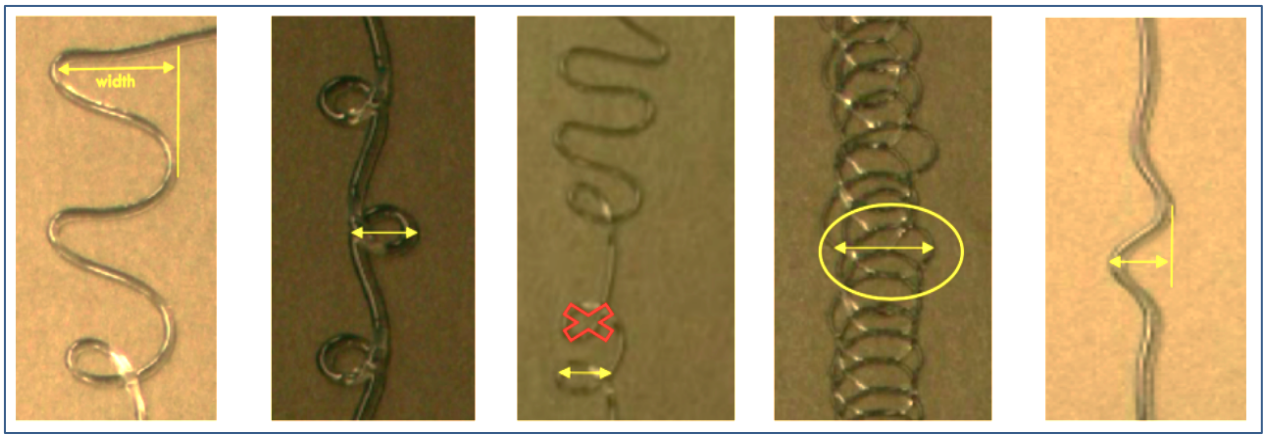

Figure 3.8: Measurements of Filament Line Width, $\boldsymbol{F_{LW}}$. (Source: By Gurkamal Saggu)

4. Filament Loop Counts, F_L.

Filament loop counts (F_L) are measured as the similar length of the opted ruler (15 cm). Measurement of the F_L is as follow, as shown in the Figure (3.9): -

- It can be counted as the total spiral forms fabricated on the sheet to the similar ruler's length (15 cm).
- If there is a presence of break, due to any external factor, then measurement distance is shortened that causes no effect on the loop density.
- When the loop is partially inside the measurement distance, then the half loop should be taken into consideration as full loop.

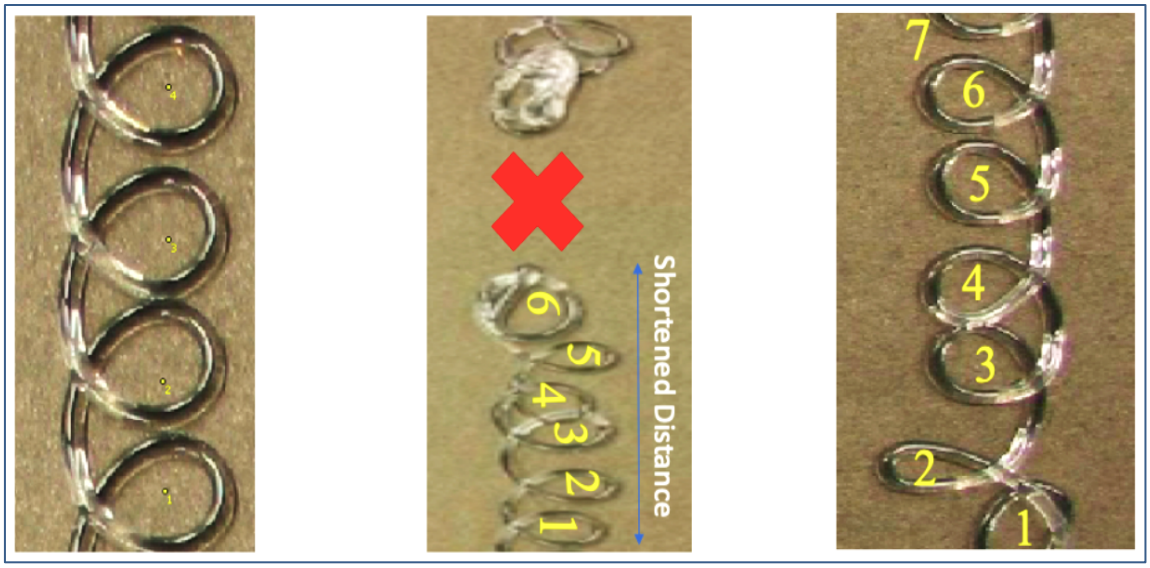

Figure 3.9: Measurements of Filament Loop Counts, F_L. (Source: By Gurkamal Saggu)

5. Filament Multiple Loops, F_{ML}.

Multiple loops can be observed, as shown in Figure (3.10), as double looping or as nested looping. Measurement of F_{ML} is quite difficult, so the multipoint tool is the efficient way of counting multiple loops in ImageJ software. Multiple loops are counted as the similar length of the measuring ruler (15 cm). Magnification tool can be used for the clearer image while marking the multipoint on the image.

6. Filament Single Loops, F_{SL}.

F_{SL} measurement is comparatively easier to record than the measurement of F_{ML}. It can be calculated manually or using multipoint tool in ImageJ software on the stretch of 15 cm ruler's length, as shown in the Figure (3.10).

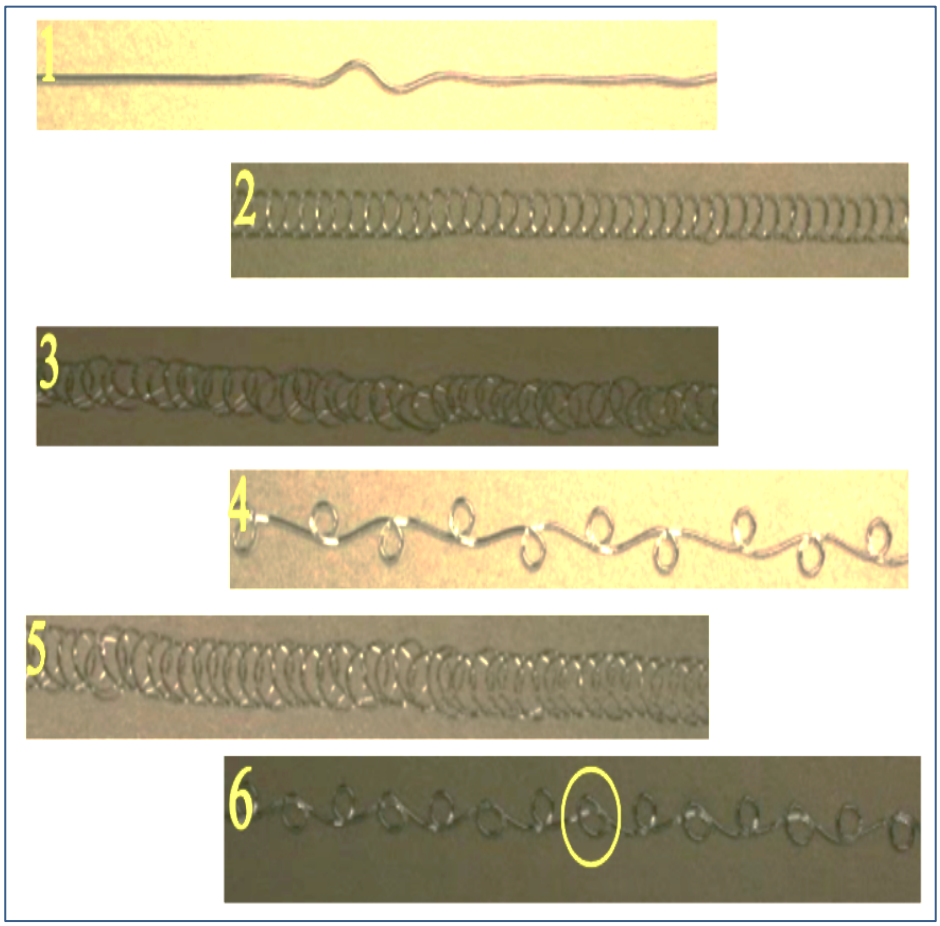

Figure 3.10: Measurements of Filament Single $\boldsymbol{F_{SL}}$ and Multiple Loops, $\boldsymbol{F_{ML}}$.(Source: By Gurkamal Saggu)

3.4.3 Bulk Printing

Bulk Printing is the production of a 3D object, as opposed to the 1D Line printing or a 2D Surface Printing. The successful attestation of Line Printing analysis here encouraged the exploration of bulk printing for technical applications. The selection of runs for Bulk Printing was finalized based on the line characteristics in the correlation with basic formulae of density. Three runs were selected to yield

lower density in-seat silicone cushion with variable firmness. Furthermore, four runs were selected to print two of fat-like and muscle-like tissues each with variable stiffness.

Attaining lower mass would be possible if focused on the lower fiber diameter and deposition height since there is less volume of material deposited (described in chapter 4). This would narrow the choice to choose smaller diameter nozzle, larger gap distance with the lower value flow rate. Another option of choosing Line Printing is through controlled multiple loops with slower print speed and larger gap distance. This would lead to produce more clustered looping, practically fabricating higher mass density. Area and loops fabrication are more subjective terms to yield voluminous form. More line width of the deposited filament would be controlled by the lower value of nozzle diameter. In addition, lower print speed and larger flow rate can print and add more loops to the surface area. The intersection arms of the loops provide more stable volume height to withstand various existing forces when applying, inducing the study on stress-strain behavior of the bulk silicone samples.

Thus, loops orientation plays vital role in examining the strength and stability when subjected to create bulk print. Figure (3.11) illustrates the Printed Bulk Model of Silicone using SWAM apparatus.

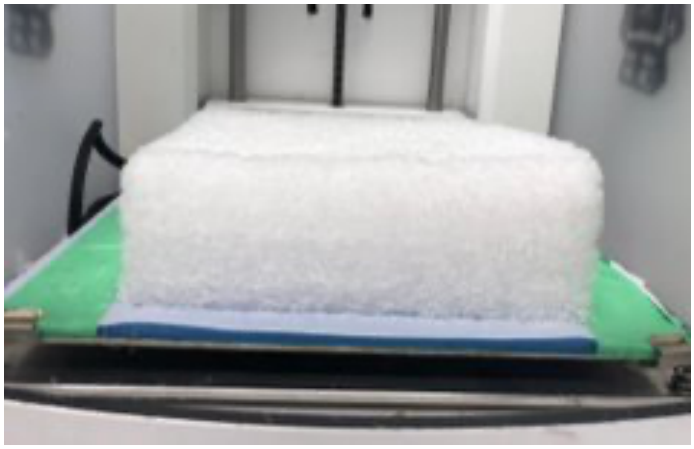

Figure 3.11: Printed Bulk Model of Silicone. (Source: By Gurkamal Saggu)

The results of Line Printing analysis encouraged the explanation regarding the Bulk Printing. Precise line pattern and its improvements would be able to yield low density product with variable firmness. Selection of the run was finalized based on the line filament characteristics with the help of basic formulae of density. Examining all the parameters thoroughly, run 7 and run 9 was chosen to print the large silicone block as in-seat car cushions. The loops are similar and consistent in run 7, while run 9

shows the consistent multiple over looping. Filament diameter and height are recorded as lesser value in both run when compared to most of the runs. Whereas, run 9 is having more value than run 7 in accordance with filament diameter and height. Therefore, they are the good indication of printing lines per layer along with layered height. However, line width of run 7 is more than run 9. It is considered relatively insignificant since it adds nothing in value to printer configurations. The line printings were chosen to produce a lower density model of in-seat car cushion. Therefore, bulk printing would use lesser material to accomplish full model.

3.5 Mechanical Testing

Compression testing is a very common testing method used to establish compressive force or crushing resistance of the material and the ability of the material to recover after the application of the specified compressive force is applied and even maintained at the specified time-period. Compression tests are used to determine under-weight behavior of the material, that is, how the materials respond after being under a heavy object for a given time. The maximum stress over the period under progressive load or constant load was determined. Compression testing is often done to break or limit. Break detection can be tested based on the type of material when testing is done at the break. All the bulk printings have undergone the force-deflection measurement according to ASTM D3574. There were seven bulk printings that were prepared. The force deflection has been done up to the 50 % of the original height of the bulk printings. The height of three parts prepared using Bulk Printing to evaluate their performance as in-car seat cushions were 57.67 mm, 51.01 mm, and 51.04 mm respectively. The average height of those blocks was 53.24 mm.

Chapter 4
Results and Discussions

4.1 Introduction

This chapter presents the results and the relationship between the printing parameters and the filament morphology using a free-forming filament technique called "Line Printing" based on 'Liquid Rope Coiling' effects. It also reports the experiments covering statistical analysis of printing parameters' effects during line printing. The characteristics of the printed filament were measured and studies in detail. In addition to the Line Printing study, this chapter also presents the method used to print block using the Bulk Printing. This is followed by the characterization and measurement of the properties of such block. The research objective was to develop a technology to enable advanced manufacturing of soft materials with controlled firmness, which in turn could be used to tailor performance of seat components or tissue for soft robotics.

The method of line printed characterized the filaments based on 6 attributes:

- Filament Diameter (F_D)
- Filament Deposition Height (F_H)
- Filament Line Width (F_{LW})
- Filament Single Loops (F_{SL})
- Filament Loop Counts (F_{LP})
- Filament Multiple Loops (F_{ML})

Experimental values alongside the mean and standard deviation values of Six Filament characteristics ($\boldsymbol{F_D, F_{LP}, F_{LW}, F_H, F_{ML}, and\ F_{SL}}$) with respect to four SWAM parameters ($\boldsymbol{x_D, x_H, x_S, and\ x_Q}$) in terms of coded values ranges from -1 (lower value) to 1 (higher value) are shown in the Table 4.1-4.3.

Filaments with different characteristics were prepared by changing the printing parameters at two levels each: nozzles speed (5 and 10 mm/s), flow rate (0.4 and 0.8 mL/min), gap distance (25 and 75 mm), and nozzle diameter (0.41 and 1.19 mm).

The experimental results for each filament characteristics are shown in shown in Figures 4.1-4.6.

Table 4. 1: Experimental values of Six Filament characteristics ($F_D, F_{LP}, F_{LW}, F_H, F_{ML}, and\ F_{SL}$) with respect to four SWAM parameters ($x_D, x_H, x_S, and\ x_Q$) in terms of coded values ranges from -1 (lower value) to 1 (higher value).

Run	x_D	x_H	x_S	x_Q	F_D	F_{LP}	F_{LW}	F_H	F_{ML}	F_{SL}
1	−1	−1	−1	−1	0.613	4.16	5.31	0.7	128.33	63.33
2	1	−1	−1	−1	1.354	0	1.57	1.32	0	0
3	−1	1	−1	−1	0.532	3.93	7.75	0.83	180	0
4	1	1	−1	−1	0.794	0.84	6.68	1.21	1.67	12.67
5	−1	−1	1	−1	0.622	1.61	4.32	0.68	4.33	28
6	1	−1	1	−1	1.013	0	1.19	1.03	0	0
7	−1	1	1	−1	0.511	2.04	7.09	0.57	40	31.67
8	1	1	1	−1	0.741	0.19	3.7	0.99	0	5
9	−1	−1	−1	1	0.607	6.42	5.36	1.09	290	0
10	1	−1	−1	1	1.360	0.78	5.07	1.85	0	11
11	−1	1	−1	1	0.549	7.67	6.45	1.17	296.67	0
12	1	1	−1	1	1.002	1.64	7.07	1.3	0	17.33
13	−1	−1	1	1	0.588	3.18	5.77	0.93	93.33	40
14	1	−1	1	1	1.403	0	2.22	1.28	0	0
15	−1	1	1	1	0.559	4.49	6.47	0.65	195	0
16	1	1	1	1	1.010	0.6	5.57	1.35	0	9.33
17	0	0	0	0	0.901	1.04	5.92	0.96	5.33	13.67
18	0	0	0	0	0.879	1.21	6.36	0.96	0.67	18
19	0	0	0	0	0.902	1.08	5.71	0.94	7.67	13
20	0	0	0	0	0.877	1.12	5.73	1.03	5.33	13.33

21	**−1**	**−1**	**−1**	**−1**	**0.610**	**4.24**	**4.33**	**0.61**	**118.33**	**65**
22	**1**	**−1**	**−1**	**−1**	**1.366**	**0**	**2.18**	**1.29**	**0**	**0**
23	**−1**	**1**	**−1**	**−1**	**0.554**	**4.02**	**7.92**	**0.84**	**210**	**0**
24	**1**	**1**	**−1**	**−1**	**0.898**	**0.82**	**6.32**	**1**	**2.33**	**12.33**
25	**−1**	**−1**	**1**	**−1**	**0.627**	**1.62**	**4.52**	**0.69**	**3**	**28.67**
26	**1**	**−1**	**1**	**−1**	**1.007**	**0**	**1.13**	**1.05**	**0**	**0**
27	**−1**	**1**	**1**	**−1**	**0.524**	**2.02**	**7.09**	**0.59**	**33.33**	**28.33**
28	**1**	**1**	**1**	**−1**	**0.832**	**0.16**	**3.72**	**0.97**	**0**	**3.33**
29	**−1**	**−1**	**−1**	**1**	**0.598**	**6.31**	**5.45**	**1.02**	**293.33**	**0**
30	**1**	**−1**	**−1**	**1**	**1.355**	**0.78**	**5.27**	**1.78**	**0**	**11.67**
31	**−1**	**1**	**−1**	**1**	**0.566**	**8.11**	**6.43**	**1.18**	**310**	**0**
32	**1**	**1**	**−1**	**1**	**0.988**	**1.62**	**7.4**	**1.39**	**1.67**	**18**
33	**−1**	**−1**	**1**	**1**	**0.589**	**3.2**	**5.61**	**0.86**	**85**	**45**
34	**1**	**−1**	**1**	**1**	**1.418**	**0**	**2.26**	**1.3**	**0**	**0**
35	**−1**	**1**	**1**	**1**	**0.572**	**4.53**	**6.57**	**0.62**	**198.33**	**0**
36	**1**	**1**	**1**	**1**	**1.077**	**0.4**	**7.09**	**1.11**	**0**	**6.33**
37	**0**	**0**	**0**	**0**	**0.888**	**1.09**	**5.88**	**1.01**	**2.67**	**15.33**
38	**0**	**0**	**0**	**0**	**0.901**	**1.11**	**6.63**	**1.01**	**1.33**	**17**
39	**0**	**0**	**0**	**0**	**0.877**	**1.11**	**6.03**	**1.16**	**2.67**	**16.33**
40	**0**	**0**	**0**	**0**	**0.882**	**1.11**	**6.29**	**1.04**	**2.67**	**15.67**
41	**−1**	**−1**	**−1**	**−1**	**0.613**	**4.2**	**4.39**	**0.71**	**121.67**	**63.33**
42	**1**	**−1**	**−1**	**−1**	**1.382**	**0**	**2.49**	**1.29**	**0**	**0**
43	**−1**	**1**	**−1**	**−1**	**0.536**	**4**	**7.74**	**0.83**	**179.33**	**0**
44	**1**	**1**	**−1**	**−1**	**0.909**	**0.87**	**6.63**	**1.12**	**3.33**	**12.67**

45	**−1**	**−1**	**1**	**−1**	**0.620**	**1.62**	**4.33**	**0.74**	**7.33**	**23.33**
46	**1**	**−1**	**1**	**−1**	**1.052**	**0**	**1.18**	**1.23**	**0**	**0**
47	**−1**	**1**	**1**	**−1**	**0.528**	**2**	**7.12**	**0.53**	**43.33**	**31.67**
48	**1**	**1**	**1**	**−1**	**0.856**	**0.09**	**3.65**	**1.1**	**0**	**2.33**
49	**−1**	**−1**	**−1**	**1**	**0.653**	**6.38**	**5.55**	**1.07**	**268.33**	**0**
50	**1**	**−1**	**−1**	**1**	**1.379**	**0.78**	**5.39**	**1.93**	**0**	**11.67**
51	**−1**	**1**	**−1**	**1**	**0.553**	**8.27**	**6.42**	**1.11**	**270**	**0**
52	**1**	**1**	**−1**	**1**	**1.034**	**1.62**	**7.31**	**1.35**	**1**	**17.67**
53	**−1**	**−1**	**1**	**1**	**0.594**	**3.2**	**5.65**	**0.77**	**90**	**45**
54	**1**	**−1**	**1**	**1**	**1.421**	**0**	**2.32**	**1.22**	**0**	**0**
55	**−1**	**1**	**1**	**1**	**0.573**	**4.62**	**6.56**	**0.64**	**211.67**	**0**
56	**1**	**1**	**1**	**1**	**1.082**	**0.53**	**6.9**	**1**	**0**	**8**
57	**0**	**0**	**0**	**0**	**0.903**	**1.09**	**5.79**	**0.99**	**4.33**	**13.67**
58	**0**	**0**	**0**	**0**	**0.890**	**1.16**	**6.27**	**1**	**0.67**	**18**
59	**0**	**0**	**0**	**0**	**0.893**	**1.16**	**6.21**	**1.04**	**0**	**18.67**
60	**0**	**0**	**0**	**0**	**0.900**	**1.16**	**5.94**	**1.12**	**0**	**18**

Table 4. 2 : Experimental mean and standard deviation values of first three Filament characteristics (F_D, F_{LP}, F_{LW}) with respect to four SWAM parameters $(x_D, x_H, x_S, and\ x_Q)$ in terms of coded values ranges from -1 (lower value) to 1 (higher value).

Run	x_D	x_H	x_S	x_Q	F_{D_mean}	F_{D_sd}	F_{LP_mean}	F_{LP_sd}	F_{LW_mean}	F_{LW_sd}
1	1	−1	1	1	1.414	0.010	0.000	0.000	2.267	0.050
2	1	−1	−1	−1	1.367	0.014	0.000	0.000	2.080	0.468
3	1	−1	−1	1	1.365	0.013	0.780	0.000	5.243	0.162
4	1	1	1	1	1.056	0.040	0.510	0.101	6.520	0.828
5	1	−1	1	−1	1.024	0.024	0.000	0.000	1.167	0.032
6	1	1	−1	1	1.008	0.024	1.627	0.012	7.260	0.171
7	0	0	0	0	0.891	0.010	1.130	0.059	6.063	0.287
8	1	1	−1	−1	0.867	0.063	0.843	0.025	6.543	0.195
9	1	1	1	−1	0.810	0.061	0.147	0.051	3.690	0.036
10	−1	−1	1	−1	0.623	0.004	1.617	0.006	4.390	0.113
11	−1	−1	−1	1	0.619	0.030	6.370	0.056	5.453	0.095
12	−1	−1	−1	−1	0.612	0.002	4.200	0.040	4.677	0.549
13	−1	−1	1	1	0.590	0.003	3.193	0.012	5.677	0.083
14	−1	1	1	1	0.568	0.008	4.547	0.067	6.533	0.055
15	−1	1	−1	1	0.556	0.009	8.017	0.311	6.433	0.015
16	−1	1	−1	−1	0.541	0.012	3.983	0.047	7.803	0.101
17	−1	1	1	−1	0.521	0.009	2.020	0.020	7.100	0.017

Table 4. 3: Experimental mean and standard deviation values of first three Filament characteristics $(\boldsymbol{F_H, F_{ML}, F_{SL}})$ with respect to four SWAM parameters $(\boldsymbol{x_D, x_H, x_S, and\ x_Q})$ in terms of coded values ranges from -1 (lower value) to 1 (higher value).

$\boldsymbol{Run}$	$\boldsymbol{x_D}$	$\boldsymbol{x_H}$	$\boldsymbol{x_S}$	$\boldsymbol{x_Q}$	$\boldsymbol{F_{H\_}mean}$	$\boldsymbol{F_{H\_}sd}$	$\boldsymbol{F_{ML\_}mean}$	$\boldsymbol{F_{ML\_}sd}$	$\boldsymbol{F_{SL\_}mean}$	$\boldsymbol{F_{SL\_}sd}$
1	**1**	**−1**	**1**	**1**	**1.267**	**0.042**	**0.000**	**0.000**	**0.000**	**0.000**
2	**1**	**−1**	**−1**	**−1**	**1.300**	**0.017**	**0.000**	**0.000**	**0.000**	**0.000**
3	**1**	**−1**	**−1**	**1**	**1.853**	**0.075**	**0.000**	**0.000**	**11.447**	**0.387**
4	**1**	**1**	**1**	**1**	**1.153**	**0.179**	**0.000**	**0.000**	**7.887**	**1.503**
5	**1**	**−1**	**1**	**−1**	**1.103**	**0.110**	**0.000**	**0.000**	**0.000**	**0.000**
6	**1**	**1**	**−1**	**1**	**1.347**	**0.045**	**0.890**	**0.840**	**17.667**	**0.335**
7	**0**	**0**	**0**	**0**	**1.022**	**0.064**	**2.778**	**2.446**	**15.889**	**2.081**
8	**1**	**1**	**−1**	**−1**	**1.110**	**0.105**	**2.443**	**0.836**	**12.557**	**0.196**
9	**1**	**1**	**1**	**−1**	**1.020**	**0.070**	**0.000**	**0.000**	**3.553**	**1.349**
10	**−1**	**−1**	**1**	**−1**	**0.703**	**0.032**	**4.887**	**2.218**	**26.667**	**2.909**
11	**−1**	**−1**	**−1**	**1**	**1.060**	**0.036**	**283.887**	**13.575**	**0.000**	**0.000**
12	**−1**	**−1**	**−1**	**−1**	**0.673**	**0.055**	**122.777**	**5.091**	**63.887**	**0.964**
13	**−1**	**−1**	**1**	**1**	**0.853**	**0.080**	**89.443**	**4.193**	**43.333**	**2.887**
14	**−1**	**1**	**1**	**1**	**0.637**	**0.015**	**201.667**	**8.822**	**0.000**	**0.000**
15	**−1**	**1**	**−1**	**1**	**1.153**	**0.038**	**292.223**	**20.367**	**0.000**	**0.000**
16	**−1**	**1**	**−1**	**−1**	**0.833**	**0.006**	**189.777**	**17.517**	**0.000**	**0.000**
17	**−1**	**1**	**1**	**−1**	**0.563**	**0.031**	**38.887**	**5.092**	**30.557**	**1.928**

4.2 Statistical Analysis

Software R Code was used to analyze the results to determine the printing parameters effect on the line printing. To be precise, the effect of printing parameters' may be defined as the change in the line printing characteristics produced by a change in the printing parametric levels. They are frequently called 'Main Effects', as they refer to experiments' primary factors of interest.

The codified mathematical model applied for 2^k - Factorial design was:

$$F_{Char} = \beta_0 + \beta_D x_D + \beta_H x_H + \beta_S x_S + \beta_Q x_Q + \beta_D\beta_H x_D x_H + \beta_D\beta_S x_D x_S + \beta_D\beta_Q x_D x_Q + \beta_H\beta_S x_H x_S + \beta_H\beta_Q x_H x_Q + \beta_S\beta_Q x_S x_Q$$

Where β_0 is the global mean and β_i are the other regression coefficients. On substituting the β_i coefficients in above equation by their values respectively, the Filament Characteristics (F_{Char}) : Filament Diameter (F_D) , Filament Deposition Height (F_H), Filament Line Width (F_{LW}), and Filament Single Loops (F_{SL}) decreases, while, Filament Loop Counts (F_{LP}), and Filament Multiple Loops (F_{ML}) increases.

4.2.1 Analysis of the Filament Diameter.

The regression coefficients table for the Filament diameter (F_D) is shown in Table (4.4).

Table 4. 4: Regression table of Filament diameter ($\boldsymbol{F_D}$) showing regression coefficients for the coded variables, factor effects, and p-values.

Regression Variables	Regression Coefficients	Effects	p-Value
β_0	$+0.855$	$+1.71$	2.2×10^{-16}
β_D	$+0.268$	$+0.54$	2.2×10^{-16}
β_H	-0.106	-0.21	2.16×10^{-15}
β_Q	$+0.051$	$+0.10$	2.29×10^{-6}
$\beta_{D:H}$	-0.073	-0.15	4.08×10^{-10}

$\beta_{D:Q}$	$+0.046$	$+0.09$	1.27×10^{-5}
L.O.F (p-value)	0.1716		
R^2	0.9491		
Adjusted R^2	0.9444		

The model obtained in table (4.4) adequately represents experimental data with a determination coefficient (R^2) of 94.91%. Three printing parameters, Nozzle Diameter, Gap Distance, and Flow Rate, show a significant effect on the Filament Diameter (F_D) including two two-way interactions, Nozzle diameter – Gap distance ($D \times H$) and Nozzle diameter – Flow rate ($D \times Q$).

Whereas Print Speed is an insignificant factor showing negligible effect. Out of three factors, Nozzle diameter shows the strongest effect followed by Gap Distance then Flow Rate.

Deducing the main polynomial equation of the Filament Diameter (F_D), the regression equation can be obtained in the coded form as:

$$F_D = 0.855 + 0.268\, x_D - 0.106\, x_H + 0.051\, x_Q - 0.073\, x_D x_H + 0.046\, x_D x_Q$$

The regression equation of the Filament Diameter (F_D) in the uncoded form is:

$$F_D = 0.345 + 0.711\, D + 0.00176\, H - 0.217\, Q - 0.0075\, D \times H + 0.59\, D \times Q$$

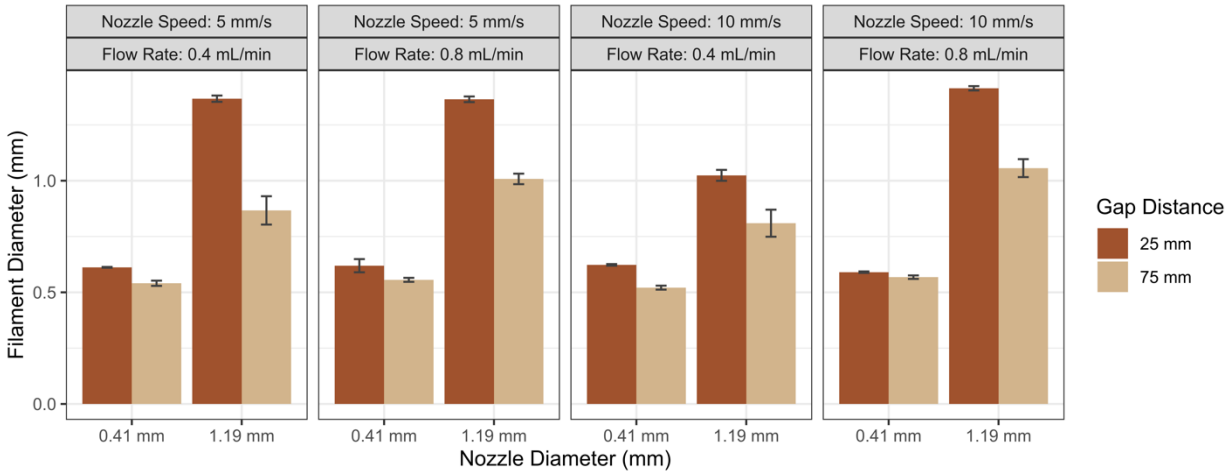

Figure 4.1: Bar plots showing the behavior of the variables Nozzle Diameter ($\boldsymbol{D}$), Gap Distance ($\boldsymbol{H}$), Nozzle Speed ($\boldsymbol{S}$), and Flow rate ($\boldsymbol{Q}$) on the average Filament diameter ($F_{\boldsymbol{D}}$).

The bar plots in Figure (4.1) show that Filament Diameter (F_D) decreases with an increase in Gap Distance. It is due to the filament entanglement based on gravity force. However, the Filament Diameter (F_D) increases with the increase in Nozzle Diameter owing to the area of the cross-section of the nozzle. For lower Nozzle Diameter, Filament Diameter (F_D) is quite similar irrespective of Print Speed, Flow Rate, and Gap distance.

For higher Nozzle Diameter, there are quite variations. The Filament Diameter resulted out to be the least value at a lower Flow Rate, and higher Nozzle Speed, and Nozzle Siameter. Whereas, for higher Nozzle Diameter, and higher Gap Distance, the Filament Fiameter decreases with the increase in Flow Rate irrespective of change in the value of Print Speed. Since Nozzle Speed has an insignificant effect on the Filament Diameter (F_D).

4.2.2 Analysis of the Filament Loop Density

The regression coefficients table for the Filament Loop Density (F_{LP}) is shown in Table (4.5).

Table 4. 5: Regression table of Filament Loop Density ($\boldsymbol{F_{LP}}$) showing regression coefficients for the coded variables, factor effects, and p-values.

Regression Variables	Regression Coefficients	Effects	p-Value
$\boldsymbol{\beta_I}$	$+2.12$	$+4.24$	$< 2.2 \times 10^{-16}$
$\boldsymbol{\beta_D}$	-1.88	-3.76	$< 2.2 \times 10^{-16}$
$\boldsymbol{\beta_S}$	-0.86	-1.72	1.74×10^{-11}
$\boldsymbol{\beta_Q}$	$+0.76$	$+1.52$	6.01×10^{-10}
$\boldsymbol{\beta_{D:S}}$	$+0.54$	$+1.08$	2.33×10^{-6}
$\boldsymbol{\beta_{D:Q}}$	-0.52	-1.04	3.79×10^{-6}
L.O.F (p-value)	5.12×10^{-11}		
$\boldsymbol{R^2}$	0.9064		
Adjusted $\boldsymbol{R^2}$	0.8978		

The determination coefficient (R^2) of the obtained model is 90.64% accurate. Nozzle Diameter, Print Speed, and Flow Rate are the three significant printing factors affecting the Filament Loop Density (F_{LP}). Gap Distance is the only insignificant factor.

Filament Loop Density (F_{LP}) is highly affected by Nozzle Diameter followed by Print Speed, and then Flow Rate. Nozzle Diameter and Print Speed shows the negative effect over Loop Density, whereas Flow Rate displays positive effect.

There are also two two-way interaction effects, one is positive effect of both Nozzle Diameter and Print Speed, and other is negative effect of both Nozzle Diameter and Flow Rate.

The main coded polynomial regression equation of the Filament Loop density (F_{LP}) is as follows:

$$F_{LP} = 2.12 - 1.88\,x_D - 0.86\,x_S + 0.76\,x_Q + 0.54\,x_D x_S - 0.52\,x_D.x_Q$$

The regression equation of the Filament Loop Density (F_{LP}) in the uncoded form is:

$$F_{LP} = 6.40 - 4.97\ D - 0.784\ S + 9.136\ Q + 0.55\ D \times S - 6.67\ D \times Q$$

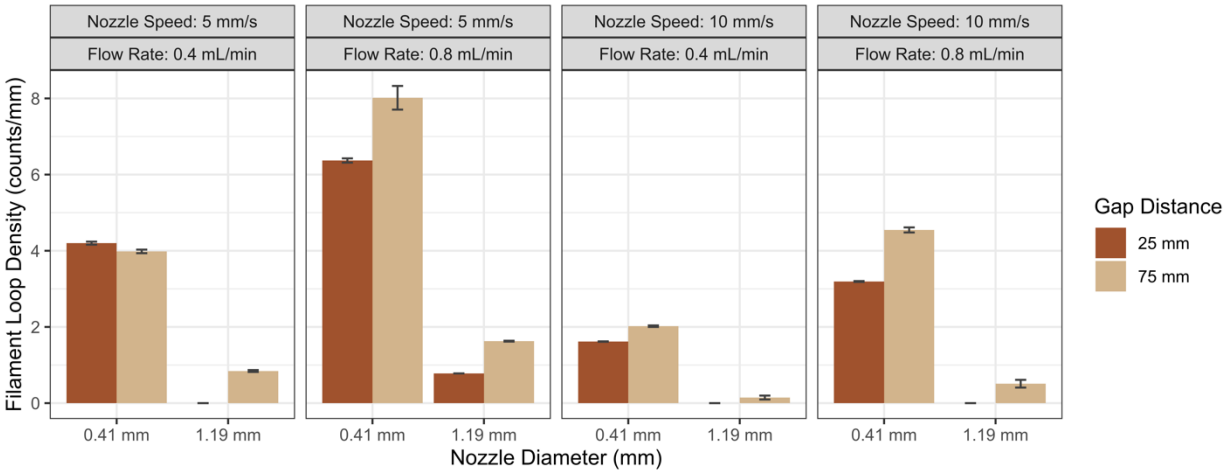

Figure 4.2: Bar plots showing the behavior of the variables Nozzle Diameter ($\boldsymbol{D}$), Gap Distance ($\boldsymbol{H}$), Nozzle Speed ($\boldsymbol{S}$), and Flow Rate ($\boldsymbol{Q}$) on the average Filament Loop Density ($\boldsymbol{F_{LP}}$).

Bar plots in Figure (4.2) depict that Filament Loop Density (F_{LP}) seems to be higher for lower Nozzle Diameter, irrespective of the value for other printing parameters, than higher Nozzle Diameter. Increasing Print Speed would lower the Filament Loop Density.

In fact, the filament tends to be deposited as a straight line when Print Speed is increased. Loop density (F_{LP}) tends to increase when smaller Nozzle Diameter is used at higher Flow Rate, however there would be lesser number of loops counts when Nozzle Diameter is increased. In this case, the Gap Distance is showing an insignificant effect.

4.2.3 Analysis of the Filament Line Width

The regression coefficients table for the Filament Line Width (F_{LW}) is shown in Table (4.6).

Table 4. 6: Regression table of Filament Line Width ($\mathbf{F_{LW}}$) showing regression coefficients for the coded variables, factor effects, and p-values.

Regression Variables	Regression Coefficients	Effects	p-Value
$\boldsymbol{\beta_I}$	$+5.355$	$+10.71$	$< 2.2 \times 10^{-16}$
$\boldsymbol{\beta_D}$	-0.831	-1.662	3.512×10^{-11}
$\boldsymbol{\beta_H}$	$+1.308$	$+2.616$	$< 2.2 \times 10^{-16}$
$\boldsymbol{\beta_S}$	-0.509	-1.018	4.50×10^{-6}
$\boldsymbol{\beta_Q}$	$+0.496$	$+0.992$	7.21×10^{-6}
$\boldsymbol{\beta_{D:H}}$	$+0.349$	$+0.698$	0.00094
$\boldsymbol{\beta_{D:S}}$	-0.426	-0.852	7.96×10^{-5}
$\boldsymbol{\beta_{D:Q}}$	$+0.480$	$+0.960$	1.25×10^{-5}
L.O.F (p-value)	3.48×10^{-15}		
$\boldsymbol{R^2}$	0.8699		
Adjusted $\boldsymbol{R^2}$	0.8524		

The determination coefficient of the analyzed Filament Line Width is 86.99% accurate. Filament Line width is only the characteristics which is affected by all the four printing parameters. Positive effect is shown by Gap Distance (H) and Flow rate (Q), whereas negative effect is shown by Nozzle Diameter (D) and Print Speed (S). Gap Distance (H) highly affects Filament Line width followed by Nozzle Diameter (D), and then Print Speed (S) and Flow Rate (Q).

There are three two-way interactions: the interaction Nozzle Diameter – Gap Distance, and the interaction Nozzle Diameter – Flow Rate both have positive effect; however, the interaction Nozzle Diameter – Print Speed has negative effect.

The main coded polynomial regression equation of the Filament Line Width (F_{LW}) is as follows:

$$F_{LW} = 5.355 - 0.831\,x_D + 1.308\,x_H - 0.509\,x_S + 0.496\,x_Q + 0.349\,x_D x_H - 0.426\,x_D x_S + 0.48\,x_D x_Q$$

The regression equation of the Filament Line Width (F_{LW}) in the uncoded form is:

$$F_{LW} = 6.251 - 4.341\,D + 0.0235\,H + 0.146\,S - 2.443\,Q + 0.036\,D \times H - 0.437\,D \times S + 6.154\,D \times Q$$

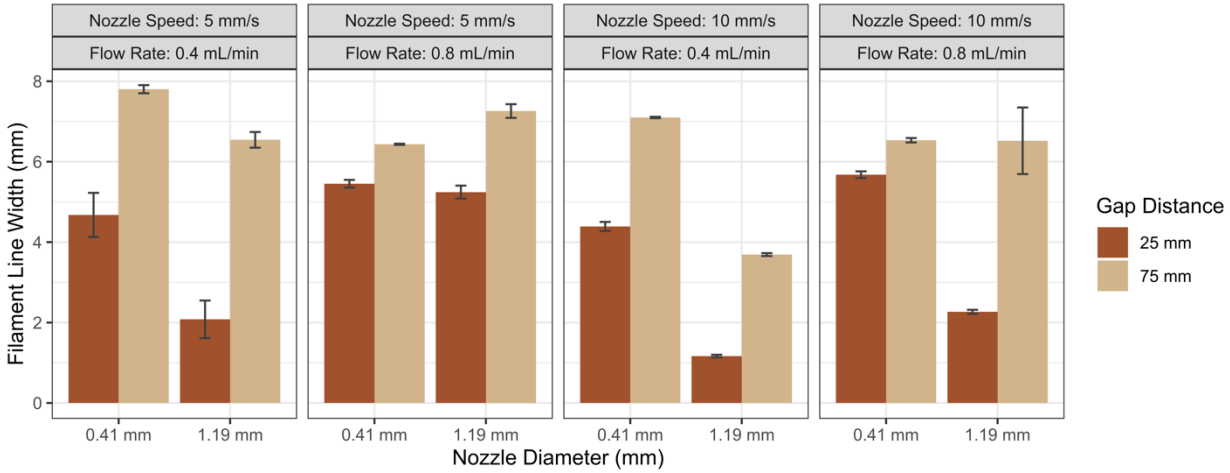

Figure 4.3: Bar plots showing the behavior of the variables Nozzle Diameter (***D***), Gap Distance (***H***), Nozzle Speed (***S***), and Flow Rate (***Q***) on the average Filament Line Width ($\boldsymbol{F_{LW}}$).

Filament Line Width (F_{LW}) is also known as the Filament Spread over the print bed. The bar plot in Figure (4.3) shows more the Gap Distance, more would be the Filament Line Width (F_{LW}). Filament Line Width (F_{LW}) is decreasing with an increase in Nozzle Diameter except when there is higher Flow Rate, and lower Print Speed.

The highest Filament Line Width can be achieved when all the printing parameters are decreased except increased Gap Distance. The lowest filament spread is caused by the lowering the Flow Rate and Gap Distance with increased Nozzle Diameter and Print Speed.

4.2.4 Analysis of the Filament Deposition Height.

The regression coefficients table for the Filament Deposition Height (F_H) is shown in Table (4.7).

Table 4. 7: Regression table of Filament Deposition Height ($\boldsymbol{F_H}$) showing regression coefficients for the coded variables, factor effects, and p-values.

Regression Variables	Regression Coefficients	Effects	p-Value
$\boldsymbol{\beta_I}$	$+1.036$	$+2.072$	$< 2.2 \times 10^{-16}$
$\boldsymbol{\beta_D}$	$+0.230$	$+0.460$	$< 2.2 \times 10^{-16}$
$\boldsymbol{\beta_H}$	-0.062	-0.124	0.00025
$\boldsymbol{\beta_S}$	-0.127	-0.254	1.125×10^{-10}
$\boldsymbol{\beta_Q}$	$+0.126$	$+0.252$	1.366×10^{-10}
$\boldsymbol{\beta_{S:Q}}$	-0.061	$+0.122$	0.00033
L.O.F (p-value)	2.02×10^{-17}		
$\boldsymbol{R^2}$	0.8708		
Adjusted $\boldsymbol{R^2}$	0.8589		

The analyzed data of Filament Deposition Height (F_H) resulted out the determination coefficient of about 87.08% accuracy. The data shows that all the printing parameters are affecting the Filament Deposition Height (F_H) significantly.

Nozzle Diameter and Flow Rate depicts positive effect than Gap Distance and Print Speed. However, there is only single two-way interaction Print Speed – Flow Rate showing decreased effect over Filament Deposition Heigh.

The main coded polynomial regression equation of the Filament Deposition Height (F_H) is as follows:

$$F_H = 1.036 + 0.23\,x_D - 0.062\,x_H - 0.127\,x_S + 0.126\,x_Q - 0.061\,x_S x_Q$$

The regression equation of the Filament Deposition Height (F_H) in the uncoded form is:

$$F_H = 0.144 + 0.59\,D - 0.0025\,H + 0.022\,S + 1.545\,Q - 0.122\,S \times Q$$

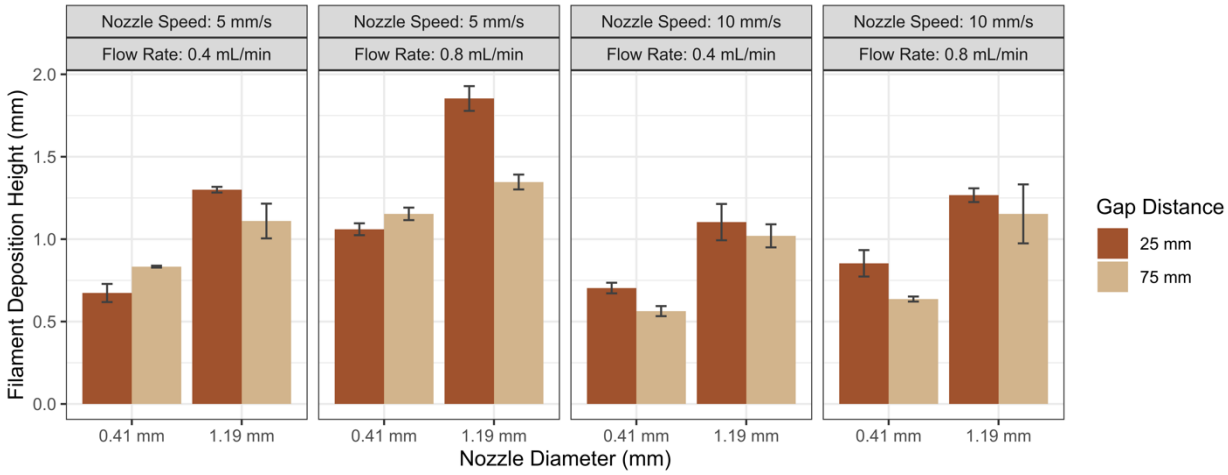

Figure 4.4: Bar plots showing the behavior of the variables Nozzle Diameter ($\boldsymbol{D}$), Gap Distance ($\boldsymbol{H}$), Nozzle Speed ($\boldsymbol{S}$), and Flow Rate ($\boldsymbol{Q}$) on the average Filament Height ($\boldsymbol{F_H}$).

The bar charts in Figure (4.4) depict that Filament Deposition Height increases with the increasing Nozzle diameter with increasing Gap Distance. More the Print Speed, lesser will be the filament deposition. However, more the Flow Rate, more will be the deposition of filament.

The highest Filament Deposition can be achieved at higher Nozzle Diameter, Flow Rate, and lower Nozzle Speed, and Gap Distance. while the lowest deposition of filament's height can be achieved at lower Nozzle Diameter and Flow Rate, and higher Gap Distance and Nozzle Speed.

4.2.5 Analysis of the Filament Multiple Loops.

The regression coefficients table for the Filament Multiple Loops (F_{ML}) is shown in Table (4.8).

Table 4. 8: Regression table of Multiple Loops ($\boldsymbol{F_{ML}}$) showing regression coefficients for the coded variables, factor effects, and p-values.

Regression Variables	Regression Coefficients	Effects	p-value
$\boldsymbol{\beta_I}$	$+61.899$	$+123.798$	$< 2.2 \times 10^{-16}$
$\boldsymbol{\beta_D}$	-76.263	-152.526	$< 2.2 \times 10^{-16}$
$\boldsymbol{\beta_S}$	-34.820	-69.64	8.65×10^{-8}
$\boldsymbol{\beta_Q}$	$+31.834$	$+63.67$	6.10×10^{-7}

$\boldsymbol{\beta_{D:S}}$	$+34.403$	$+68.81$	1.14×10^{-7}
$\boldsymbol{\beta_{D:Q}}$	-32.028	-64.06	5.37×10^{-7}
L.O.F (p-value)	$< 2.2 \times 10^{-16}$		
$\boldsymbol{R^2}$	0.8569		
Adjusted $\boldsymbol{R^2}$	0.8436		

The Filament Multiple Loops (F_{ML}) regression data shows the data determination coefficient (R^2) of about 85.69% correctly. Nozzle Diameter, Print Speed, and Flow Rate affect the Filament Multiple Loops significantly. Nozzle Diameter and Print Speed affect the Filament Multiple Loops negatively while Flow Rate affects it positively. Gap distance has negligible effect over multiple loops. There are two two-way interactions: Filament Multiple Loops are influenced positively by interaction Nozzle Diameter – Print Speed and negatively by interaction of Nozzle Diameter – Flow Rate.

The main coded polynomial regression equation of the Filament Multiple Loops (F_{ML}) is as follows:

$$F_{ML} = 61.9 - 76.26\, x_D - 34.82\, x_S + 31.834\, x_Q + 34.403\, x_D x_S - 32.028\, x_D x_Q$$

The regression equation of the Filament Multiple Loops (F_{ML}) in the uncoded form is:

$$F_{ML} = 241.84 - 213.7\, D - 42.154\, S + 487.82\, Q + 35.28\, D \times S - 410.77\, D \times Q$$

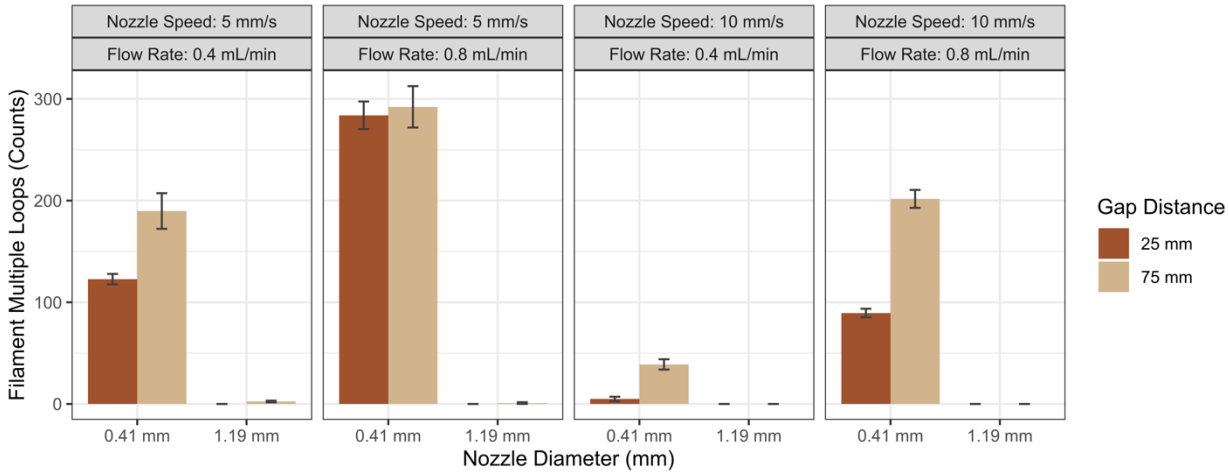

Figure 4.5: Bar plots showing the behavior of the variables Nozzle Diameter ($\boldsymbol{D}$), Gap Distance ($\boldsymbol{H}$), Nozzle Speed ($\boldsymbol{S}$), and Flow Rate ($\boldsymbol{Q}$) on the average Filament Multiple Loops (F_{ML}).

The bar charts in Figure (5) show that Filament Multiple Loops (F_{ML}) cannot be formed by larger Nozzle Diameter (D) irrespective of any other printing parameters, Gap Distance (H), Nozzle Speed (S), and Flow Rate (Q).

Increased Flow Rate (Q) tends to form more multiple loops for lower Print Speed (S) whereas multiple loops' counts are lesser for higher Print Speed (S).

4.2.6 Analysis of the Filament Single Loops.

The regression coefficients table for the Filament Single Loops (F_{SL}) is shown in Table (4.9).

Table 4. 9: Regression table of Filament Single Loops ($\boldsymbol{F_{SL}}$) showing regression coefficients for the coded variables, factor effects, and p-values.

Regression Variables	Regression Coefficients	Effects	p-Value
$\boldsymbol{\beta_I}$	$+14.1$	$+28.2$	3.350×10^{-13}
$\boldsymbol{\beta_D}$	-6.96	-13.92	9.081×10^{-5}
$\boldsymbol{\beta_H}$	-4.56	-9.12	0.007502
$\boldsymbol{\beta_Q}$	-3.56	-7.12	0.0351
$\boldsymbol{\beta_{D:H}}$	$+8.35$	$+16.7$	4.918×10^{-6}
$\boldsymbol{\beta_{D:Q}}$	$+6.17$	$+12.34$	0.000434
L.O.F (p-value)	0.7628453		
$\boldsymbol{R^2}$	0.5649		
Adjusted $\boldsymbol{R^2}$	0.5246		

The determination coefficient (R^2) of Filament Single Loops (F_{SL}) is about 56.49%. This response filament characteristics is negatively affected by all the parameter, Nozzle Diameter, Gap Distance, and Flow Rate, except Print Speed. Both two-way interactions Nozzle Diameter – Gap Distance and Nozzle Diameter – Flow Rate affect single loops positively.

The main coded polynomial regression equation of the Filament Single Loops (F_{SL}) is as follows:

$$F_{SL} = 14.1 - 6.96\,x_D - 4.56\,x_H - 3.56\,x_Q + 8.35\,x_D x_H + 6.17\,x_D x_Q$$

The regression equation of the Filament Single Loops (F_{SL}) in the uncoded form is:

$$F_{SL} = 120.404 - 108.13D - 0.8674H - 81.1Q + 0.856D \times H + 79.103D \times Q$$

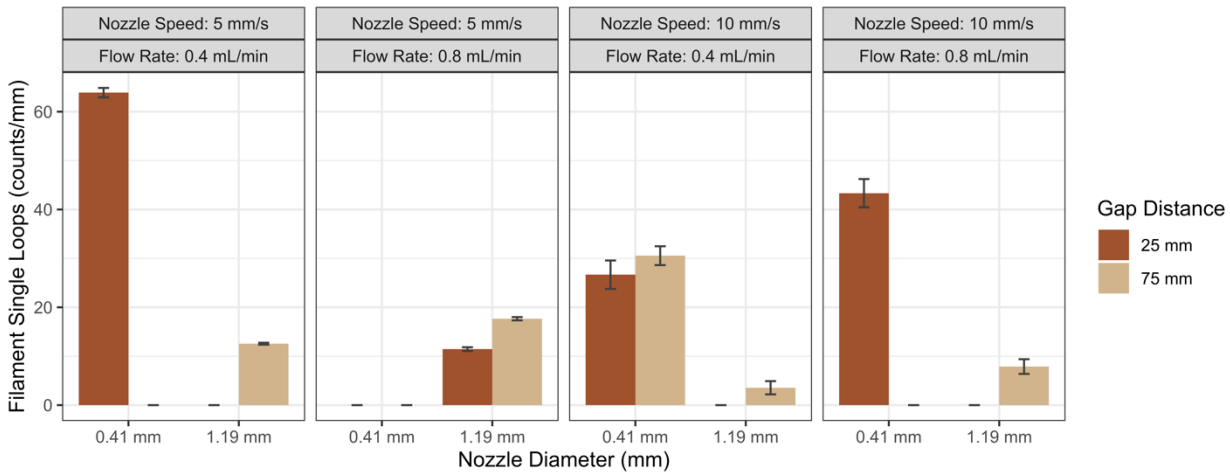

Figure 4.6: Bar plots showing the behavior of the variables Nozzle Diameter ($\boldsymbol{D}$), Gap Distance ($\boldsymbol{H}$), Nozzle Speed ($\boldsymbol{S}$), and Flow Rate ($\boldsymbol{Q}$) on the average Filament Single Loops ($\boldsymbol{F_{SL}}$).

The bar plots in Figure (4.6) depict that single loops cannot be formed by larger Nozzle Diameter and lower Gap Distance irrespective of other two parameters, Nozzle Speed and Flow Rate. But when Gap Distance is increased with increasing Flow Rate and Nozzle Diameter, the filament tends to have single loops. The single loops are the most in the case lower value of printing parameters however when only Gap Distance is increased, single looped filament tend to change its phase to multiple.

4.3 Empirical Relation

Regression analysis was applied to derive the statistical model of the 'Line Printing' to explain the looping effect while fabrication. Due to the existence of the inverse relationship between the flow rate and the print speed, the empirical formula was generated.

This empirical formula can predict the transformation of the depositing filament during 3D printing, from steady to looped filament. The transformation in the deposited filament occurs due to the "Rope Coiling effect" because of fluid instability. The filament instability could be better understood by this

empirical formula. This empirical formula defines the looping condition for the Line Printing. It should be noted that the flow rate of the filament and the speed of the print head are two independent variables.

The empirical relation is generated based on the two elementary boundary conditions:

a) $Q = 0$ and $V = \infty$, No Filament deposition.

b) $V = 0$ and $Q = \infty$, Looped Filament deposition.

The first boundary condition defines the working of the SWAM with no feed, while the print head is moving at very high speed. Therefore, it is the condition for no filament deposition. Note that any condition with $Q = 0$ would lead to not printing, so a better boundary condition would be one that denotes a relatively very small flow rate, or $Q \rightarrow 0$.

The second condition defines the looped filament deposition at high flow rate of the feed. In this case, the falling filament forms a series of regular loops at fixed point onto the horizontal surface as there is no movement of the print head. Similarly, if $V = 0$ there will be no filament since only a point will be printed. So, the condition with $V = 0$ can be replaced by a better boundary condition to denote a very small velocity, or $V \rightarrow 0$.

The empirical formula is written mathematical as

$$G_L = \frac{\partial (Q)}{\partial (V)} \quad \text{.....……..... Eqn (i)}$$

Where, G_L may be defined as the ratio of change in Flow Rate (Q) to the change in the printer's head speed (V). It should be noted that the other two printing value, Nozzle Diameter (D) and Gap Distance (H), are held as constant parameters but can never be zero. The value of G_L is predicted by Eqn (ii) and Eqn (iii), on the based on the above-mentioned boundary conditions that are applied in the Eqn (i) respectively.

$$G_L\,(Q,V) = 0 \begin{cases} Q \rightarrow 0 \\ V \rightarrow \infty \end{cases} \quad \text{.....……..... Eqn (ii)}$$

$$G_L\,(Q,V) = \infty \begin{cases} Q \rightarrow \infty \\ V \rightarrow 0 \end{cases} \quad \text{.....……..... Eqn (iii)}$$

Another empirical relation can be generated in terms of stream velocity (V_i) and average velocity ($< V >$) of printing. Stream velocity is the velocity which has been described in the literature of Barnes [56]. It defined as the rate of change of the silicone fluid with respect to a frame of reference and is a function of time. While the average velocity of silicone, herein, falling on the base of printing bed under the effect of gravity has been calculated. Consider the small cylindrical cross-section area of the falling silicone under the gravity (g) as shown in the Figure (4.7). Diameter of the small section would be similar as that of nozzle diameter and is represented by d. Using free falling object equation:

$$V_i^2 = < V >^2 + 2gh\,;$$

$$< V >^2 = V_i^2 - 2gh\,;$$

$$< V >^2 = \frac{Q}{A} - 2gh\,.$$

Similarly, the empirical relation of G_L, ratio between stream velocity (V_i) and average velocity ($< V >$) of printing on the two elementary boundary conditions, can be deduced as;

a) $< V > = 0$ and $V = \infty$, No Filament deposition.

b) $V = 0$ and $< V > = \infty$, Looped Filament deposition.

The above empirical relation follows the same criterion as generated between Print Speed (V) and Flow Rate (Q).

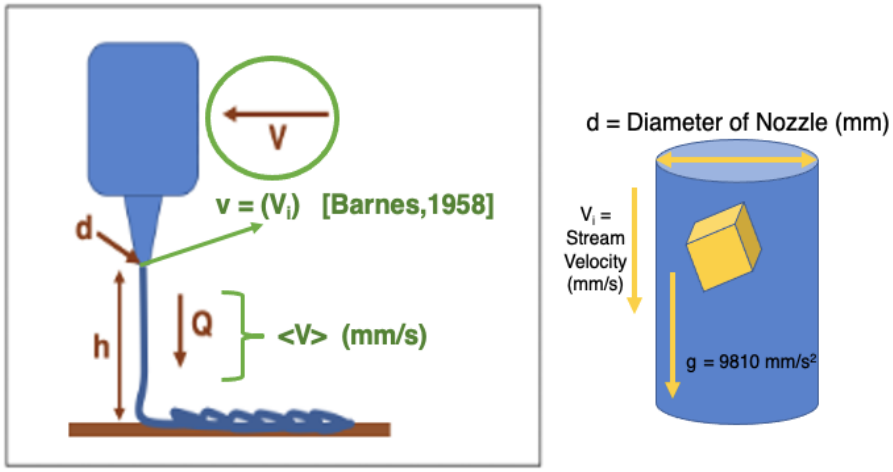

Figure 4.7 : Demonstration of average velocity ($< \boldsymbol{V} >$) and stream velocity ($\boldsymbol{V_i}$) in falling silicone from nozzle of the SWAM. (Source: created by Gurkamal Saggu)

Dimensional Analysis

Dimensional analysis is a means of simplifying a physical problem by appealing to dimensional homogeneity to reduce the number of relevant variables and to check equations. Dimensional analysis can determine the dimensions of physical quantities in terms of fundamental dimensions; mass $[M]$, length $[L]$, time $[T]$, and temperature $[\theta]$, to introduce the physical modelling. Dimensional homogeneity is a useful tool for checking formulae. For this reason, it is helpful when analysing a physical problem to retain algebraic symbol for as long as possible, only substituting numbers right at the end. During inspection. It has been inspected that G_L is having the dimension of deposition area (A) when it is the ratio of Flow Rate (Q) and Print Velocity (V), however, it is dimensionless when it is the ratio of Average velocity of falling silicone $(< V >)$ to the Print Velocity (V) [74].

Obtaining an expression in non-dimensional form for the G_L of the falling silicone with the Flow Rate of Q and Print Velocity (V), depositing a circular cross-section area of A onto the printing bed.

Step 1: Identifying the physical variable which are G_L, A, V, Q as:

$$[G_L] = M^0L^2T^0$$
$$[A] = M^0L^2T^0$$
$$[V] = M^0L^1T^{-1}$$
$$[Q] = M^0L^3T^{-1}$$

Step 2: Establishing the number of independent dimensional and non-dimensional group

number of physical variables $(n) = 4$

number of fundamental dimensions $(m) = 3$

number of non-dimensional group $(\Pi_s) = 4 - 3 = 1$

Step 3: Create the Π_1 by non-dimensionalising the remaining variable as;

$$\Pi_1 = G_L A^a V^b Q^c$$
$$[M^0L^0T^0] = [M^0L^0T^0]\,[M^0L^2T^0]^a[M^0L^1T^{-1}]^b[M^0L^3T^{-1}]^c$$

comparing the powers on both sides and left with:

$$0 = 2 + 2a + b + 3c$$
$$0 = -b - c$$

the values of a, b, c come out to be $-1,0,0$ respectively.

$$\Pi_1 = G_L A^{-1} V^0 Q^0$$

$$G_L = (\Pi_1)\, A$$

This concludes that the G_L is having the dimension of deposition area which is the factor occurred due to the Flow Rate when it calculated as the ratio of Flow Rate to Print Velocity.

Similarly, generating an expression in non-dimensional form for G_L of falling silicone through a nozzle at the certain gap distance with the average velocity of $(< V >)$ and is printed on the bed with the velocity of nozzle as V.

Step 1: Identifying the physical variable which are $G_L, V, < V >$ as:

$$[G_L] = M^0 L^0 T^0$$

$$[V] = M^0 L^1 T^{-1}$$

$$[< V >] = M^0 L^1 T^{-1}$$

Step 2: Establishing the number of independent dimensional and non-dimensional group

number of physical variables $(n) = 3$

number of fundamental dimensions $(m) = 3$

number of non-dimensional group $(\Pi_s) = 3 - 3 = 0$

As a result, it can be concluded that G_L will be dimensionless in this case.

The Line Printing can be clearly understood based on these two empirical relations as shown in the Figure (4.8). If the boundary condition 1 is applied, then there would be no deposition or there would be chances of the occurrence of breaks due to the highest print velocity. As it moves further to the boundary condition 2, it would lead to the maximum looped coil at one steady point when the printing stage is almost static, meaning that the Print Velocity is almost equals to zero. Another point can be made that the deposition spreading would getting wider as well.

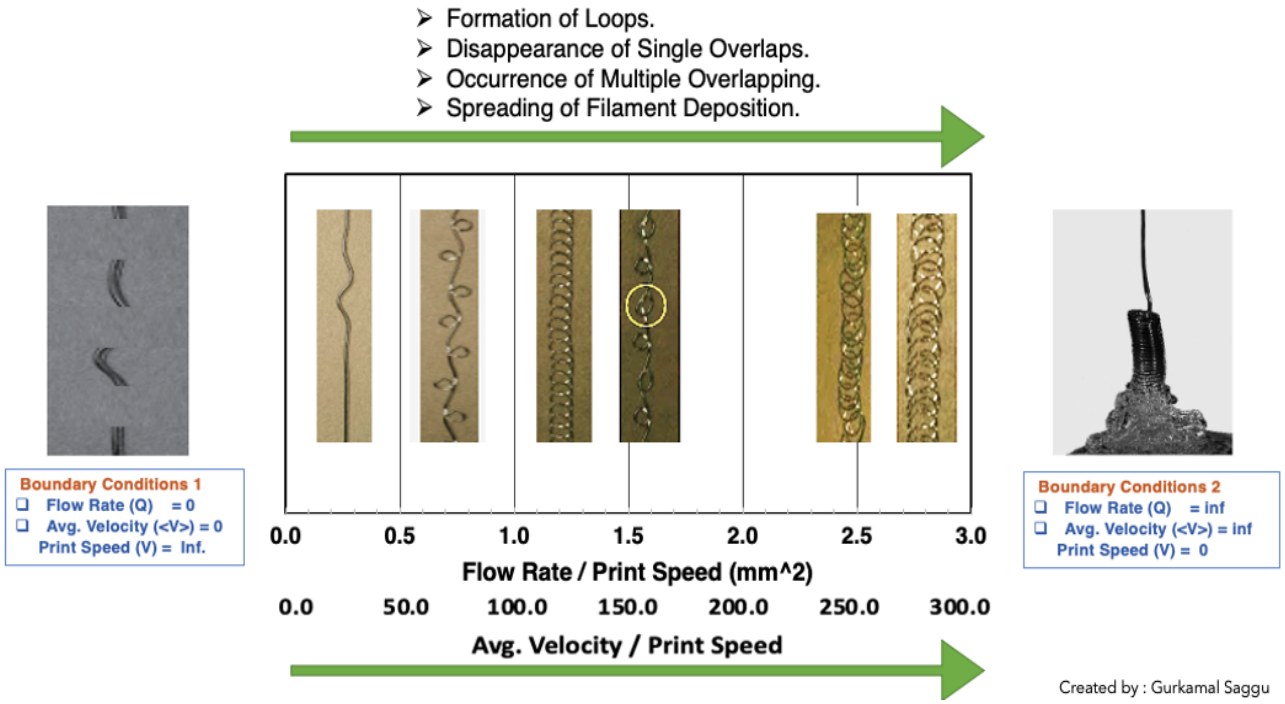

Figure 4.8: Transformation of Line Printing based on the two mentioned empirical formulae (Source by: Gurkamal Saggu)

4.4 Analysis of Filament Characteristics (F_{Char}) as a function of Flow to Speed Ratio (G_L)

The filament characteristics are further explained on the based empirical ratio, G_L. The results for six Filament Characteristics F_{Char} are plotted as a function G_L in Figure (4.9) and Figure (4.11).

Loops, irrespective of nozzle sizes, are lower at lower flow rates (Q) and higher print speeds (V) and vice versa. Loop counts are almost the same at higher flow rates and higher print speeds, or lower flow rates and lower print speeds. Increasing gap distance (H) would also lead to have a greater number of loops as well.

It shows the uphill pattern in both cases of the nozzle sizes as seen in the Figure (4.9a). It indicates that there is a positive linear relationship between F_L and G_L. As a result of increased G_L ratio, the F_L will increase as well. Higher loops in Line Printing can be obtained by using smaller nozzle size, whereas the loops are lesser in number using larger nozzle size.

Loops might be deposited as single loops or multiple loops. Figure (4.9b) and Figure (4.9c) show the plot of the F_{SL} and F_{ML} respectively as a function of G_L. It is evident from the curve that multiple loops are increasing with the increasing G_L ratio.

However, they are mainly observed in a lower nozzle size as compared to those nozzles having larger diameter. The larger nozzle, thus, prints more single loops than multiple loops. To be precise, the loop counts are possible to be controlled based on the G_L.

The transformation of the filament can also be understood thoroughly on controlling the loops, as an effect of G_L. Another evident from the curves is that single loops are being converted into multiple loops with higher G_L using smaller nozzle size.

On the contrary, indeed, the larger nozzle size would only transform the straight filament to single looped filament.

The transformation of the filament can be understood by the Filament Line Width Characteristic, F_{LW} on the basis on G_L ratio. The Line Width of the filament deposited by smaller nozzle has an insignificant effect of the G_L ratio, because the fabrication is already happened in the coiled phase. The single and multiple looped filaments tend to have similar line width, whereas the line width seemed to be higher during the mix loops transition state. The mix loop can be defined as the transition state at which single loops are developing into multiple loops due to the increased instability.

The transformation of the filament deposition as shown in the Figure (4.10).

The transformation of the filament can be understood by the Filament Line Width Characteristic, F_{LW} on the basis on G_L ratio. The Line Width of the filament deposited by smaller nozzle has an insignificant effect of the G_L ratio, because the fabrication is already happened in the coiled phase.

The single and multiple looped filaments tend to have similar line width, whereas the line width seemed to be higher during the mix loops transition state. The mix loop can be defined as the transition state at which single loops are developing into multiple loops due to the increased instability.

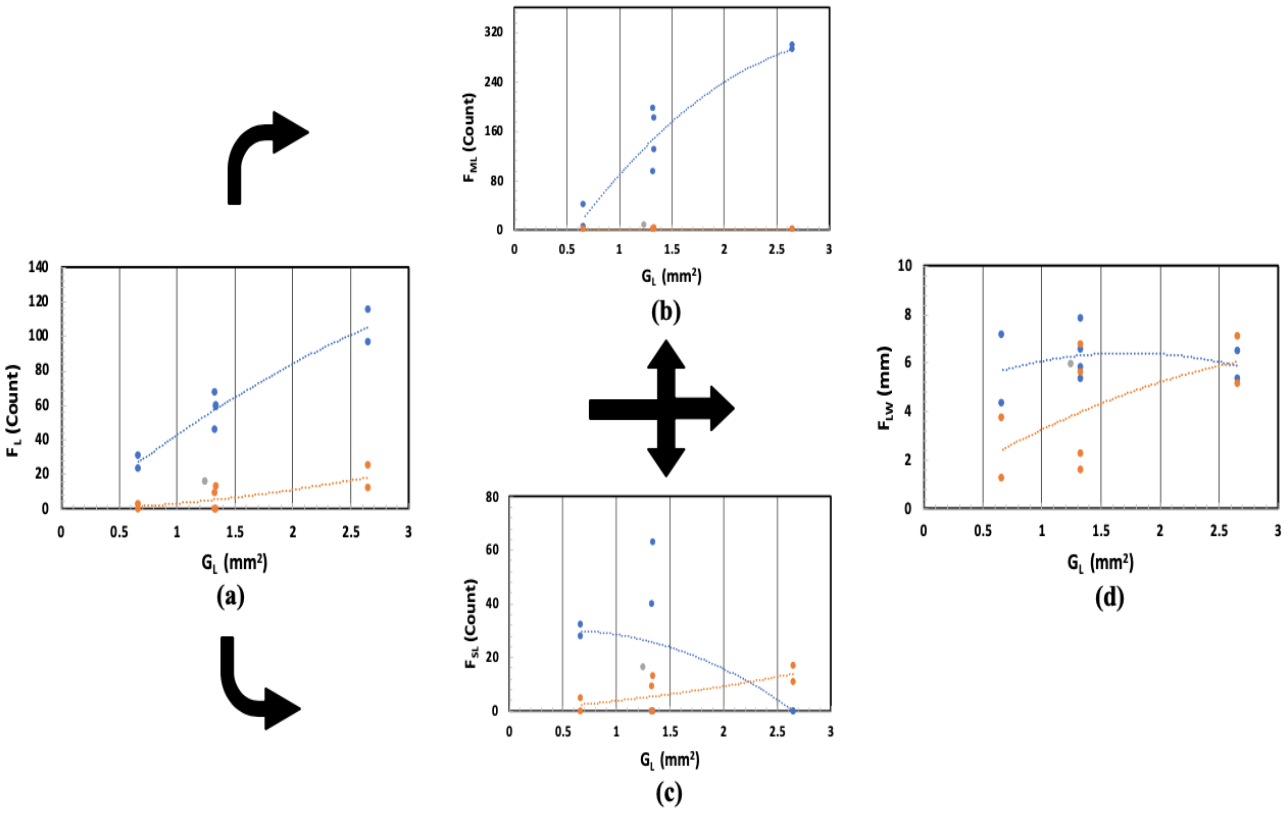

Figure 4.9: Line graphs depicting the four Filament Characteristics $(\boldsymbol{F_{Char}})$ versus Flow to Speed ratio $(\boldsymbol{G_L})$. Nozzle diameter in the figure is displayed based on the three-color representations: blue color represents the smaller diameter variations, grey color represents the center point variation, and orange color represents the variation of larger diameter. (a) depicts the Nozzle diameter variations when Filament Loop $(\boldsymbol{F_L})$is plotted against Flow to Speed ratio $(\boldsymbol{G_L})$. (b) depicts the Nozzle diameter variations when Filament Single Loop $(\boldsymbol{F_{SL}})$ is plotted against Flow to Speed ratio $(\boldsymbol{G_L})$. (c) depicts the Nozzle diameter variations when Filament Multiple Loop $(\boldsymbol{F_{ML}})$ is plotted against Flow to Speed ratio $(\boldsymbol{G_L})$. (d) depicts the Nozzle diameter variations when Filament Line Width $(\boldsymbol{F_{LW}})$ is plotted against Flow to Speed ratio $(\boldsymbol{G_L})$.

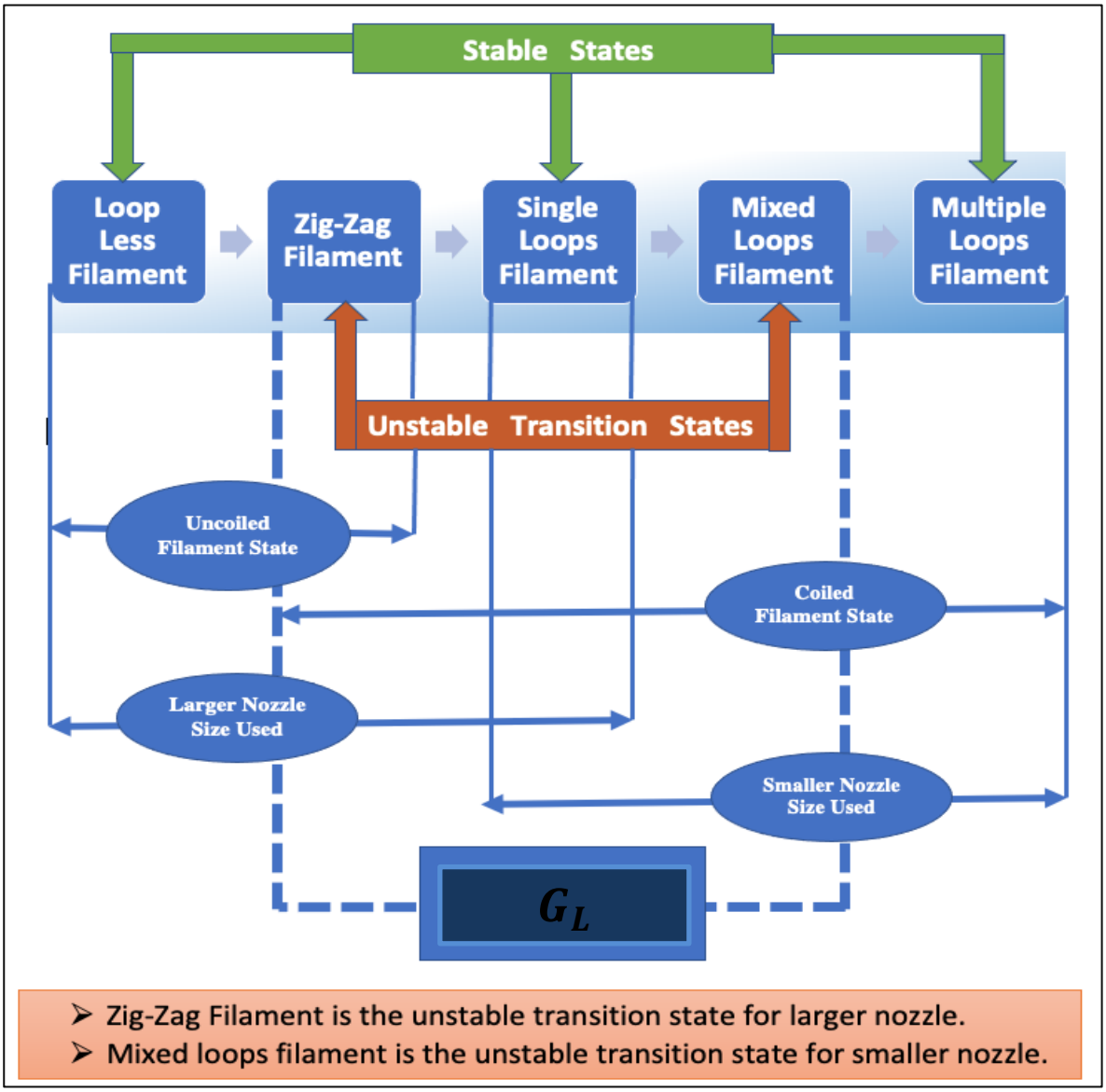

Figure 4.10: Diagram illustrates the transformation of the filament deposition having two states of transition: stable state and unstable transition state. Stable states: Loop less filament, single loops filament, and multiple loops filament. Unstable transition state: Zig-zag filament and mixed loops filament. (Source: by Gurkamal Saggu).

For larger nozzle, the line width seems to be increasing with G_L ratio. It makes more sense, because the filament transition is occurring at the zig-zag line to print single looped filament from straight filament. Similarly, zig-zag line is the transition state at which straight filament transformed itself to the single looped filament.

Instability of the filament is relatively high at the transition state because of filament transformation. The transition state in the filament fabrication occurs mainly when, $G_L = 1m^2$.

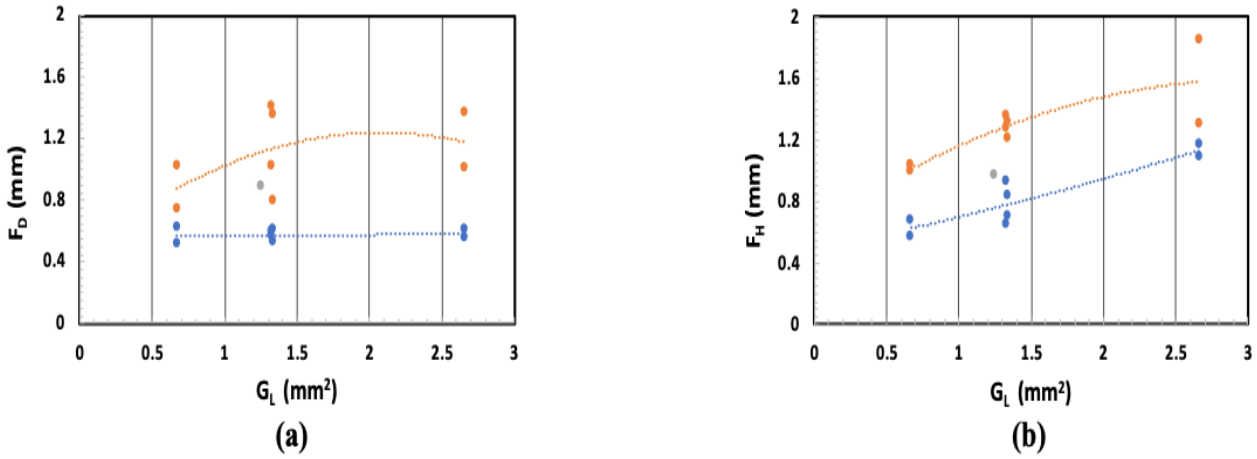

Figure 4.11: Line graphs depicting the two Filament Characteristics $(\boldsymbol{F_{Char}})$ versus Flow to Speed ratio $(\boldsymbol{G_L})$. Nozzle diameter in the figure is displayed based on the three-color representations: blue color represents the smaller diameter variations, grey color represents the center point variation, and orange color represents the variation of larger diameter. (a) depicts the Nozzle diameter variations when Filament diameter $(\boldsymbol{F_D})$ is plotted against Flow to Speed ratio $(\boldsymbol{G_L})$. (b) depicts the Nozzle diameter variations when Filament height deposition $(\boldsymbol{F_H})$ is plotted against Flow to Speed ratio $(\boldsymbol{G_L})$.

Filament Diameter, as shown in Figure (411), is almost consistent with the increasing G_L ratio, since it is highly dependent on the nozzle sizes as:

$$F_D \cong D \qquad \text{.....Eqn (iv)}$$

Deposition Height of the filament (F_H) is another characteristic which is increasing with G_L ratio and the nozzle sizes, as shown in (Fig 3(b)). Deposition Height is highly dependent on the volume deposited as an effect of the volumetric flow rate of the filament as well as the nozzle sizes. With the gap distances, filament gets thinner in diameter and tends to attain steady by coiling itself. Therefore, more deposition height is due to the more volume deposited because of the looping effects of the filament instability.

4.5 Application of SWAN for Seat Cushion Manufacturing

Based on the parameters obtained in previous sections, three blocks were designed with an attempt to achieve materials with controlled properties. The goals are to explore SWAM for controlling firmness by bulk printing materials while minimizing density.

Three samples, with the experimental conditions given in Table (4.10), were printed to represent seat cushions: SC 1, SC 2, and SC 3.

Table 4. 10: Experimental conditions that are used to print all the three Seat Cushion.

Samples	Nozzle Diameter (mm)	Gap Distance (mm)	Flow Rate (ml/min)	Print Speed (mm/s)
Seat Cushion 1	0.84	50	0.8	10
Seat Cushion 2	0.41	25	0.8	5
Seat Cushion 3	0.41	75	0.4	10

The stress is in the unit of kPa, and time is in the unit of seconds. This graph of stress is the function of time i.e.,

$$\text{Stress} = \text{fn (Time)}$$

The stress relaxation curve consists of two sections: the increasing strain rate section and the constant strain rate section. Overall, the stress of each sample become constant to attain equilibrium stress modulus after achieving the maximum stress modulus. It can also be concluded that after reorganizing their physical viscoelastic structure, each replicate can sustain roughly 90% of the maximal stress modulus for a longer time-period. Each car in-seat cushion obtained the maximum stress modulus within 25 seconds. Moreover, all of them attained their constant equilibrium stress modulus in just another 25 seconds and remains stable for longer time-period. Figure (4.12) shows the line graph depicts the stress relaxation curve of three seat cushion samples.

Table 4. 11: Result of all the three seat cushions with their density, density of pure silicone, average height, and maximum force deflection at 50 % of the total height respectively.

Samples	Density of Samples (g/cc)	Density of pure Silicone (g/cc)	Average Height(mm)	Max. Force Deflection@ 50% (N)
Block A	0.501	2.33	57.69	319.8096
Block B	0.315	2.33	51.04	158.7312
Block C	0.297	2.33	51.041	87.9310

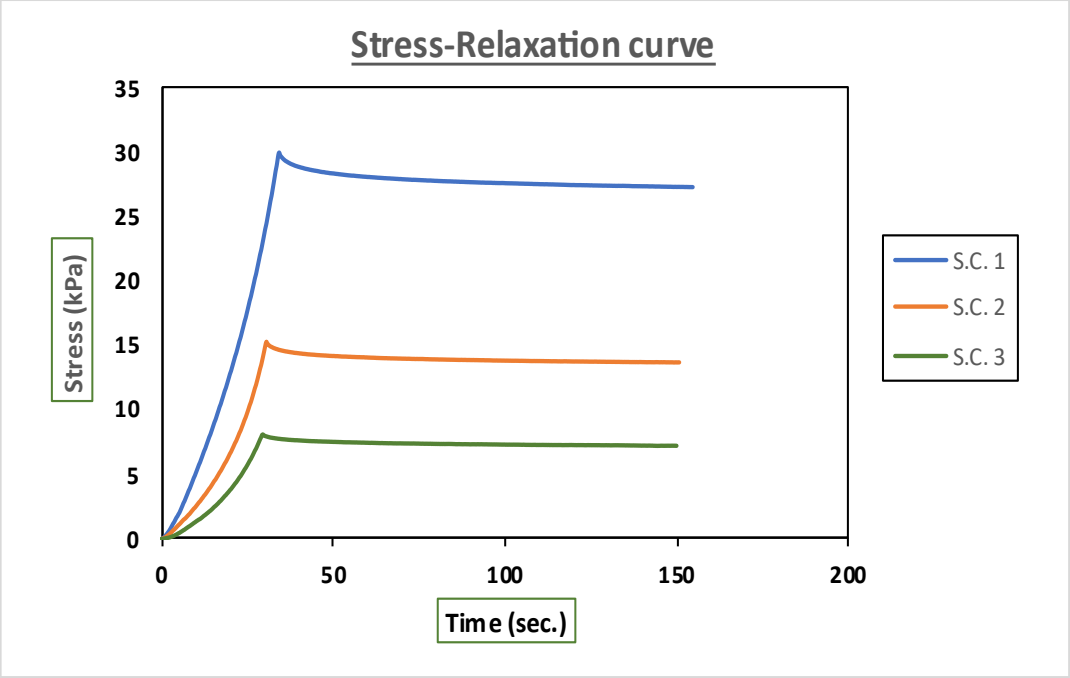

Figure 4.12: Line graph represent the Stress-relaxation curve of three different Seat Cushions.

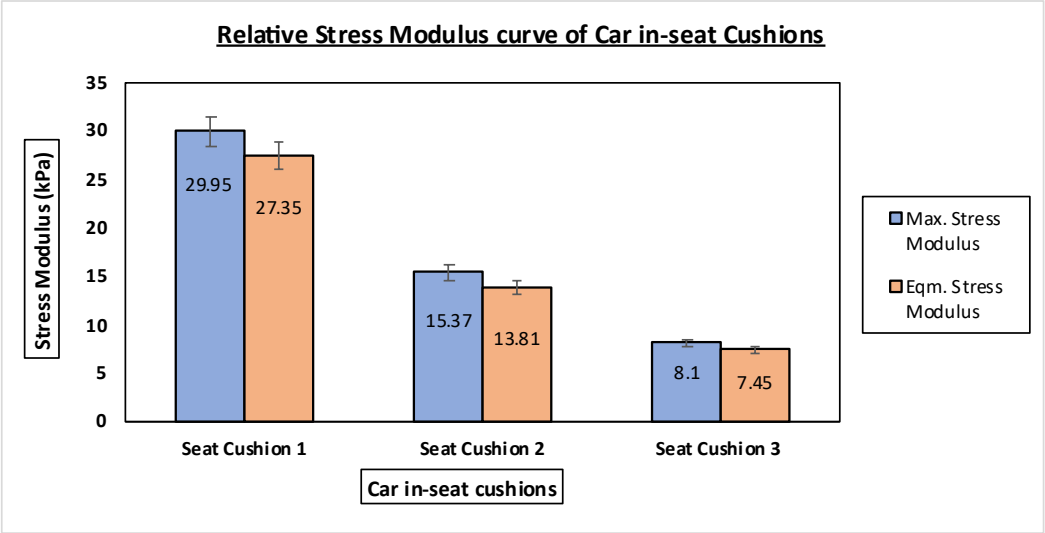

Figure 4.13: Bar graph represents the Relative Stress Modulus curve three of Car-in-seat Cushions. Blue color determines Maximum Stress Modulus and orange determines Equilibrium Stress Modulus.

The bar graph, as shown in the Figure (4.13) illustrates the maximum stress modulus (blue color) and equilibrium stress modulus (orange color) of each seat cushion. The maximum stress modulus of cushion 1, cushion 2, and cushion 3, are 29.95 kPa, 15.37 kPa, and 8.1 kPa respectively. The equilibrium stress modulus of cushion 1, cushion 2, and cushion 3, are 27.35 kPa, 13.81 kPa, and 7.45 kPa respectively.

The equilibrium stress moduli are 91.32 %, 89.85 %, and 91.98 % of the maximum stress modulus withstood by cushion 1, cushion 2, and cushion 3 respectively. The -seat cushion 1 can withstand the highest stress modulus followed by cushion 2, whereas the car in-seat cushion 3 can withstand the least stress.

The stress-strain curve, as shown in Figure (4.14), has been drawn out the conclusion of the changing stress applied on the specimen with the strain up to 50 %. The seat cushion 1 can withstand the highest stress among all the cushions. The stress-strain curve can also conclude that seat cushion 3 has the lesser porous structure due to thinner looped filament while the seat cushion 1 has the least pores due to thicker filament and lesser loops.

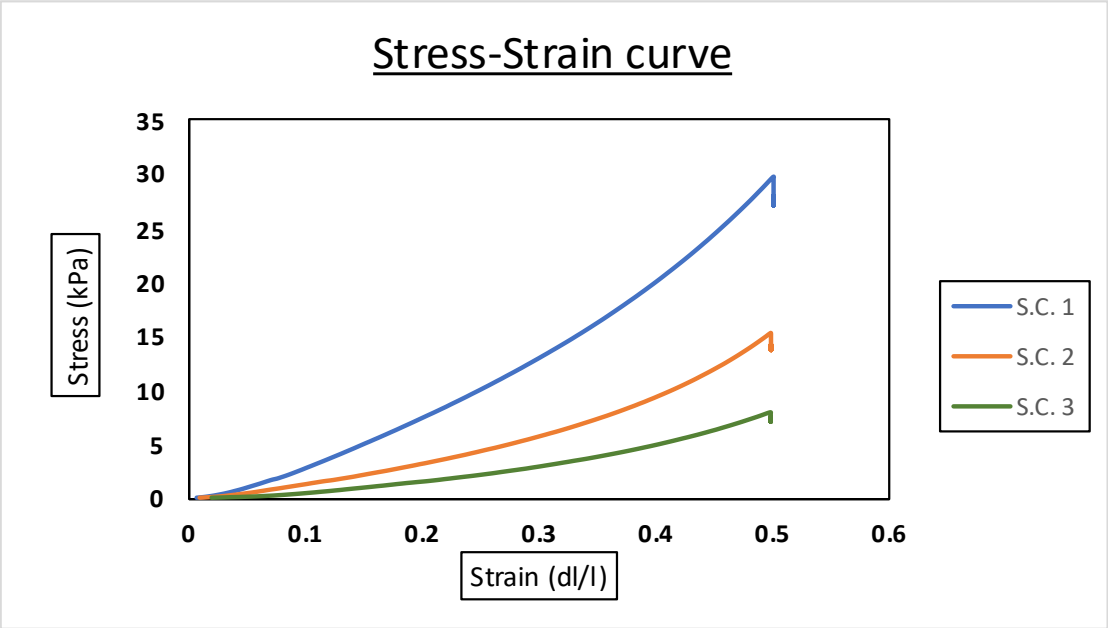

Figure 4.14: Line graph represents Stress-Strain curve of the three seat cushions.

The energy absorption can be concluded by the area under the stress-strain curve. It has been drawn in the bar graphs as shown in the Figure (4.15).

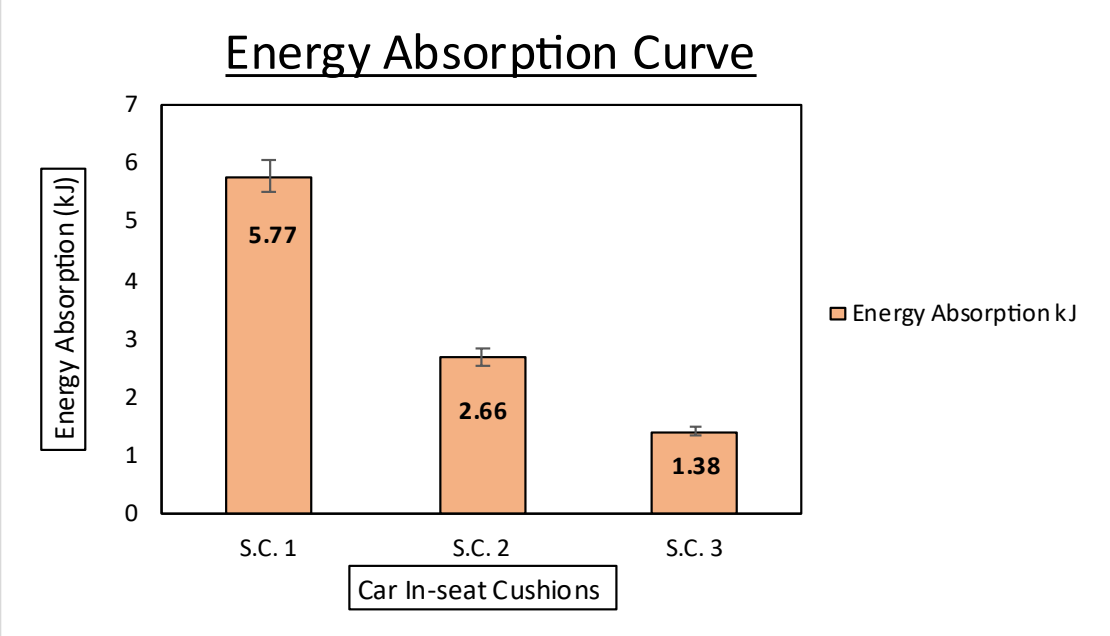

Figure 4.15: Bar graph illustrates the Energy Absorption curve of three Car In-seat Cushions.

The energy absorption has been calculated in the unit of kJ and is labeled by the y-axis. The x-axis labels seat cushions. Interestingly, the seat cushion 1 absorb almost the thrice amount of the energy absorbed by the seat cushion 3 and the double amount of the energy absorbed by the seat cushion 2. The seat cushion 1, seat cushion 2, and seat cushion 3 absorbs 5.77 kJ, 2.66 kJ, and 1.38 kJ respectively.

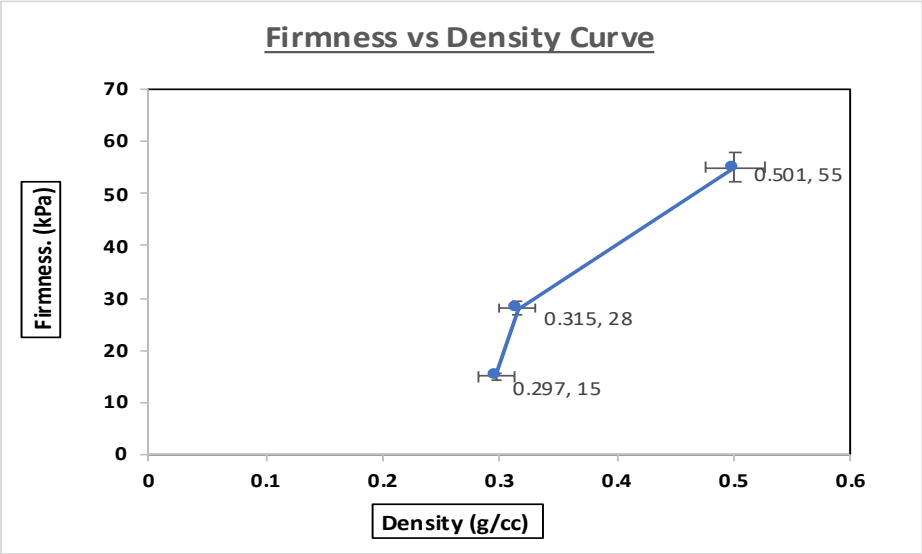

Figure 4.16: Line graph illustrates Firmness versus Density variation of three Car In-seat Cushions.

The firmness-density curve, as represented by the Figure (4.16), has been concluded out from the above data. The firmness is also defined by the young modulus of the specimen. The young's modulus of seat cushion 1, seat cushion 2, and seat cushion 3 is 55 kPa, 28 kPa, and 15 kPa respectively. The density of the seat cushion 1, seat cushion 2, and seat cushion 3 is 0.501 g/cc, 0.315 g/cc, and 0.297 g/cc respectively. It has been found that the young moduli are almost the sum of the maximum stress moduli and the equilibrium stress moduli of each specimen. However, there is no direct relationship between the firmness and density.

4.6 Tissue for Soft Robotics

Soft robots, in contrast to traditional machines and robots, are made mostly of fluids, gels, soft polymers, and other easily malleable substances. These materials have many of the same elastic and rheological qualities as soft organic matter, allowing the robot to continue to function even when stretched or compressed.

The forces exchanged between the robot and the surface must be uniformly distributed across a broad contact area to avoid the robot from penetrating into the surface and causing damage or mechanical

immobility. This necessitates compliance matching, or the idea that interacting materials should have equal mechanical stiffness to distribute internal load uniformly and reduce interfacial stress concentrations.

Young's modulus, on the other hand, is a helpful metric for comparing the stiffness of materials used in soft robots. Most of the robots are composed of materials, namely metals, and hard plastics that have modulus of greater than $10^9\ Pa$ or $10^9\ N/m^2$. The modulus of most natural creatures' materials, such as skin and muscle tissue, is on the range of 10^2-$10^6\ N/m^2$. That is, living creatures' materials are 3–10 orders of magnitude less stiff than standard robot materials. This enormous discrepancy in mechanical compliance is one of the main reasons why inflexible robots are typically biologically unsuitable and even unsafe for close human interaction, and why they seldom display the rich multifunctionality that flexible robots do [73].

Discussion about the firmness of fat and muscle and to design the conditions for printing the tissues as follow:

1. A higher strength and lower density composite elastomeric materials for the robotic body were designed so that the robot could operate at higher constant pressure.

2. A Line printing is the main concept that is used to carry out the printing procedures of the tissues to fabricate variety of the tissues. Lower the nozzle diameter, higher the gap distance would provide you the lower density tissue. Higher the flow rate and the print speed along with the lower gap distance would surely increase the firmness as shown in the Figure (4.17) and Table (4.12).

The prototype values were selected based on achieving soft tissues replicas and the conditions of the printing parameters are shown in the Table (4.12).

Table 4. 12: Experimental conditions that are used to print all the Soft Tissues.

Specimen	Nozzle Diameter (mm)	Gap Distance (mm)	Flow Rate (ml/min)	Print Speed (mm/s)
Soft Tissue 1	0.41	50	0.4	5
Soft Tissue 2	0.84	25	0.8	10
Soft Tissue 3	0.41	25	0.8	10
Soft Tissue 4	1.19	25	0.8	10

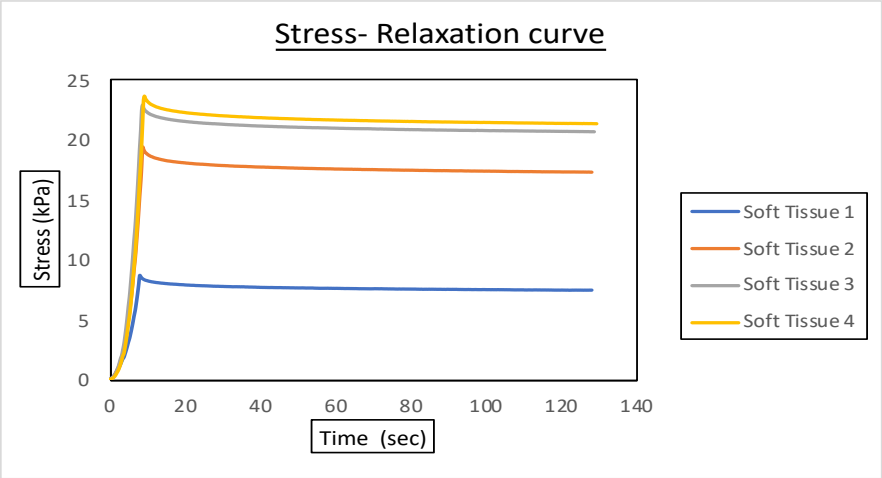

Figure 4.17: Line graph illustrates Stress-relaxation curve of four Soft Tissues.

The line graphs depict the stress relaxation curve of four prototypes for soft tissue. The stress is in the unit of kPa, and time is in the unit of seconds. This graph of stress is the function of time i.e.,

$$\text{Stress} = \text{fn (Time)}$$

The stress relaxation curve consists of two sections: the increasing strain rate section and the constant strain rate section. Overall, the stress of each soft tissue prototypes become constant to attain equilibrium stress modulus after achieving the maximum stress modulus. It can also be concluded that each prototype can withstand around 85-90% of the maximum stress modulus for a longer time-period after rearranging their physical viscoelastic structure.

Each prototype obtained the maximum stress modulus within 10 seconds. Moreover, all of them attained their constant equilibrium stress modulus in just another 10 seconds and remained stable for a longer time-period.

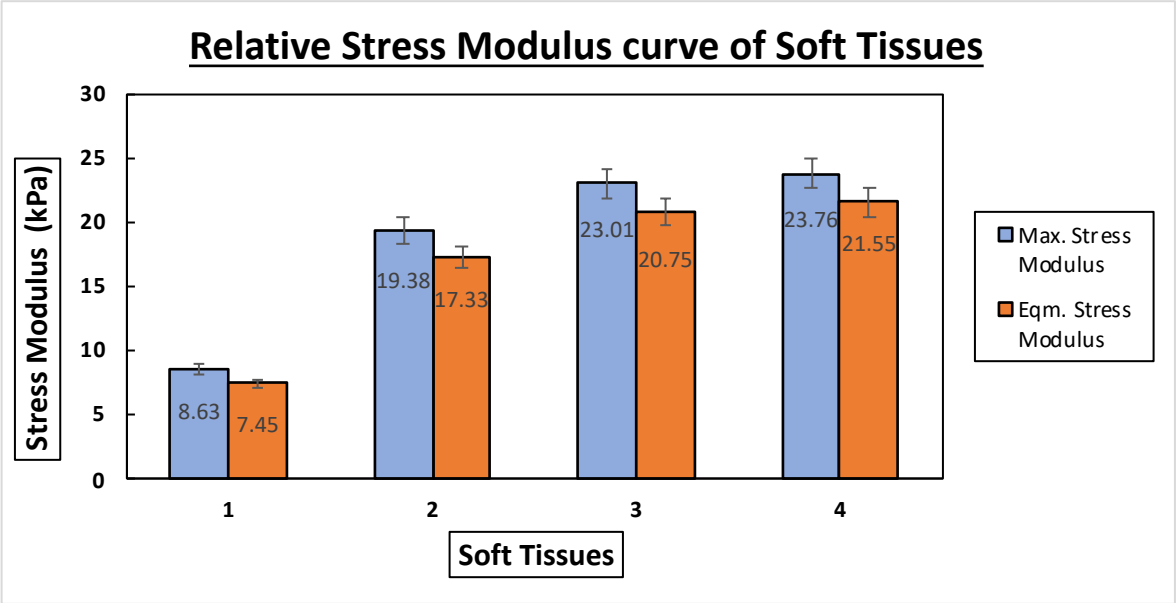

Figure 4.18: Bar graph illustrates Relative Stress Modulus curve of four Soft Tissues.

The bar graph has been illustrating the maximum stress modulus (blue color) and equilibrium stress modulus (orange color) of each tissue counterfeits.

The maximum stress modulus of prototype 1, prototype 2, prototype 3, and prototype 4 are 8.63 kPa, 19.38 kPa, 23.01 kPa, and 23.76 kPa. The equilibrium stress modulus of prototype 1, prototype 2, prototype 3, and prototype 4 are 7.54 kPa, 17.33 kPa, 20.75 kPa, and 21.55 kPa respectively.

Each prototype would have attained the constant equilibrium stress modulus which is nearly equal to 85-90% of the maximum stress modulus. The maximum and equilibrium stress modulus of prototype 3 and prototype 4 is almost similar. Whereas the relative moduli of prototype 1 is the least.

The stress versus strain graph has drawn out the conclusion of how the stress has been acted on the various type of prototype differently at the same strain rate. The stress over prototype 1 has been increasing gradually as it proceeds to 50% of the strain.

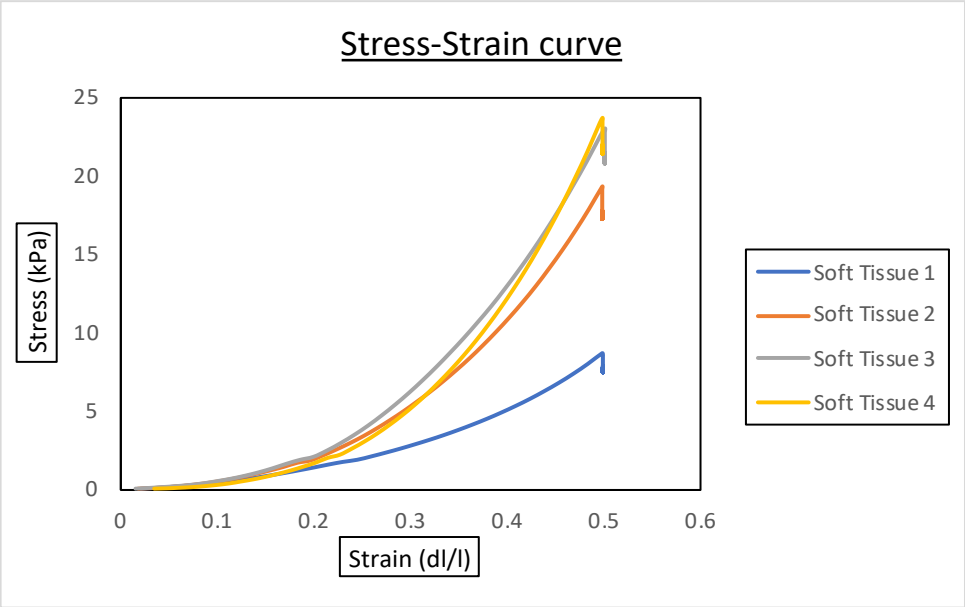

Figure 4.19: Line graph illustrates Stress-Strain curve of four Soft Tissues.

It can be concluded that the line printing in prototype 1 has thinner filament diameter and thinner deposition height due to the smaller nozzle diameter. It can also be concluded that line width is of higher value due to the increased falling height. Thereby, loops can be predicted as the mixed loops. Prototype 1 can be considered as the soft tissue. Prototype 2 would have the thicker filament with thicker deposition height but having more congested mixed loops due to it being more dense and slightly stiffer than skin 1. Prototypes 3 and 4 can be considered more loops with thicker filament diameter and thicker deposition height. This would make these skins even more stiff than the former one. Due to the less porosity, the prototype can attain more stress faster than more porous prototype. The polymeric entanglement in the structure helps in determining the stress moduli, young moduli as well as the energy absorption.

Furthermore, the young moduli can be evaluated through the tangent method across the stress- strain curve of each prototype profile. The young moduli of each prototype specimen are almost the sum of the maximum stress modulus and equilibrium stress modulus. The young modulus of prototype 1 - 4 are 15.2 kPa, 34.9 kPa, 41.9 kPa, and 44.7 kPa respectively. Prototypes 3 and 4 are stiffer than prototype 2 followed by prototype 1.

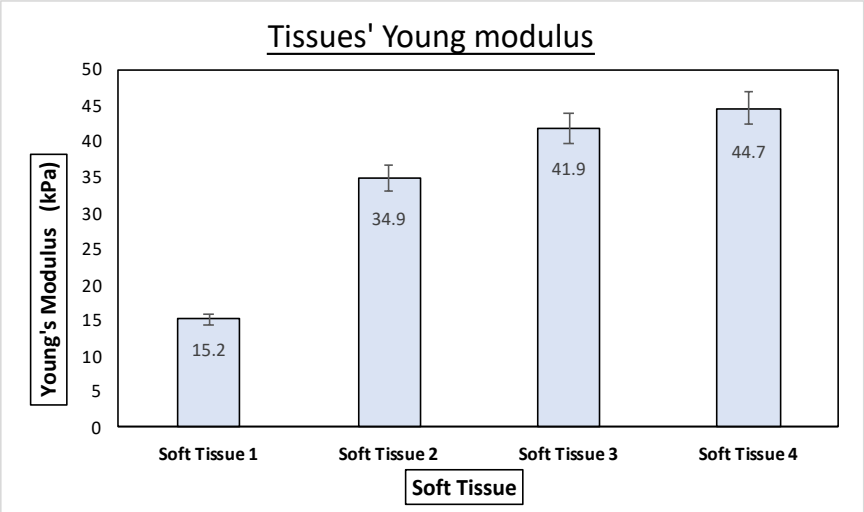

Figure 4.20: Bar graph illustrates Young's Modulus curve of four Soft Tissues.

The energy absorption curve has been drawn by calculating the area under the stress-strain curve of the prototypes. Interestingly, the prototype 3 has absorbed the maximum energy of 3.26 kJ followed by prototype 4 with an energy consumption of 3kJ. Prototype 2 absorbed energy (i.e., 2.73 kJ) almost double compared to the energy absorbed by prototype 1 (i.e., 3 kJ). The maximum energy absorbed by prototype 3 might be the reason for more or thicker diameter loops than prototype 4.

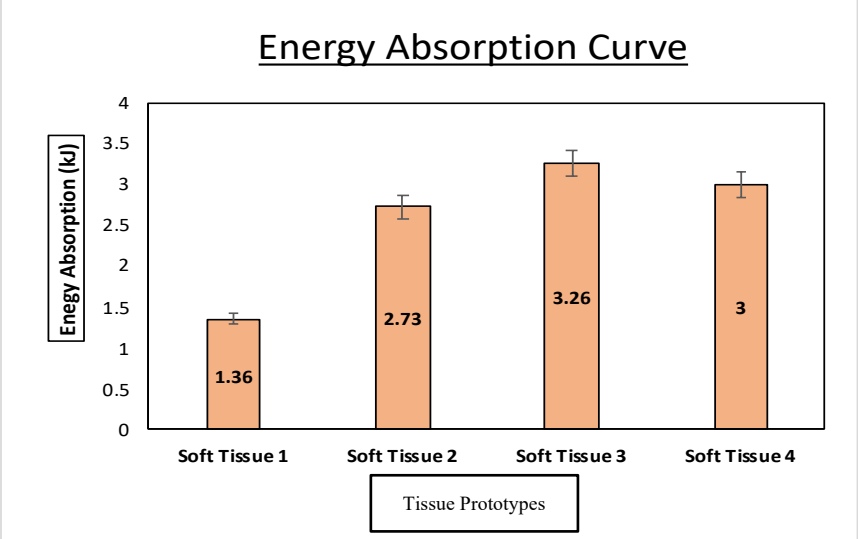

Figure 4.21: Line graph illustrates Stress-relaxation curve of four Soft Tissues.

Chapter 5
Conclusions

Silicone has a broad range of different usage in additive manufacturing due to its versatile physical and chemical characteristics. Based on the innovative SWAM applications, silicone has been chosen as the optimum alternative for elastomeric components in terms of durability and flexibility. Silicone can be conceived of as a low-cost core element for SWAM applications. The following conclusions can be drawn after a comprehensive examination of its rheology, and flow behavior:

1. Silicone has been researched for paste printing in a novel SWAM setup to investigate the new line printing approach that use the whipping method by optimizing four major printing parameters: Nozzle Diameter, Gap Distance, Flow Rate, and Print Speed. The thesis notably concludes the Liquid Rope Coiling effect on the falling silicone from SWAM's moving nozzle, which was coined by George Barnes in 1958. Due to the four distinct regimes: viscous, gravitational, inertial, and inertia-gravitational, this completely impacts the pattern as well as the transformation of the filament production over the printing bed. Filament Diameter, Filament Height, Filament Loops (Single and Multiple Loops), and Filament Line Width are the six distinct filament properties studied. The statistically examined results revealed a correlation between SWAM parameters and filament characteristics, trying to bridge the gap in additive paste manufacturing studies on the volume of deposition characterized by different printing parameters.

2. The empirical relationship between Flow Rate and Print Speed could well be assessed using line printing. Based on the variance of Nozzle Diameter and Gap Distance, a new term called G_L ratio, or Flow Rate to Print Speed ratio, has been established to depict the transformation of filament fabrication from loop-less filament to looped filament. For printing various types of silicone foam constructions, line printing would be an appropriate approach.

3. The line printing approach was used by SWAM to enable the development of the prototype for automotive cushioning. Therefore, silicone can be printed for "Automotive Application – Cushioning" as a robust, lightweight, and flexible component. With statistical analyses of characteristics, the bulk printing of car in-seat cushion has become possible. Line printing characteristic of overlapping plays a crucial role to achieve strength through the interconnectedness between the layers. The mechanical compression results of the seat cushion

have successfully shown that variable density and variable firmness for cushioning can be controlled and fabricated, however there is no direct relations between these two terms. Moreover, the silicone car in-seat cushion printed through SWAM would certainly consider as the alternatives to the PUR cushions in automotive in future, though they both are the good elastomeric components share almost similar mechanical properties.

4. Another application of SWAM has been illustrated in developing prototype for tissue replica through line printing technique. Therefore, silicone can be fabricated as a biocompatible, soft, and Visco-elastomeric component for 'Soft Robotics'. The obtained result has proved that the fabrication of soft or lower firmness tissues can be printed by controlling the printing parameters. This would be an opportunity in the field of soft robotics to transform hard bodied robot into humanoid robots by the silicone tissue coverings. This would open the new possibilities of effective learning especially to the autistic children in future.

Chapter 6

Future Aspects

1. 3D printing relies on modelling on the combination of important parameters (flow rate) to study the regime of line printing in 3D printing.
2. SWAM would be used further to scale up the production in different ways: parallel silicone printing, multiple printing, and variable density layered printing.
3. The forecasting can be done based on the new research work: Continuation of Inertial Control Liquid Rope Coiling effect.
4. This thesis is the outcome of a novel investigation concerning new counterfeits such as shoe soles, mattress paddings, delicate tissues, and mats.

Bibliography

[1] N. Vijay, “Reimagining the future with 3D printing,” *infosys Am. Head Manuf. Pract.*

[2] “Beamler Additive Manufacturing,” *Materials (Basel).*

[3] A. Rosenthal, “How 3D Printing could revolutionize the future of development.,” *Soc. Good Ser. Emerg. Technol.*, 2018.

[4] “3D printing market size, share & trends analysis reports by material, by component (hardware, services), by printer type (destop, industrial), by technology, by software,by applications,by vertical, and by segment forecast (2020 - 2027),” *Gd. view Res.*, no. Report I.D : 978-1-180380002, p. 250.

[5] N. J. Englewood Cliffs and M. Burns, “Automated Fabrication: Improving productivity in manufacturing,” *PTR Prentice Hall*, p. 8,15,49, 1993.

[6] “Euro Moulders.” .

[7] U. Andree and H. Oliver, “Johnson conntrols premiers synergy seat Gen3 seating concept at the International Motor Show (IAA),” *Johnson controls UK press*, 2013.

[8] M. . Hirschler, “Polyurethane foam and fire safety,” *Polym. Adv. Technol.*, pp. 521–529, 2008.

[9] S. Liang, M. Neisius, H. Mispreuve, R. Naecher, and S. Gaan, “Flame retardancy and thermal decompositionof flexible polyurethane foams:structural influence of organophosphorus compounds,” *Polym. Degrad. Stab.*, pp. 2428–2440, 2012.

[10] S. Liang, M. Neisius, H. Mispreuve, R. Naecher, and S. Gaan, “Flame retardant flexible polyurethane foams from novel DOPO-phosphonamidate additives.,” *Polym. Degrad. Stab.*, pp. 180–188, 2015.

[11] D. Price, Y. Liu, G. J. Mimes, R. Hull, B. K. Kandola, and A. R. Horrocks, “An investigation into the mechanism of flame retadancy and smoke suppression by melamine in flexible polyurethane foam.,” *Fire Matter*, pp. 201–206, 2002.

[12] A. Andersson, A. Magusson, S. Troedsson, F. H. . Maurer, and S. Lundmark,

"Intumescent foams- A novel flame retardant system for flexible PUR foams.," *J.Applied Polym. Sci.*, pp. 2269–2274, 2008.

[13] S. Thomas McKenna and T. Richard Hull, "The fire toxicity of PUR foams," *Fire Sci. Rev.*

[14] G. Hartzell, "Overview of combustion toxicology," *Toxicology*, p. 115, 1993.

[15] H. . Kaplan, A. . Grand, and G. Hartzell, "Toxicity and the smoke problem," *Fire Saf. J.*, p. 11.

[16] "Methylene Diphenyl Di-isocyanate (MDI), Toluene Di-isocyanate (TDI), and Polyurethane (PUR) market (2011-2016)," *Mark. Mark. Rep.*, 2011.

[17] A. M. Alcour *et al.*, "Educators' views on using humanoid robots with autistic learner in special education settings in the England," *Cent. Res. autism Educ. - London*.

[18] "American psychiatric association," 2013.

[19] C. L. Straten, A. Chen, E. Barakova, I. Smeekens, J. Glennon, and J. Buitlaar, "Effects of robots ' intonation and bodily appearance on robot-mediated communicative treatment outcomes for children with autism spectrum disorder.," *Pers. Ubiquit. Comput. 22*, pp. 379–390, 2018.

[20] B. Scassellati, H. Admoni, and M. Mataric, "Robots for use in Autism Research," *Ann.Rev. Biomed. Enginnering.14*, pp. 275–294, 2012.

[21] C. Duarte, "Successful Artificial Intelligence (AI) Implementation starts with people," *T.M. Tecnology*.

[22] W. R. Prototyping, "Rapid Prototyping," 2019. .

[23] Y. Yan *et al.*, "Rapid Prototyping and Manufacturing Technology: Principle, Representative Technics, Applications, and Development Trends," *Tsinghua Sci. Technol.*, vol. 14, no. SUPPL. 1, pp. 1–12, 2009, doi: 10.1016/S1007-0214(09)70001-X.

[24] J. Kerns, "How 3D Printing is changing Auto Manufacturing." .

[25] S. H. Huang, P. Liu, A. Mokasdar, and L. Hou, “Additive manufacturing and its societal impact: A literature review,” *Int. J. Adv. Manuf. Technol.*, vol. 67, no. 5–8, pp. 1191–1203, 2013, doi: 10.1007/s00170-012-4558-5.

[26] J. Herzberger, J. M. Sirrine, C. B. Williams, and T. E. Long, “Polymer Design for 3D Printing Elastomers: Recent Advances in Structure, Properties, and Printing,” *Prog. Polym. Sci.*, vol. 97, p. 101144, 2019, doi: 10.1016/j.progpolymsci.2019.101144.

[27] S. O. Onuh and Y. Y. Yusuf, “Rapid prototyping technology: Applications and benefits for rapid product development,” *J. Intell. Manuf.*, vol. 10, no. 3, pp. 301–311, 1999, doi: 10.1023/A:1008956126775.

[28] T. Wohlers and T. Gornet, “History of additive manufacturing Introduction of non-SL systems Introduction of low-cost 3D printers,” *Wohlers Rep. 2012*, pp. 1–23, 2012.

[29] J. P. Kruth, M. C. Leu, and T. Nakagawa, “Progress in additive manufacturing and rapid prototyping,” *CIRP Ann. - Manuf. Technol.*, vol. 47, no. 2, pp. 525–540, 1998, doi: 10.1016/S0007-8506(07)63240-5.

[30] S. Jasveer and X. Jianbin, “Comparison of Different Types of 3D Printing Technologies,” *Int. J. Sci. Res. Publ.*, vol. 8, no. 4, pp. 1–9, 2018, doi: 10.29322/ijsrp.8.4.2018.p7602.

[31] A. Hamidi and Y. Tadesse, “3D Printing of very soft elastomer and sacrificial carbohydrate glass/elastomer structures for robotic applications.,” pp. 1–9, 2020.

[32] J. S.Plott, *Extrusion-based Additive Manufacturing of Silcone Elasomer Parts*, vol. العدد الحا, no. 1. 2017.

[33] A. Finkle and Charles, “Silicone molding (Structur3d),” 2019. .

[34] N. Guo and M. C. Leu, “Additive manufacturing: Technology, applications and research needs,” *Front. Mech. Eng.*, vol. 8, no. 3, pp. 215–243, 2013, doi: 10.1007/s11465-013-0248-8.

[35] R. Truby and J. Lewis, “Printing Soft Matter in three dimensions,” *Nature*, p. 540,

2016.

[36] G. Robert, S. Aronson, W. Charleston, and Va, “U . S . Patent Nov . 26 , 1985,” *Fluid. bed Disch. Process*, no. 19, 1985, [Online]. Available: https://patentimages.storage.googleapis.com/dd/ad/8e/f23409e3205668/US4555183.pdf.

[37] R. Community and H. E. Everyone, “My Developments following the pioneers at Reprap - My aim is to help others build technology and eventually Universal Paste extruder - Ceramic , Food and Real Chocolate 3D Printing ... 1) - The Universal Paste Extruder,” 2020.

[38] W. Launches, T. H. E. First, P. Extruder, and F. O. R. Ceramic, “WASP launches the new professional clay extruder,” pp. 1–16, 2020, [Online]. Available: http://www.wasproject.it/w/en/wasp-launches-the-new-professional-clay-extruder/.

[39] C. Amza, A. Zapciu, and D. Popescu, “Paste Extruder—Hardware Add-On for Desktop 3D Printers,” *Technologies*, vol. 5, no. 4, p. 50, 2017, doi: 10.3390/technologies5030050.

[40] F. . Kipping and L. . LLoyd, “XLVII Organic derivatives of silicone triphenylsilicone and alkyloxysilicone chlorides,” *J.Chem.Soc.Trans.79*, pp. 449–459, 1901.

[41] C. Nouvelle, “‘Les Sillicones: preparation et performances,’” pp. 847–852, 1990.

[42] H. . Moretto, M. Schulze, and G. Wagner, “Silicones,” *Ullman’s encylopedia Ind. Chem.*, 2005.

[43] DeBuyle.F., “Silicones sealants and structural adhesives,” *Int. J. Adhes. Adhes.*, pp. 411–422, 2001.

[44] E. P. Plueddeman, “Silane coupling agents,” *Pluenum.Press, New York*, 1982.

[45] “http://chemiedidaktik.uni-wuppertal.dc/fileadmin/chemie/chemiedidaktik/disido/en/info/m-fact/crossmod.htm.” .

[46] “Adhesives,” *https://www.adhesives.org*.

[47] “https://www.adhesives.org/adhesives-sealants/adhesives-sealants-overview/sealant-technologies.” .

[48] “https://www.vijaysystems.com/blog/what-are-fire-stop-sealants.” .

[49] “‘Fire and rescue incident statistics: England.’”

[50] “Fire Statistics: United Kingdom 2003,” *https://www.communities.gov.uk/pub/894/*. .

[51] “Department for Transport : U.K.”

[52] “Do you need to carry a fire extinguisher in your car?,” *https://www.mocktheorytest.com/resources/fire-extinguisher-car/*.

[53] “NFPA report-vehicle fire trends and patterns (2010),” *Natl. fire Prot. Assoc.*

[54] “What rubber materials can withstand high heat?,” *Martins rubber Co.*

[55] “http://knowledgecenter.mearthane.com/polyurethanetemperaturerange.” .

[56] G. Barnes and R. Woodcock, “Liquid rope-coil effect,” *Am. J. Phys.*, pp. 26, 205–209, 1958.

[57] G. I. Taylor, “Instability of jets, threads, and sheets of viscous fluid,” *Proc. Intl. congr. Appl. Mech. Springer*, 1968.

[58] J. O. Cruichshank, “Low-Reynolds-number instabilities in stagnating jet flows,” *J. Fluid Mech.*, vol. 193, pp. 111–127, 1988.

[59] B. Tchavdarov, A. L. Yarin, and S. Radev, “Buckling of thin jets,” *J. Fluid Mech.*, vol. 253, pp. 593–615, 1993.

[60] J. O. Cruickshank and B. R. Munson, “viscous fluid buckling of plane and axisymmetric jets,” *J. Fluid Mech.*, 1981.

[61] A. Bol, “Flow Visualization (A course in the physics and Art of fluid flow,” *https://www.flowvis.org/2015/01/06/falling-honey-exhibits-the-rope-coiling-instability/*. .

[62] M. Habibi, “Coiling Instability in Liquid and Solid Ropes,” *Fluid Dyn.*, 2007.

[63] B. Fry, L. McGuire, and A. Shah, “An Experimental study of frequency regimes of Honey Coiling,” 2008.

[64] M. Maleki, M. Habibi, R. Golestanian, N. M. Ribe, and D. Bonn, “Liquid rope coiling on a solid surface,” *Phys. Reserv. Lett. 93,214502*, 2004.

[65] N. M. Ribe, M. Habibi, and D. Bonn, “The cook’s instability: coiling of a thread of honey,” *Phys. Reserv.*, 2007.

[66] L. Mahadevan, W. S. Ryu, and A. D. T. Samuel, “Correction: Fluid ‘Rope Trick’ investigated,” *Nat. 403*, p. 502, 2000.

[67] G. Barnes and R. MacKenzie, “Height of fall versus frequency in liquid rope-coil effect,” *Am. J. Phys.*, pp. 27, 112–115, 1959.

[68] S. Chiu-Webster and J. R. Lister, “The fall of a Viscous thread onto a moving surface: A ‘Fluid-Mechanical sewing Machine,’” *J. Fluid Mech.*, vol. 569, pp. 89–111, 2006.

[69] J. I. Lipton and H. Lipton, “3D printing variable stiffness foams using Viscous Thread Instability (VTI),” *Sci. Rep.*

[70] J. Crane, R. Crestani, and M. Cotteleer, “3D opportunity for end-use products (Additive manufacturing builds a better future),” *A Deloitte Ser. Addit. Manuf.*

[71] P. Scarfe and E. Lindsay, “Air muscle actuated low cost humanoid hand,” *Int. J. Adv. Robot. Syst.*, vol. 3, no. 2, pp. 139–146, 2006, doi: 10.5772/5745.

[72] C. Majidi, “Soft Robotics: A Perspective - Current Trends and Prospects for the Future,” *Soft Robot.*, vol. 1, no. 1, pp. 5–11, 2014, doi: 10.1089/soro.2013.0001.

[73] M. T. Tolley *et al.*, “A Resilient, Untethered Soft Robot,” *Soft Robot.*, vol. 1, no. 3, pp. 213–223, 2014, doi: 10.1089/soro.2014.0008.

[74] N. . Edwin, R. B. Bird, and W. E. Stewart, *Transport Phenomena*. 2018.